

THE UNIVERSITY
of EDINBURGH

This thesis has been submitted in fulfilment of the requirements for a postgraduate degree (e.g. PhD, MPhil, DClinPsychol) at the University of Edinburgh. Please note the following terms and conditions of use:

This work is protected by copyright and other intellectual property rights, which are retained by the thesis author, unless otherwise stated.
A copy can be downloaded for personal non-commercial research or study, without prior permission or charge.
This thesis cannot be reproduced or quoted extensively from without first obtaining permission in writing from the author.
The content must not be changed in any way or sold commercially in any format or medium without the formal permission of the author.
When referring to this work, full bibliographic details including the author, title, awarding institution and date of the thesis must be given.

Exploring the heterogeneity of perivascular cells

Joan Casamitjana

BSc, MSc

2021

Declaration

This is the result of my own work and includes only work issued from my sole work, except when specifically indicated.

The data shown here has not been submitted for any other degree or professional qualification. This thesis does not exceed 100,000 words as stipulated by the College of Medicine and Veterinary Medicine.

Joan Casamitjana

Abstract

Perivascular cells have been identified as *in vivo* progenitors of mesenchymal stem cells (MSCs), these being widely used as adult stem cells in multiple clinical conditions. Indeed, pericytes can differentiate into mesodermal lineages when cultured in induction media. Compared to MSCs, pericytes represent a more refined population of cells. As the interest to identify and isolate pure populations of pericytes increased, several markers have simultaneously and independently become reference pericyte identifiers. Nevertheless, the term "pericyte" exclusively refers to cells in a specific anatomical position -cells in the perivascular area of small blood vessels and embedded within its basal lamina- and *in situ* can be found around multiple types of vessels, in varying morphology and immunophenotype. This heterogeneity is being explored but remains largely unknown.

To investigate perivascular cell heterogeneity, we have used multiple well established pericyte markers (CD146, αSMA, NG2, leptin receptor [LepR], PDGFRβ, PDGFRα) across multiple tissues, including foetal and adult human (heart, skeletal muscle, bone marrow, subcutaneous white adipose tissue), murine (heart, skeletal muscle) and porcine tissues (heart, subcutaneous white adipose tissue). Immunohistological analysis was used to identify different pericyte subtypes, as well as their tissue distribution. Flow cytometry allowed pericyte subtype quantification and, when possible, cell sorting was performed for subsequent culture. When long-term cell cultures were established, cell lines at low passages were used in multiple in vitro assays to characterise their mesenchymal potential, including clonogenesis, growth, migration, metabolic activity

or mesodermal cell differentiation ability.

Analysis focused on LepR showed presence of subtypes in the foetal and adult bone marrow, but when sorted, presented donor-related differences *in vitro*. Foetal cardiac histological analysis revealed different distribution of perivascular layers within cardiac compartments, with homogeneous coverage of PDGFRβ^+ and PDGFRα^+ perivascular layers but significantly different for αSMA$^+$ (p-value$<$0.0001). Subsets based on PDGFRβ and PDGFRα were present in both foetal human and adult murine tissues, but when sorted cell cultures were not achieved. NG2$^+$ pericytes presented high mortality following enzymatical tissue dissociation, but were successfully isolated and sorted. *In vitro*, NG2 subtypes presented donor-dependent variations in multiple assays, but the NG2- subset performed better when results were homogeneous.

Together, this work shows the existence of multiple subtypes within generally assumed homogeneous pericyte populations. Variability concerns tissue distribution, with respect to the specific marker used, both within a specific tissue and across different tissues, and *in vitro* mesenchymal developmental potentials. Also, this work highlights donor-related differences within human tissues. In addition, current practices and terminology use, or misuse, involving perivascular and mesenchymal cells isolation, cell culture and later use are discussed.

Lay Abstract

Mesenchymal stem cells (MSCs) are a sort of stem cell that generate multiple types of tissues such as bone or muscle. They have been explored in the field of tissue regeneration, widely used in clinical trials to regenerate and repair broken bones and infracted hearts among others. Nevertheless, as opposed to other type of stem cells, little is known about their identity and the method of isolation is non-specific and therefore collects multiple cell types simultaneously.

The work presented in this thesis focuses on understanding the basic biology of a particular type of cell, found around the blood vessels that supply every cell in our body. These cells, the perivascular cells, have been shown to have the ability to generate other tissues, such as bone, fat or muscle when you put them in the right set of conditions in the laboratory, thus being characterised as MSCs progenitors. Yet these perivascular cells are very diverse, both in shapes and proteins they expose on their cell surface, and the current methods we possess to isolate them do not capture this diversity.

This work explores this heterogeneity by isolating fractions of the perivascular cells using combinations of specific cell surface markers, and looking at their numbers, tissue distribution and abilities when isolated and put in culture, such as growth rate or differentiation ability to turn into other cell types. Perivascular cells of multiple organs were used from human, mouse and pig donors.

The analysis revealed that indeed a multitude of subtypes exist when using specific combinations of markers across all tissues analysed. Distribution variabilities across

organs does not occur similarly for all the subtypes explored. Similarly, the different subsets do not survive equally the process of cell isolation, and only some of them were successfully cultured. Assays on cultured cells showed large donor-related differences, making the analysis of particular subtypes inconclusive, while revealing significant differences on another specific subtype.

Together, this work shows the existence of multiple subtypes of perivascular cells with clear and significant differences. Variability concerns tissue distribution, with respect to the specific marker used, both within a specific tissue and across different tissues, and the features they exhibit in culture. Also, this work highlights donor-related differences within human tissues. In addition, current practices and terminology use, or misuse, involving perivascular and mesenchymal cells isolation, cell culture and later use are discussed.

Acknowledgements

This PhD has been a great adventure, in and outside the lab. In my first international adventure, I have made many friends that have helped me through these wonderful 5 years.

First, my family and friends back at home, supporting me even though we were over 1,600km away, and even came visit me few times.

In the laboratory, everyone in Péault and Crisan's groups, in particular Isaac, Zaniah, Diana, Mario, Telma, David, Iain, Bianca, James, Mihaela and Bruno. Also to Bertrand, with whom I had fun coding FIJI scripts, and Ana, helping me organise yoga classes for the centre.

I wanted to thank the Folk society, where I learnt many tunes, songs and dances, and where I spent many nights in pubs and sessions, making me a true ceilidh master. And the EUHWC, where I discovered Scotland through munros with Anna.

And finally, Robin, one of my dearest friends that made easier at the end of this PhD, probably the hardest and most stressful period of my life.

Publications, presentations and other conferences

Publications

Diana Sá da Bandeira*, **Joan Casamitjana***, Mihaela Crisan. Pericytes, integral components of adult hematopoietic stem cell niches. Pharmacol Ther. 2017 Mar;171:104-113. doi: 10.1016/j.pharmthera.2016.11.006. Epub 2016 Nov 28. *__Co-first authors__.

Carolyn A. Meyers, **Joan Casamitjana**, Leslie Chang, Lei Zhang, Aaron W. James , Bruno Péault. Pericytes for Therapeutic Bone Repair. Adv Exp Med Biol. 2018;1109:21-32. doi: 10.1007/978-3-030-02601-1_3. In: Birbrair A. (eds) Pericyte Biology - Novel Concepts. Advances in Experimental Medicine and Biology, vol 1109. Springer, Cham

Bianca Vezzani, Mario Armando Gomez-Salazar, **Joan Casamitjana**, Carlo Tremolada, Bruno Péault. Human Adipose Tissue Micro-Fragmentation for Cell Phenotyping and Secretome Characterization. J. Vis. Exp. (152), e60117, doi:10.3791/60117 (2019).

Mario Armando Gomez-Salazar, Zaniah Nashira González, **Joan Casamitjana**, Mihaela Crisan, Bruno Péault. Five decades later, are mesenchymal stem cells still relevant? Front. Bioeng. Biotechnol.. **Accepted**. doi: 10.3389/fbioe.2020.00148

Poster presentations

2016. Scottish Cardiovascular Forum, Belfast (UK). *Characterising CD295/Leptin Receptor positive perivascular stem cells in multiple human tissues.* **Joan Casamitjana** and Bruno Péault.

2016. CVS symposium, Edinburgh (UK). Characterizing CD295 positive pericytes in multiple human tissues. **Joan Casamitjana** and Bruno Péault.

2017. CVS symposium, Edinburgh (UK). *Heart pericytes for cardiac pericytes.* **Joan Casamitjana**, Gillian A. Gray and Bruno Péault. Runner-up in the Imaging competition.

2018. High content imaging meeting, Edinburgh (UK). Imaging competition.

2018. CVS symposium, Edinburgh (UK). *Heart pericytes for cardiac pericytes.* **Joan Casamitjana**, Gillian A. Gray and Bruno Péault.

2018. Till&McCulloch meeting, Ottawa (Canada). *Characterising human and porcine heart pericytes for cardiac regeneration.* **Joan Casamitjana**, Montserrat Rigol, Gillian A. Gray and Bruno Péault.

Other conferences and seminars attended

2017. British Heart Foundation joint meeting, Cambridge (UK).

2018. ICMC Karolinska Institutet Symposium, Stockholm (Sweden).

Contents

Declaration iii

Abstract v

Lay Abstract vii

Acknowledgements ix

Publications, presentations and other conferences xi

List of Figures xxiv

List of Tables xxvi

Abbreviations xxx

1 INTRODUCTION 1

1.1 General introduction 1

1.2 Mesenchymal stem/stromal cells 2

1.2.1 Characteristics 2

1.2.2 MSCs in the clinic 3

1.2.3 A perivascular origin of MSCs 4

1.3 Vascular anatomy 4

1.3.1 Pericytes 5

1.3.2 Vascular smooth muscle cells 6

1.3.3 Adventitial cells 6
1.3.4 Perivascular fibroblasts 7
1.4 Perivascular cell markers 8
1.4.1 Reporter mice 17
1.4.2 Perivascular cell markers are homogeneous across species . . . 17
1.5 The role of perivascular cells during development 18
1.5.1 Ontogeny 18
1.5.2 Meso-angioblasts 19
1.5.3 Blood vessel formation 19
1.6 Perivascular cell role in homeostasis 20
1.6.1 Vascular support 20
1.6.2 Perivascular cell specialisation 20
1.6.3 Native response to tissue injury 22
1.7 Hypothesis and aims 23

2 GENERAL METHODS 25

2.1 Tissue procurement 25
2.1.1 Human foetal tissues 25
2.1.2 Human adult tissues 25
2.1.3 PDGFRβ reporter mice 26
2.1.4 Porcine tissues 27
2.2 Flow cytometry and cell sorting 27
2.2.1 Cell isolation 27
2.2.2 Unsorted cells as classical MSC 30
2.2.3 Cellular cell surface antibody labelling 30
2.2.4 Intracellular antibody cell labelling 32
2.2.5 Flow analysis 33
2.2.6 Cell sorting 33

2.3 Cell culture 35
2.3.1 Primary culture and cell line establishment 35
2.3.2 Cell line maintenance 36
2.3.3 *In vitro* assays 38
2.4 Histology and imaging techniques 42
2.4.1 Tissue preparation 42
2.4.2 Sectioning 44
2.4.3 Immunohistochemistry 45
2.4.4 Immunocytochemistry 49
2.5 Microscopy, image acquisition and data processing 50
2.5.1 Macro scripting 50
2.5.2 Widefield fluorescence 50
2.5.3 High content imaging 51
2.5.4 Whole slide scanning 51
2.5.5 Bright field 51
2.5.6 Image analysis 51
2.6 Statistics 52

3 Leptin Receptor **55**

3.1 Introduction 55
3.2 Hypothesis and Aims 56
3.3 Results 56
3.3.1 LepR is expressed on a fraction of pericytes in human bone marrow 56
3.3.2 LepR is expressed on a fraction of pericytes in human subcutaneous fat 59
3.3.3 LepR is expressed in other human foetal tissues 59
3.3.4 Do LepR$^{+/-}$ perivascular cells exhibit different potential *in vitro*? 60
3.3.5 Brief summary 67

3.4 Discussion 67
3.4.1 LepR is expressed by a fraction of pericytes and adventitial cells in adult and foetal tissues 67
3.4.2 LepR does not functionally discriminate subtypes of PCs based on the assays performed 69
3.4.3 Foetal samples exhibit dramatic donor dependent differences . . 69

4 NG2 and αSMA 71

4.1 Introduction 71
4.2 Hypothesis and Aims 72
4.3 Results 72
4.3.1 Different vessels in close proximity to each other possess distinct perivascular layers 72
4.3.2 Mef2c is exclusively expressed on CD146$^+$$\alpha$SMA$^+$NG2$^+$ cells in a transient fashion. 73
4.3.3 Different cardiac compartments have significantly different vascularisation levels, while constant during development 77
4.3.4 The epicardium is enriched in vessels with an αSMA$^+$ perivascular layer compared to the compact myocardium 79
4.3.5 Native response of cardiac pericyte subsets to myocardial infarction in a large animal 80
4.3.6 Porcine pericytes can be detected *in situ* using human pericyte markers 81
4.3.7 Pericyte markers are detected in non-perivascular areas following acute myocardial infarction 83
4.3.8 αSMA can be detected by intracellular flow cytometry in human tissues 87

4.3.9 Subsets of human pericytes based on CD146, αSMA and NG2 can be detected by intracellular flow cytometry 88

4.3.10 CD146$^+$NG2$^+$ pericytes exhibit high mortality rate while undergoing cell isolation 89

4.3.11 Do surviving CD146$^+$NG2$^{+/-}$ pericytes exhibit a different potential *in vitro*? 96

4.4 Discussion 117

4.4.1 There is heterogeneity within perivascular cells 117

4.4.2 Impact of anoikis 118

4.4.3 The technical issues of human tissue handling 119

5 PDGFRα and PDGFRβ 121

5.1 Introduction 121

5.2 Hypothesis and Aims 121

5.3 Results 122

5.3.1 PDGFRα and β are expressed in the perivascular layer of the majority of blood vessels in the human foetal heart 122

5.3.2 Subsets of PDGFRβ^+ cells based on other pericyte markers are present in murine tissues 124

5.3.3 PDGFRα and β label porcine perivascular cells 127

5.3.4 FACS analysis of PDGFRα and β expressing cells in human tissues 127

5.3.5 FACS analysis of PDGFRα and β expressing cells in murine tissues 130

5.3.6 Early attempts to analyse pig cells by flow cytometry 132

5.3.7 Brief summary 132

5.4 Discussion 133

5.4.1 PDGFRα and β identify subsets of perivascular cells in porcine, murine and human tissues 133
5.4.2 Faint extracellular labelling hinders cell sorting and later culture . 133
5.4.3 *In vitro* and *in vivo* characteristics of the subtypes based on PDGFRα and β derived from human tissues remains unknown . 134
5.4.4 Overall conclusion 134

6 General discussion **137**
6.1 Major findings 137
6.2 Perivascular cell populations need to be standardised 138
6.2.1 Perivascular cell nomenclature is obsolete 139
6.2.2 Cellular immunophenotype should be used as the new standard 139
6.2.3 New markers are still required 140
6.2.4 Hierarchy within perivascular cells 141
6.3 Important factors to consider when studying perivascular cells 142
6.3.1 Organ architecture 142
6.3.2 Variability due to blood vessel type 143
6.3.3 Tissue age 143
6.4 Final remarks 144

Appendices **177**

Macros **179**
.1 Stitching Operetta whole scan images 179
.2 Blood vessel quantification 184
.3 Adipogenesis/osteogenesis quantification 187

List of Figures

1.1 **Schematic representation of the physical interactions between pericytes and endothelial cells.** 5

1.2 **Schematic representation of the a large blood vessel.** 7

1.3 **Summary of the markers used for the identification of perivascular cells in 68 different studies.** 17

2.1 **Schematic representation of the method to isolate pericytes, adventitial cells and unsorted classical MSCs.** 35

3.1 **Leptin receptor in the human bone marrow.** 58

3.2 **Leptin receptor in the human subcutaneous white adipose tissue.** . 59

3.3 **Leptin receptor in the human foetal heart and skeletal muscle.** . . . 60

3.4 **FACS plots for foetal human perivascular LepR subset sorting.** . . 61

3.5 **CFUf assay reveals no conclusive differences when comparing subtypes of PCs based on LepR.** 63

3.6 **Growth in culture reveals no conclusive differences when comparing subtypes of PCs based on LepR.** 65

3.7 **Adipogenesis assay does not reveal consistent differences between subtypes based on LepR.** 66

3.8 **LepR^{+} adventitial cells and LepR^{-} pericytes exhibit higher osteogenic potential.** 68

4.1 **Different vessels in close proximity to each other possess distinct perivascular layers.** 73
4.2 **Foetal perivascular cells differently express developmental cardiac markers.** 75
4.3 **Mef2c is not expressed on cardiac tissues ranging 11 to 17 weeks of development.** 76
4.4 **Blood vessel quantification on foetal cardiac whole sections.** . . . 78
4.5 **Human foetal epicardium is less vascularised than the compact myocardium.** 79
4.6 **The human foetal epicardium contains a higher percentage of αSMA$^+$ perivascular layered blood vessels than the compact myocardium.** 80
4.7 **Porcine adipose-resident pericytes express the same markers as human pericytes.** 81
4.8 **Porcine cardiac pericytes express the same markers as human pericytes.** 82
4.9 **Porcine pericytes in a 2-day post-myocardial infarction heart.** . . . 84
4.10 **Pericytes in a non-infarcted area of the pig heart.** 85
4.11 **Pericytes in a 60 days post-myocardial infarction pig heart.** 86
4.12 **Subsets of CD146$^+$ pericytes based on αSMA expression can be detected by intracellular flow cytometry.** 88
4.13 **Subsets of pericytes based on CD146, αSMA and NG2 can be detected by intracellular flow cytometry.** 89
4.14 **The majority of NG2$^+$ pericytes are positive for the cell death marker live/death e780.** 90
4.15 **Sequential digestion did not improve NG2$^+$ survival.** 92
4.16 **Apoptosis inhibitors and metalloproteases did not improve NG2 yield.** 95
4.17 **Foetal pericyte subset sorting.** 97

4.18 **NG2$^-$ pericyte derived populations contain a higher proportion of PDGFRα than the NG2$^+$ after 5 passages.** 99
4.19 **NG2$^-$ pericytes exhibit higher metabolic activity.** 100
4.20 **Scratch assays revealed donor dependent differences in cell cultures when tested for their migration ability.** 102
4.21 **NG2$^-$ pericytes exhibit higher proliferation potential than NG2$^+$ pericytes.** 104
4.22 **Tested subtypes behaved in a donor dependent manner when tested for their clonogenic ability.** 106
4.23 **NG2$^-$ pericytes exhibit higher osteogenic potential.** 108
4.24 **NG2$^-$ pericytes exhibit higher osteogenic potential.** 109
4.25 **NG2$^-$ pericytes exhibit higher osteogenic potential.** 110
4.26 **Osteogenesis quantifications.** 111
4.27 **NG2$^-$ pericytes exhibit no skeletomyogenesis potential.** 112
4.28 **NG2$^-$ pericytes exhibit higher cardiomyogenic potential in two of the three donors tested.** 114
4.29 **Quantification of diferentiated muscle cells by immunocytochemistry.** 115

5.1 **PDGFRα and β are expressed in the perivascular layer of the majority of blood vessels in the human foetal heart.** 123
5.2 **Pbag PDGFRβ-GFP$^+$ cells co-express multiple perivascular markers in the murine heart.** 125
5.3 **Pbag PDGFRβ-GFP$^+$ cells co-express multiple perivascular markers in the murine skeletal muscle.** 126
5.4 **Porcine pericytes express PDGFRα and β.** 127
5.5 **PDGFRα^+ and β^+ cells in human tissues.** 129
5.6 **PDGFRα^+ and β-GFP$^+$ cells in murine tissues.** 131
5.7 **Flow cytometry analysis of porcine tissue.** 132

6.1 **CD39 is expressed on VSMCs but not on pericytes in human tissues.** 141

List of Tables

1.1 **Markers used in the identification of perivascular cells.** 13

1.2 **Summary of the markers used for the identification of perivascular cells in 68 different studies.** Presence of the perivascular markers (+) was noted in 68 published studies, by either immunohisto or cytochemistry, flow cytometry, qPCR or protein level quantification methods. . . . 14

1.3 Example of some reporter mice used in the identification of PCs. 18

2.1 Human tissues used. 26

2.2 Murine tissues used. 26

2.3 Flow cytometry antibodies used against human cell surface antigens. ms=Mouse 31

2.4 Flow cytometry isotype controls. Used at same dilutions as the primary antibodies. 31

2.5 Flow cytometry dyes used for human intracellular labelling. ms=Mouse . 32

2.6 Sorted immunophenotypes. 34

2.7 Culture media used. 42

2.8 Unconjugated primary antibodies. rb=rabbit, hu=human, ms=mouse, p=pig. 47

2.9 Conjugated primary antibodies. hu=human, ms=mouse, p=pig. 48

2.10 Secondary antibodies. 48

4.1 FACS sorting of $CD146^{+}NG2^{+/-}$ pericyte subsets. 97

4.2 Foetal skeletal muscle derived NG2$^{+/-}$ pericytes in culture. Best performers in each assay are indicated. 115

Abbreviations

αSMA α Smooth muscle actin.

$^{\circ}$C degrees Celsius.

AF Alexa fluor.

ALP Alkaline phosphatase.

AM Adipogenic medium.

APC Allophycocyanin.

BV Brilliant violet.

CFU-f Colony forming unit-fibroblast assay.

Cy Cyanide.

DAB 3,3'-diaminobenzidine.

DAPI 4',6-diamidino-2-phenylindole.

DMEM High glucose Dulbecco's modified Eagle medium with Glutamax.

DMSO Dimethyl sulfoxide.

ECM Extracellular matrix.

ECs Endothelial cells.

EGM-2 Endothelial cell growth medium 2.

FACS Fluorescence activated cell sorting.

FCS Foetal calf serum.

FITC Fluorescein isothiocyanate.

FSC-A Forward scatter area.

FSC-H Forward scatter heigth.

GFP Green fluorescent protein.

GM Growth medium.

HRP Horseradish peroxidase.

HSCs Haematopoietic stem cells.

hu Human.

ICC Immunocytochemistry.

IHC Immunohistochemistry.

LepR Leptin receptor.

Mef2c Myocardial enhancer factor 2c.

ms Mouse.

MSCs Mesenchymal stem/stromal cells.

NG2 Neural glial antigen 2.

O/N Over-night.

OCT Optimal cutting temperature compound.

OM Osteogenic medium.

p Pig.

P/S Penicillin/streptomycin.

PBS Phosphate buffered saline.

PCs Perivascular cells.

PDGFRα Platelet derived growth factor receptor α.

PDGFRβ Platelet derived growth factor receptor β.

PE Phycoerythrin.

PE/Cy7 Phycoerythrin/cyanine 7.

PFA Paraformaldehyde.

PSR Picrosirius red.

rb Rabbit.

RBC Red blood cell lysis buffer.

rcf Relative centrifugal force.

RGS-5 Regulator of G-protein signalling 5.

ROI Region of interest.

RT Room temperature.

SF-MHC Slow fast myosin heavy chain.

SGM Standard growth medium.

SSC-A Side scatter area.

TGFβ Transforming growth factor β.

V Violet.

VSMCs Vascular smooth muscle cells.

vWF von Willebrand factor.

Chapter 1

INTRODUCTION

1.1 General introduction

The work presented in this thesis investigates the heterogeneity within perivascular cells. Perivascular cells have consolidated their position as mesenchymal progenitor cells, still there is no unique marker specific for each cell type. While most studies use a unique marker to isolate and describe the characteristics of a particular cell population, they fail to explore the diversity of subpopulations that span from the existence of multiple perivascular cell markers. This thesis focuses on describing the native distribution and *in vitro* potential of subsets of pericytes and adventitial cells as described previously in our group using well described perivascular cell markers. This step is crucial to understand the true complexity and diversity of the cells composing blood vessel walls.

1.2 Mesenchymal stem/stromal cells

1.2.1 Characteristics

In 1867, Conheim suggested for the first time that the bone marrow (BM) is not only populated by haematopoietic cells [1]. In the 1960s, Friedenstein described a population of cells coming from rodent BM that can adhere to plastic and included fibroblast colony forming cells [2]. These cells looked heterogeneous in culture, but mainly presented a spindle-shaped morphology. Later on, those cells were proven to differentiate into osteocytes, chondrocytes, adipocytes and myocytes [3]. In 1991, Caplan coined the term mesenchymal stem cells (MSCs), by analogy to their embryonic counterparts [4]. The term 'stem' was later altered to 'stromal' by some authors to avoid misunderstanding of the pluripotency of these cells [5].
In 2006, the International Society for Cellular Therapy established the minimal criteria for defining multipotent mesenchymal stromal cells [6] stating that MSCs are:

- plastic adherent cells in standard culture conditions,
- express the cell surface markers CD105, CD73 and CD90; while lacking the cell surface markers CD45, CD34, CD14 or CD11b, CD79α or CD19, and HLA-DR,
- able to differentiate *in vitro* into osteocytes, adipocytes and chondrocytes.

Beyond these minimal criteria, characterisation of MSCs has gone further attributing them special roles. MSCs have been described to support haematopoiesis in long term cultures *in vitro* [7], create a haematopoietic microenvironment [8] and favour haematopoietic stem cell (HSCs) engraftment and haematopoietic cell repopulation when transplanted together [9]. Immunomodulatory capacities have been largely described in allogenic MSC transplants, increasing their therapeutic potential. MSCs mediate immunosuppression by cell-to-cell contact and factor secretion [10]. Furthermore, the MSC secretome -cellular products including growth factors and cytokines released into the extracellular compartment, sometimes by means of extracellular

vesicles- seems to have effects beyond the immune system, releasing trophic factors [10, 11] that may have crucial angiogenic and antiapoptotic effects. These effects could prolong injured tissue survival and promote tissue repair, reduction of the inflammatory response, revascularisation of the tissue and potentially recruit local progenitor cells, although the secretome is variable among MSCs from different anatomical positions and functions [12].

Even with the establishment of minimal criteria, there has been a lack of information on the native identity of MSCs. Several groups have attempted to establish new markers, which has been controversial, again due to the anatomical variability of MSCs [13].

1.2.2 MSCs in the clinic

Since their discovery, MSCs have been proposed as the best candidates for a multitude of conditions, from regenerating hearts and injured muscles, synthesising new tendons and skin, to regulating the immune system. Indeed, MSC abundance, easy extraction and subsequent culture make these cells prime candidates for clinical use. Over 1,000 different clinical trials using MSCs have taken place to date (clinicaltrials.gov). Nevertheless, these trials have produced very variable results raising questions about whether these cells are still suited to treat some conditions.

As to why these trials have produced such variable outcomes, the cell type that is actually being used must be examined. Most trials are still selecting cells for use by a single indirect cell to plastic adherence step, resulting in completely uncharacterised cell lines. This method of selection does not exclude numerous cell types that would not be of any regenerative interest, such as fibroblasts. A much more pure and refined population of MSCs may be beneficial.

1.2.3 A perivascular origin of MSCs

While MSCs are exclusively an *in vitro* product generated when cells are placed in culture and demonstrated to possess the minimal characteristics described above (section 1.2.1), the main mechanism of isolation remains extremely simple, but results in collection of numerous cell types simultaneously. Cells are selected indirectly, by cell attachment to plastic following tissue dissociation, thus selecting all adherent cell types. The major question, still now investigated, is: what are the *in vivo* counterparts of the MSCs?

As multiple origins were investigated, it was first suggested, then well established, that mesenchymal progenitors reside on the blood vessel walls, thus MSCs can be isolated from virtually all vascularised tissues [14]. Indeed, populations residing on the vessel walls, when in culture, display MSCs characteristics [15–19]. These cell populations have been successfully isolated from multiple tissues including skeletal muscle, bone marrow, white adipose tissue, placenta, pancreas, umbilical cord, heart, kidney, infrapatellar fat pad and liver [16, 20–33]. Other mesenchymal progenitors in lower frequencies can be found in other locations , such as interstitial fibroblasts.

Despite discovering the location of MSCs progenitors *in vivo*, multiple cell types compose the blood vessel wall and heterogeneity is to be expected.

1.3 Vascular anatomy

Blood vessel architecture is directly dependent on the type of blood vessel and the specific organ it vascularises. Structured in two to three layers, blood vessels change their perivascular components to acquire the specific features necessary for their proper function. The innermost layer, the *tunica intima*, is strictly populated by endothelial cells (ECs). The second and third layers, the *tunica media* and *tunica adventitia* (only present on large vessels), are populated by a diversity of cells of generally mesoder-

mal origin that constitute the perivascular cells (PCs).

1.3.1 Pericytes

Pericytes are large stellate cells that form a discontinuous layer and are in close contact with the endothelial cell layer of capillaries (diameter 4-10μm), and constitute a continuous layer around microvessels (arterioles and venules; diameter 10-100μm). Historically first described in 1873 by Rouget [34, 35], then in 1923 by Zimmermann [36], pericytes were first suggested to be involved in regeneration in the early 1970s [37], and specifically suggested to be MSCs progenitors [38, 39]. It is now clear that pericytes are progenitors of *bona fide* MSCs both *in vitro* and *in vivo*. Pericytes are able to differentiate into chondrocytes, adipocytes and osteocytes regardless of their tissue of origin [15–17], as well as other mesodermal lineages such as skeletal and cardiac muscle [40, 41]. Pericytes have been linked with mesenchymal abilities such as haematopoietic cell support [42–44], immunomodulatory and proangiogenic effects.

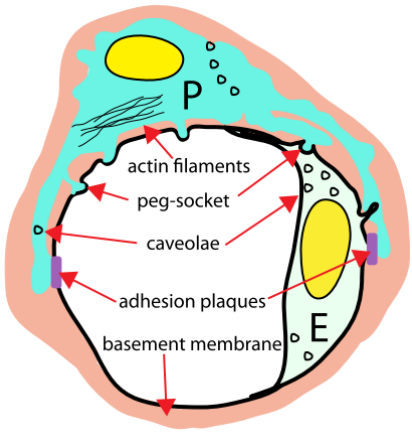

Figure 1.1: **Schematic representation of the physical interactions between pericytes and endothelial cells.** Schematic representation adapted from Armulik *et al.* (2010) [45], representing a pericyte (P) and endothelial cell (E) and their interactions in a cross section of a capillary.

1.3.2 Vascular smooth muscle cells

Residents of the *tunica media*, vascular smooth muscle cells (VSMCs) are contractile cells associated mostly with veins and arteries. In large vessels they are usually found in multiple and compact layers, shaping the vessel. Classical VSMCs can be easily differentiated from pericytes, while in reality VSMCs and pericytes form a continuum changing with the vessel, thus becoming more difficult to differentiate in smaller vessels. VSMCs and pericytes share the same lineage, as well as several markers [46].

1.3.3 Adventitial cells

Adventitial cells are a particular type of cell found within the *tunica adventitia* of larger vessels characterised by expression of the haematopoietic cell marker CD34. This particular cell can also give rise to classical MSCs in culture [18, 47]. Adventitial cells can also differentiate into VSMCs, and start expressing other perivascular cell markers in culture [48, 49]. Furthermore, when compared to pericytes, they exhibit a more primitive state, thus it has been theorised that adventitial cells are more progenitor-like than other perivascular cells [50].

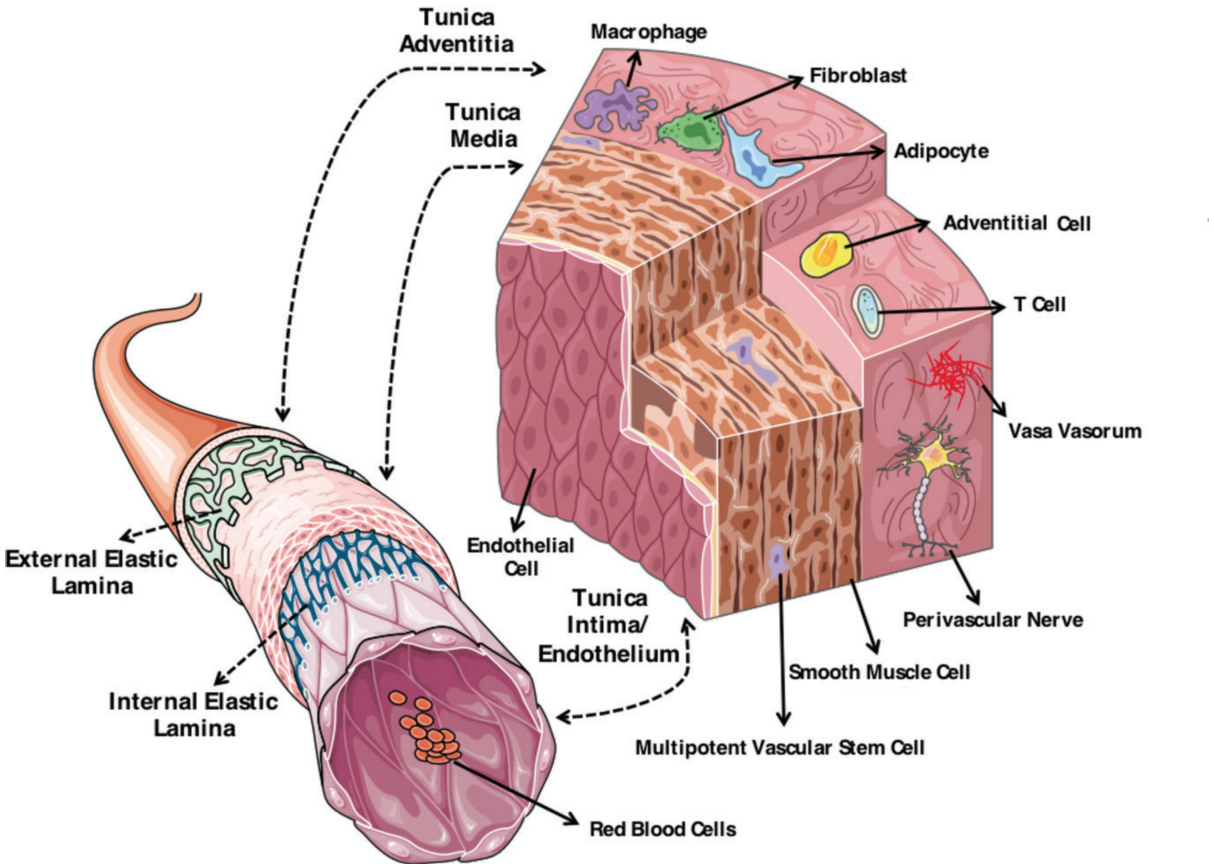

Figure 1.2: **Schematic representation of the a large blood vessel.** Schematic representation adapted from di Luca *et al.* (2018) [51], representing an artery and the different cell types present in the vessel wall, including VSMCs in the *tunica media* and adventitial cells in the *tunica adventitia*.

1.3.4 Perivascular fibroblasts

Perivascular fibroblasts are resident cells to the vessel wall able to produce a fibrotic response following injury, thus their true identity might overlap with that of the previously described PCs. They can reside in both the *tunica media* and the *tunica adventitia*, and be identified with multiple markers, shared with other PCs [52–55].

1.4 Perivascular cell markers

Whereas the identification of endothelial cells is simple, using a unique marker such as CD31, CD144, von Willebrand factor (vWF) or specific lectins, no unique marker exists for any particular type of PCs. Over the past two decades, a fairly loose spectrum of markers has been established to identify PCs, although as these overlap with other cell types they must be used in combination with markers for other cell lineages.
In situ, PCs can be easily identified using a single marker and their anatomical location with respect of the endothelium. For non-imaging techniques, proper identification of cells requires a larger combination of markers, which include at least an endothelial, a haematopoietic and a perivascular cell marker. Here are listed all major markers used to identify PCs.

Alkaline phosphatase

Alkaline phosphatase (ALP) is a group of membrane bound isoenzymes that catabolise phosphate esters located in the extracellular matrix [56]. It is found in pericytes, mainly studied in skeletal muscle [57–59]. ALP is also expressed across multiple tissues in a number of cancer cells, embryonic and induced pluripotent stem cells, thus it has been linked to stemness [60–62]. ALP is also a marker for osteoblastic differentiation [63].

αSMA

Also known as aortic or alpha smooth muscle actin, αSMA is an actin specific to smooth muscle cell lineages. As an actin, αSMA plays roles in cell motility, structure and integrity, as found in contractile pericytes [64]. αSMA is expressed in a subset of pericytes, VSMCs and is also widely used as a marker for myofibroblasts in fibrotic lesions [65].

CD13

CD13, also known as aminopeptidase N or alanyl-aminopeptidase, is an enzyme involved in the degradation of specific peptides. CD13 has been described as a pericyte marker mainly used to detect brain pericytes [66]. However, it can also be found on ECs, VSMCs and fibroblasts [45].

CD34

CD34 is a transmembrane phosphoglycoprotein, that was first described to identify haematopoietic progenitors, and since then has been used as a canonical marker of these progenitors [67]. Nevertheless, CD34 is found in multiple types of progenitor cells, ECs, keratinocytes and fibroblasts [68]. CD34 is the main marker used to identify adventitial cells, but can also identify perivascular fibroblasts [18, 47].

CD146

Also known as cell surface glycoprotein MUC18 and melanoma cell adhesion molecule, CD146 is a cell membrane glycoprotein that binds to laminins. CD146 is widely studied in cancer for its role in cell adhesion with cells and matrix and subsequent migration and proliferation [69]. CD146 is expressed by pericytes but also by ECs, VSMCs, fractions of lymphocytes and tumour cells [8, 16, 69–72].

Desmin

Desmin is an intermediate filament mostly expressed in muscle cells. Desmin can also be found in fibroblasts, pericytes, VSMCs and some astrocytes [65, 73–78].

Gli1

Gli1 is a zinc finger transcription factor first associated with glioblastomas. Gli1 is one of the most novel markers for perivascular cells and has been primarily linked to the fibrotic response after injury. Gli1 is expressed in pericytes, VSMCs, adventitial cells and perivascular fibroblasts, as well as cancer cells [48, 55].

Leptin receptor

Leptin receptor (LepR), also known as CD295 and OB-R, is a type I transmembrane glycoprotein class I cytokine receptor [79]. The ligand for LepR is leptin, an adipocyte-produced hormone linked to lipid metabolism and obesity [80]. Leptin/LepR signalling on MSCs was shown to be involved in immune homeostasis, reproduction, haematopoiesis, angiogenesis, haematological malignancies [81, 82] and bone formation [83]. LepR is expressed on pericytes surrounding sinusoids in the murine bone marrow directly supporting HSCs quiescence [43, 84]. Human pericytes in adipose tissue and bone marrow expressing LepR support engraftable HSCs [27].

PDGFRα and PDGFRβ

Platelet-derived growth factor receptor α (PDGFRα) and β (PDGFRβ), also known as CD140a and CD140b respectively, are membrane receptors of the tyrosine kinase family. They can form homodimers (α/α or β/β) or heterodimers (α/β). Each dimer will have specificity for a combination of the five known ligands. These ligands are dimers formed by combinations of PDGF-A, -B, -C or -D [85].

PDGFRα is a main marker for identifying fibroadipogenic progenitors, a particular mesodermal progenitor that has been characterised as a key player in the fibrotic response in injured muscle. These are located in perivascular areas [52], and span pericytes and VSMCs among other cell types [86].

PDGFRβ plays a key role during capillary sprouting and pericyte recruitment via PDGF-B/PDGFRβ signalling [73, 87]. PDGFRβ is one of the most used markers for pericyte identification. PDGFRβ is also expressed by VSMCs, interstitial fibroblasts and glial cells [88].

Nestin

Also known as a neuroectodermal stem cell marker, nestin is an intermediate filament protein [89]. Nestin is expressed in pericytes [90]. Nestin is also found expressed in neural stem cells, ECs, myofibroblasts and cancer cells [91–95].

NG2

Neuron-glial antigen 2 (NG2), also known as chondroitin sulphate proteoglycan 4, is a proteoglycan involved in cell proliferation and migration during vasculogenesis, binding to extracellular matrix. NG2 is one of the main markers used to identify pericytes. NG2 is specific to arteriolar pericytes, rarely found in venular vessels when undergoing remodelling [96]. NG2 is also present on macrophages, glial cells and various tumour cells, VSMCs and adventitial cells [18, 49, 96].

RGS-5

The regulator of G-protein signalling 5 (RGS-5) is a protein belonging to the RGS family, which are players in the inhibition of the downstream signalling of receptors coupled to G-proteins [97]. RGS-5 can be detected in pericytes and VSMCs, as well as ECs, tumorous cells and astrocytes [97–100]. It has been primarily linked to neovascularisation.

X-lacZ4

X-lacZ4 is not a marker but a transgenic mouse line [101]. A lacZ transgene was inserted and specifically labels some mesodermal cell lineages, including pericytes, VSMCs and muscle progenitors [45, 75, 102, 103].

Vimentin

Vimentin is an intermediate filament primarily identified in muscle cells. Vimentin is expressed on ECs, pericytes, VSMCs and myofibroblasts [104, 105].

3G5

3G5 is the name of a monoclonal antibody that detects the 3G5 cell surface ganglioside antigen. 3G5 is expressed on pericytes, as well as neurons, pancreas islet cells, thyroid follicular cells and mast cells [106–109].

This extensive selection of markers used in the identification of perivascular cells above listed and below summarised (Table 1.1) is just an indicator on how vastly heterogeneous and complex the perivascular component is.

Only a few of these markers are used simultaneously in published studies to identify perivascular cell populations of interest. This can be appreciated on Table 1.2, where the PCs markers used in 68 different studies were identified. Even then, the majority of published works use a single PCs marker for isolation, while showing co-expression of one or two other PCs markers as a validation method for their specific population. Common PCs validation markers are PDGFRβ and NG2, while CD34 is used as endothelial and haematopoietic, and αSMA as a fibroblast marker.

Table 1.1: **Markers used in the identification of perivascular cells.** Markers listed are used to positively (+) or negatively (-) identify the following cell types composing the vasculature. When labelling cells for FACS, three markers are at least required: an endothelial and haematopoietic marker to exclude those cell lineages and a perivascular one for positive selection. When sorting from skeletal muscle, a myogenic progenitor marker should also be added to exclude that lineage.

Marker	**EC**	**Pericyte**	**VSMC**	**Adv cell**	**Fibroblast**	**Lineages**	Reference
CD31	+	-	-	-	-		[110]
CD144	+	-	-	-	-		[111]
vWF	+	-	-	-	-		[110, 112]
Lectins	+	-	-	-	-		[113]
CD45	-	-	-	-	-	Haematopoietic	[114]
CD56	-	-	-	-	-	Myogenic	[115, 116]
ALP	-	+	+	-	-		[57–59]
αSMA	-	+	+	-	+		[65]
CD13	+	+	+	-	+		[45]
CD34	+	-	-	+	+		[18, 47, 110]
CD146	+	+	+	-	-		[16, 72]
Desmin	-	+	+	-	+		[65, 73]
Gli1	-	+	+	-	+		[48, 55]
LepR	-	+	+	+	-		[43, 84]
PDGFRα	-	+	+	-	+		[86]
PDGFRβ	-	+	+	-	+		[73, 88]
Nestin	+	+	+	-	+		[90, 93, 94]
NG2	-	+	+	+	+		[18, 49, 96]
RGS-5	-	+	+	-	-		[98]
Vimentin	+	+	+	-	+		[104, 105]
X-lacZ4	-	+	+	-	-		[75, 102]
3G5	-	+	-	-	-		[106]

Table 1.2: **Summary of the markers used for the identification of perivascular cells in 68 different studies.** Presence of the perivascular markers (+) was noted in 68 published studies, by either immunohisto or cytochemistry, flow cytometry, qPCR or protein level quantification methods.

Reference	Year	ALP	αSMA	CD13	CD34	CD146	Desmin	Gli1	LepR	PDGFRβ	PDGFRα	Nestin	NG2	RGS-5	Vimentin	X-lacZ4	3G5
[104]	1987						+								+		
[117]	1988	+															
[106]	1988																+
[64]	1991		+														
[118]	1992		+				+										
[66]	1994			+													
[70]	1994					+											
[119]	1997									+							
[107]	1998		+														+
[73]	1999		+				+			+							
[108]	2001		+														+
[102]	2001		+							+	+					+	
[101]	2001															+	
[98]	2003		+				+			+			+	+			
[120]	2003									+				+			
[75]	2003		+				+			+	+		+			+	
[65]	2004		+				+										
[15]	2004		+														+
[97]	2005		+			+	+			+				+			
[74]	2005		+				+			+			+				
[14]	2006		+	+	+												
[77]	2006						+								+		
[96]	2006		+										+				

Table 1.2 – continued from previous page

Reference	Year	ALP	αSMA	CD13	CD34	CD146	Desmin	Gli1	LepR	PDGFRβ	PDGFRα	Nestin	NG2	RGS-5	Vimentin	X-lacZ4	3G5
[57]	2007	+	+	+	+	+	+			+			+				
[8]	2007	+			+	+				+							
[72]	2008			+	+	+				+			+				
[16]	2008	+	+	+	+	+				+			+				
[109]	2008		+				+										+
[17]	2008		+		+					+							
[53]	2008		+		+		+			+			+				
[121]	2008									+						+	
[122]	2008		+		+			+		+							
[86]	2009				+	+				+	+						
[45]	2010			+						+						+	
[76]	2010						+			+			+				
[18]	2010		+	+	+	+	+			+		+	+		+		
[52]	2010		+		+						+						
[88]	2011		+							+			+	+		+	
[58]	2011				+		+			+	+						
[71]	2011		+		+	+				+		+					
[47]	2012		+		+	+				+			+		+		
[123]	2012		+		+	+				+		+	+				
[43]	2012	+							+	+	+	+					
[24]	2012				+	+											
[124]	2012				+	+											
[125]	2012	+	+										+				
[103]	2012											+				+	
[90]	2013				+	+				+	+	+	+				
[28]	2013				+	+				+							

Table 1.2 – continued from previous page

Reference	Year	ALP	αSMA	CD13	CD34	CD146	Desmin	Gli1	LepR	PDGFRβ	PDGFRα	Nestin	NG2	RGS-5	Vimentin	X-lacZ4	3G5
[27]	2013		+		+	+			+			+	+				
[42]	2013		+						+			+	+				
[126]	2013		+		+					+			+				
[127]	2013		+	+						+	+	+	+				
[49]	2013		+			+				+			+				
[128]	2014									+		+	+				
[129]	2014	+	+		+	+	+			+	+		+		+		
[130]	2014		+		+	+		+		+			+				
[84]	2014								+	+	+						
[55]	2015		+		+	+		+		+	+	+	+				+
[131]	2015		+			+				+							
[132]	2015		+				+			+			+				
[133]	2015		+							+	+		+				
[134]	2016		+	+			+			+			+	+			
[48]	2016				+			+		+					+		+
[100]	2016		+											+			
[31]	2016		+		+	+				+			+				
[135]	2017		+	+						+			+	+			
[78]	2018		+	+		+	+			+			+				

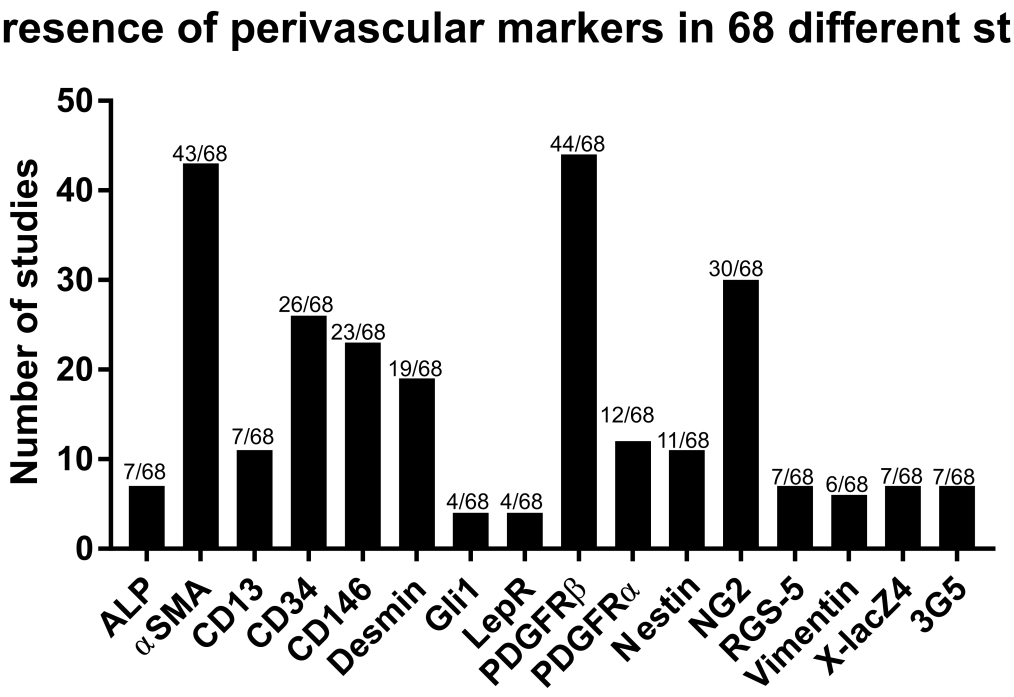

Figure 1.3: **Summary of the markers used for the identification of perivascular cells in 68 different studies.** Presence of the perivascular markers was noted in the 68 published studies examined on Table 1.2, by either immunohisto or cytochemistry, flow cytometry, qPCR or protein level quantification methods.

1.4.1 Reporter mice

Multiple mouse reporter lines have been generated to exploit PCs markers, some of which are summarised in Table 1.3. These mouse lines have been used to isolate cells and do cell lineage tracing to understand further the origin and potential of the labelled cells.

1.4.2 Perivascular cell markers are homogeneous across species

PCs markers are homogeneous across multiple animal species. So far, other than human, mouse and rat, studies have been performed on dog [141], sheep [142], horse [143, 144] and fish.

Table 1.3: Example of some reporter mice used in the identification of PCs.

Marker	Reporter mice	References
αSMA	αSMA-Cre	[126]
	αSMA-CreER	[126]
	αSMA-mCherry	[136]
	αSMA-RFP	[136]
	αSMA-tk	[126]
Collagen1a1	Coll-GFP	[53, 137, 138]
Gli1	Gli1-CreER	[48]
LepR	LepR-Cre	[43]
Nestin	Nestin-GFP	[43, 139]
NG2	NG2-Cre	[126]
	NG2-dsRed	[90]
	NG2-mTmG	[136]
PDGFRα	PDGFRαn-GFP	[133]
PDGFRβ	PDGFRβ-eGFP	[134]
	PDGFRβ-mTmG	[140]
	PDGFRβ-tk	[126]
	PDGFRβ-YFP	[126]
RGS-5	RGS-5-GFP	[132]
XlacZ4	XlacZ4	[101]

1.5 The role of perivascular cells during development

1.5.1 Ontogeny

Perivascular cells have their origin from multiple sources. In general, head and thymus perivascular cells are believed to originate from the neural crest [145], thus derived from the ”mesectoderm”, while others derive from the mesothelium, thus the mesoderm. Most tissues form from multiple origins e.g. the aorta originates from neural crest, somites, secondary heart field and the splanchnic mesoderm [46,121,146–148]. In addition, some perivascular cells might transdifferentiate from endothelial cells following epithelial-to-mesenchymal transition.

As to the origin of pericytes and VSMCs, some works suggest that pericytes differentiate into the VSMCs, while this matter will be difficult to investigate as long as clear differences between these two cell types have not been established [133]. Most re-

cently it has also been suggested that adventitial cells are more primitive and can differentiate into both pericytes and VSMCs [48, 50].

1.5.2 Meso-angioblasts

Haemangioblasts are cells that during development can generate haematopoietic and endothelial cell lineages. Following this definition, the existence of a similar cell type has been proposed that would give rise to mesodermal and endothelial cell lineages: the meso-angioblast [149]. Experiments performed injecting quail dorsal aorta cells into chick embryos showed chimerism and integration of the injected cells into multiple tissues and later developing into the expected tissue, including bone and muscle. Interestingly, these meso-angioblasts, originating from the wall of the aorta, also integrated into the recipient vessel walls, both into large and smaller vessels. These progenitor cells can also be found post-natally in the vessel wall, expressing CD34 and Sca1 [149–153].

1.5.3 Blood vessel formation

Formation of new blood vessels requires interaction between ECs and pericytes. This occurs via multiple signalling pathways leading to multiple bonds formed between the two cell types involving peg-and-socket, gap junctions, cadherins and other adhesion molecules.

The most studied signalling pathway in blood vessel formation involves PDGF-B/PDGFRβ. Angiogenic ECs secrete PDGF-BB which binds into the extracellular matrix, forming a concentration gradient. Pericytes expressing PDGFRβ are attracted to the ECs then establish bonds and form new blood vessels [154]. This mechanism is supported by TGFβ, angiopoietin-1/Tie2, HB-EGF/EGFR, SDF-1α/CXCR4, Shh and Notch [46, 148,

155].

The involvement of pericytes in angiogenesis is also relevant in tumorous growth. It has been suggested that a number of tumours can only develop with a key contribution of the neovascularisation promoted by pathological pericytes.

1.6 Perivascular cell role in homeostasis

1.6.1 Vascular support

The main function of the perivascular cells is to provide structure, resistance and integrity to the blood vessel. The VSMCs provide elastic force to resist the blood pressure in arteries and arterioles. Together with pericytes they provide contractility to control blood flow on smaller vessels [136, 156–158].

Perivascular coverage of the blood vessels differs between tissues. A lower coverage translates into a more permeable blood vessel. The nervous system vasculature is the most covered, at a 1-3 EC per 1 pericyte ratio, similarly to the retina. Intermediate coverages can be found in the kidneys at a 5:2 EC:pericyte ratio. Coverage is among the lowest at a 100:1 EC:pericyte ratio in the skeletal muscle [148, 159].

1.6.2 Perivascular cell specialisation

As blood vessels adapt to satisfy the needs of the organ they vascularise, some PCs can acquire more unique features and are relevant to mention.

Blood brain barrier

Brain pericytes, although similar in many features, seem to respond differently to cell signalling thus making them unique to the rest of the body [148]. Blood vessels in the brain have an additional layer composed by astrocyte prolongations. The astrocytes are tightly bound to the pericytes via multiple junctions and adhesion molecules. Alterations in either the interaction between pericytes with endothelial cells or astrocytes can increase the permeability of the vessels leading to pathological conditions [45].

Mesangial cells

Mesangial cells are specialised pericytes located exclusively in renal glomeruli. Mesangial cells play a role in the filtration capabilities of the kidneys, by regulating blood flow and their contribution to tissue response to injury. Together with renal VSMCs, they are believed to originate from a common PDGFRβ^+ ancestor [53, 85, 119, 157, 160]. Recently, it has been documented that mesangial cells produce renin, a key player in the renin-angiotensin system that regulates blood pressure [31].

Hepatic stellated cells

Hepatic stellated cells as specialised liver pericytes, also known as Ito cells. They reside in the subendotheial space of Disse, a compartment between sinusoidal ECs and parenchymal cells. They were first described in 1876 by Carl von Kupffer as stellated cells, then again in 1952 by Toshito Ito as perisinusoidal fat storing cells particularly rich in vitamin A [161, Chapter 9]. Hepatic stellated cells share many pericyte markers, including PDGFRβ, αSMA, vimentin or desmin, while possessing unique ones such as GFAP (glial fibrillary acidic protein), p75 (nerve growth factor receptor) or LRAT (lecithin-rethinol acyltransferase) [162].

Hepatic stellated cells are suggested to originate from both mesoderm and neural

crest. They have exhibited some degree of regenerative potential by differentiating into hepatocytes following partial hepatectomy. Nevertheless, they have been primarily linked to fibrosis as main producer of collagen following injury [161, Chapter 9]. Hepatic stellated cells transdifferentiate into myofibroblasts, mediated by multiple signalling pathways TGFβ, PDGF and CTGF (connective tissue growth factor) [163, 164].

1.6.3 Native response to tissue injury

PCs have shown the ability to generate multiple mesodermal tissues both *in vitro* and when injected *in vivo*. Their native response upon tissue injury is not that clear. There are indications of a role of perivascular cells, notably pericytes, in tissue regeneration, by direct differentiation or release of protective molecules [59, 165].

A significant amount of independent studies support the involvement of PCs in the fibrotic response, while some still reject it [126]. Fibrosis is characterised by the deposition of proteins into the ECM, particularly collagen I and III, resulting in pathological conditions. Myofibroblasts involved in tissue fibrosis can originate from resident myofibroblast progenitors, epithelial cells undergoing epithelial-to-mesenchymal transition, endothelial cells undergoing endothelial-to-mesenchymal transition, and circulating fibrogenic cells [166]. While there are multiple resident myofibroblast progenitors, all studies indicate a perivascular involvement.

Upon injury, massive expansion of PDGFRβ^+, PDGFRα^+ and NG2$^+$ takes place within fibrotic depositions, also expressing collagen1a1 and αSMA thus identifying them as myofibroblasts. TGFβ1, secreted by epithelial cells, induces the later production of PDGF-B. PDGFRβ^+ PCs detach from the vessel wall and differentiate into myofibroblasts. Inhibition of TGFβ1, PDGFRβ, VEGFR2 lead to a significant reduction of myofibroblasts and fibrotic response [53, 54, 167]. The majority of these cells have been identified to descend from a population of FoxD1$^+$ cells in lung and kidney, as the main source of myofibroblasts [138, 160]. In skeletal muscle and dermis, ADAM12, a metalloprotease involved with TGFβ has been identified as a transient marker for a

cell population that will generate over half of the myofibroblasts present after injury. Blockage of ADAM12 not only reduced the amount of myofibroblasts generated but increased the expression of regenerative genes Igf1 and Igf2, while ablation of the ADAM12$^+$ cells lead to a fully healed tissue. Gli1 was identified in lung, bone marrow, kidney, heart, liver and skeletal muscle, as a marker for myofibroblast progenitors, residing in the perivascular area [48, 55, 140]. Proper identification of the exact cell populations would enable successful pharmacological approach [137, 159, 168].

While it is clear that PCs are involved in this pathologic response, the heterogeneity within the PCs compartment is highlighted. ADAM12$^+$ cells represent less than 1% of the total stromal cells 4 days following injury, FoxD1-derived less than 8% and Gli1 expression ranged 0.01-0.17% of the stromal cells in the tissues screened. These populations produced the majority of endogenous fibrogenesis, while not all of it indicating other mesenchymal cells are involved in the response [55, 138, 169]. In fact, within the known PCs, subpopulations based on their fibrotic response can be identified. In spinal cord injury, type A pericytes expressing Glast, representing 10% of the total pericytes, detach from the blood vessels, change their phenotype into a more myofibroblastic state and produce ECM, while the rest of pericytes, type B, remain attached [170]. In skeletal muscle, type I pericytes, NG2$^+$nestin$^-$, produce a fibrogenic response, while type II pericytes, NG2$^+$nestin$^+$ exhibit a more myogenic profile [90, 171].

1.7 Hypothesis and aims

The above review of the literature indicates that the perivascular cell compartment is insufficiently characterised. Heterogeneity must be investigated to elucidate the potential of the different subsets of PCs. This work explores subtypes of two well established populations of perivascular cells, first described in our group, CD146$^+$CD34$^-$CD31$^-$CD45$^-$CD56$^-$ pericytes and CD34$^+$CD146$^-$CD31$^-$CD45$^-$CD56$^-$ adventitial cells, basing the sub-

types examined on three major combinations of markers:

- Leptin receptor
- NG2 and αSMA
- PDGFRβ and PDGFRα

The general hypothesis of this thesis is that functionally distinct of perivascular cells exit within the currently characterised perivacular populations.
For each group of subtypes, the general aims are to:

1. Characterise the *in situ* localisation of perivascular cell subsets.
2. Isolate perivascular cell subtypes using flow cytometry.
3. Assess functional differences between sorted subtypes *in vitro*.

Chapter 2

GENERAL METHODS

2.1 Tissue procurement

2.1.1 Human foetal tissues

Human foetal tissue samples were procured after elective surgical abortion, with full ethics permission of the NHS Lothian Research Ethics Committee (REC 08/S1101/1). Foetal samples were from 9 to 20 weeks of gestation. Samples were dissected 4-48h post intervention, and harvested tissues where stored in 2% (v/v) foetal calf serum (FCS, Life Science Production) in phosphate buffered saline (PBS, Sigma Life Sciences) at 4°C until use for up to 24h.

2.1.2 Human adult tissues

Adipose tissue was collected following informed consent from patients undergoing liposuction or abdominoplasty for cosmetic purposes, from the Murrayfield and Shawfair Park hospital, Edinburgh, UK. Samples were stored as provided for a maximum period of 24h.

Adult femoral heads were obtained following informed consent from patients under-

going hip replacement surgeries, and kindly provided by Dr. Iain Murray and Prof. Hamish Simpson. Samples were stored in 1% (v/v) penicillin/streptomycin (P/S, Invitrogen) in PBS at 4°C until use, up to 24h.

Number of samples are summarised in Table 2.1.

Table 2.1: Human tissues used.

Tissue	Type	Label	n Number
Bone Marrow	Foetal	FBM	9
Bone Marrow	Adult	ABM	6
Skeletal Muscle	Foetal	SkM	13
Heart	Foetal	H	19
White adipose tissue	Adult	ADP	5

2.1.3 PDGFRβ reporter mice

Pbag transgenic mice expressing enhanced green fluorescent protein (eGFP) under the PDGFRβ promotor, genotype tg(PDGFRβ-eGFP)JN169Gsat/Mmucd, were kindly provided by Dr. Phoebe Kirkwood from Dr. Philippa Saunders' laboratory, Centre for Inflammation Research, University of Edinburgh.

Number of samples are summarised in Table 2.2.

Table 2.2: Murine tissues used.

Mouse line	Reporter	Tissue
Pbag	PDGFRβ-GFP	Heart
Pbag	PDGFRβ-GFP	Skeletal muscle
WT	-	Heart
WT	-	Skeletal muscle

2.1.4 Porcine tissues

Samples were kindly donated by Dr. Montserrat Rigol, from the IDIBAPS-Hospital Clinic in Barcelona, Catalonia. Pigs aged 2 months underwent acute myocardial infarction under local regulations. Cardiac infarcted and non-infarcted areas where dissected and snap frozen. Tissues were transported to Edinburgh, where samples were sectioned and further processed.
Fresh adipose and cardiac samples were provided by Dr. Cristina Esteves, from the Roslin Institute, University of Edinburgh.

2.2 Flow cytometry and cell sorting

2.2.1 Cell isolation

Human foetal and murine soft tissue

Tissue was washed 3 times in PBS and transferred into a petri dish. Tissue was dissected according to organ and size. When possible, a piece of the tissue was preserved for histological analysis (see section 2.4). Tissue was transferred into a petri dish containing 5mL of high-glucose Dulbecco's modified Eagle medium with Glutamax (DMEM, Gibco) and mechanically minced, using scissors or scalpels, into pieces (max. 0.5cm). Minced tissue was transferred into a sterile container with the working digestion medium.

Human foetal bone marrow

Limbs were washed by immersion 3 times in PBS and transferred into a petri dish. Skin was removed and discarded. Bones were dissected out by cutting the ligaments, then

processed as mentioned in above for foetal tissues. Long bones were gently scraped using a scalpel to remove remaining muscle. Cartilage surrounding the epiphysis was removed with a scalpel and bone marrow exposed. Long bones were transferred into a petri dish containing 5mL of DMEM, and cut open longitudinally, exposing the bone marrow. If required, one of the long bones was cut transversally and one of the halves was kept for histology. Marrow was gently flushed out using the DMEM present in the petri dish and a pipette. Medium and bones were transferred into a container with the standard digestion mix containing 0.5mg/mL of collagenase I, collagenase II and collagenase IV (all from Gibco), and incubated for 45-60min in a shaking water bath at 37°C.

Human adult bone marrow

The external area of the femoral head was dried with sterile gauzes. Holding the femoral head by hand with the help of gauzes, the marrow exposed on the cut site was scooped out using a metal spoon and transferred into a container with DMEM. The femoral head was then wrapped in multiple gauzes and put into a sterile durable bag. Using a hammer, the femoral head was cracked open. Carefully, with the aid of forceps and a bone clipper, pieces of trabecular bone (1cm) containing marrow were transferred into the container where the scooped marrow was transferred.

Enzymatic digestion

Tissues in the container were covered with a digestion mix containing 0.5mg/mL of collagenase I, collagenase II and collagenase IV (all from Gibco), and incubated for 45-60min in a shaking water bath at 37°C. The digestion solution for soft tissues was supplemented with 0.125mg/mL of DNAse I (Roche).

After digestion, the digestion medium and remaining tissues are poured through 500μm, 100μm, 70μm and 40μm cell strainers (Greiner Bio-one) placed on top of 50mL cen-

trifuge tubes, with one wash using 5mL of FACS buffer (2%FCS,PBS) per tube to collect remaining cells. Bones were cleaned by adding 5mL of FACS buffer and vortexed for 1min at least twice. The isolated cell suspension was centrifuged at 300rcf for 5min at RT. Supernatant was discarded and pellet was re-suspended in 2-6mL of hybri-max red blood cell lysis buffer (RBC, Sigma-Aldrich), depending on the size and redness of the pellet, and incubated up to 10min at RT. FACS buffer was added up to 45mL of cell suspension, gently mixed by inversion to dilute RBC and centrifuged at 300rcf for 5min at RT. Pellet was re-suspended in 0.5-2.5mL, depending on the pellet size, in FACS buffer.

Adult adipose tissue

White subcutaneous fat was dissected out using forceps and a scalpel, carefully avoiding blood clots, large blood vessels with coagulated blood and large connective areas. With scalpels and scissors, fat was minced and transferred into a container. Final volume of 100-200mL of minced fat was digested with 0.5mg/mL collagenase II in DMEM for 60min in a shaking water bath at 37°C.

After digestion, all of the solution was transferred into 50mL centrifuge tubes and centrifuged at 300rcf for 5min at RT. Three layers formed in the tube, with a top layer containing undigested adipose tissue and oil, a medium aqueous phase and a lower cell pellet. Carefully, the top layer was removed by decantation. Pellet was re-suspended using the supernatant and centrifuged again using the same conditions. The remaining oil and supernatant were removed by aspiration, and pellets re-suspended in FACS buffer. Cell suspensions were merged and centrifuged using the same conditions. Supernatant was discarded and pellet was re-suspended in 5-10mL of FACS buffer. Cell suspension was poured through 500μm, 100μm, 70μm and 40μm cell strainers (Greiner Bio-one) placed on top of 50mL centrifuge tubes, with one wash using 5mL of FACS buffer (2%FCS,PBS) per tube to collect remaining cells. The isolated cell

suspension was centrifuged at 300rcf for 5min at RT. Supernatant was discarded and pellet was re-suspended in 2-6mL of hybri-max red blood cell lysis buffer (RBC, Sigma-Aldrich), depending on the size and redness of the pellet, and incubated up to 10min at RT. FACS buffer was added up to 45mL of cell suspension, gently mixed by inversion to dilute the RBC and centrifuged at 300rcf for 5min at RT. Pellet was re-suspended in 0.5-2.5mL to the pellet size in FACS buffer.

2.2.2 Unsorted cells as classical MSC

Mechanical and enzymatic dissociation of cells is sufficient to isolate MSCs progenitors, while remaining unpurified [172, 173]. Cultures established from unsorted cell plating from the final cell suspension as obtained as described above were considered classical MSCs.

2.2.3 Cellular cell surface antibody labelling

Single cells were re-suspended in the appropriate volume of FACS buffer and incubated for at least 10min at 4°C. Cell suspension was split in the required number of tubes, with a minimum volume of 50μL per tube. Cells were labelled by addition of the antibodies into the tubes as detailed in Table 2.3, and with the appropriate isotypes as detailed in Table 2.4 in the same concentration as the specific antibody. Cells were incubated for 30min in the dark at 4°C. After the incubation, 200-300μL of FACS buffer was added to each tube and tubes were centrifuged at 300rcf for 6min at RT. Supernatant was discarded by decantation and washing was repeated. Pellet was resuspended in a final volume of 300μL of FACS buffer and cell suspension was transferred into a new tube after passing through a 40μm strainer cap. Cells were kept on ice until analysis. 5 min prior to analysis, dead cells were stained using DAPI at 0.1 mg/mL. DAPI penetrates the cell membrane of dead or dying cells, binding to the DNA

thus labelling non-viable cells.

In order to properly calibrate the cytometer, tubes labelled with a single fluorochrome-conjugated antibodies were required. These single stain controls were prepared by using BD CompBead Plus anti-mouse Ig (BD Biosciences, 51-9006274) following the same staining protocol.

Table 2.3: Flow cytometry antibodies used against human cell surface antigens. ms=Mouse

Antigen	Fluorochrome	Species	Dilution	Company&Catalog number
CD31	V450	ms	1:400	BD Horizon 561653
CD34	BV605	ms	1:100	Biolegend 343530
CD34	FITC	ms	1:100	BD Pharmingen 555821
CD34	PE	ms	1:100	BD Pharmingen 555822
CD45	V450	ms	1:400	BD Horizon 560368
CD56	V450	ms	1:400	BD Horizon 560360
CD146	BV711	ms	1:100	BD Horizon 563186
NG2	FITC	ms	1:100	Millipore AB5320A4
PDGFRβ	APC	ms	1:100	Biolegend 323608
PDGFRα	PE/Cy7	ms	1:300	Biolegend 323508
LepR	AF647	ms	1:300	BD Pharmingen 564376

Table 2.4: Flow cytometry isotype controls. Used at same dilutions as the primary antibodies.

IgG	Fluorochrome	Company&Catalog number
mouse IgG1	V450	BD Horizon 560373
mouse IgG1	BV711	BD Horizon 563044
mouse IgG1	BV605	Biolegend 400162
mouse IgG1	FITC	BD Pharmingen 555748
mouse IgG1	APC	BD Pharmingen 555751
mouse IgG1	PE	BD Pharmingen 555574
mouse IgG1	PE/Cy7	BD Pharmingen 557872

2.2.4 Intracellular antibody cell labelling

Single cells were re-suspended in the appropriate volume of FACS buffer and incubated for at least 10min at 4°C. Cell suspension was split in the required number of tubes, with a minimum volume of 50μL per tube. Cells were incubated with the live/death e780 for 30min on ice in the dark. 300μL of FACS buffer was added and tubes centrifuged for 7min at 350rcf at 4°C. Supernatant was discarded and cells re-suspended in 100μL of FACS buffer. Cell surface labelling was performed as explained above. 300μL of FACS buffer was added and tubes centrifuged for 7min at 350rcf at 4°C and supernatant discarded. Cells were resuspended in 100μL of FACS buffer. 100μL of fixation buffer was added (eBioscience fix and perm kit), tubes were gently mixed and incubated for 45min at RT in the dark. Tubes were centrifuged at 600rcf for 5min and supernatant discarded. Cells were resuspended in 200μL of ice-cold absolute methanol, gently mixed and incubated for 40min on ice in the dark. 300μL of FACS buffer was added and tubes centrifuged for 7min at 600rcf and supernatant discarded. Cells were resuspended in 100μL of FACS buffer. Intracellular labelling was performed by adding the antibody at the appropriate dilution and incubating the tubes for 60min on ice in the dark. After the incubation, 200-300μL of FACS buffer was added to each tube and tubes were centrifuged at 600rcf for 6min at RT. Supernatant was discarded by decanting it off the pellet; this wash was then repeated. Pellet was resuspended in a final volume of 300μL of FACS buffer and the cell suspension was transferred into a new tube after passing through a 40μm strainer cap. Cells were kept on ice until analysis.

Table 2.5: Flow cytometry dyes used for human intracellular labelling. ms=Mouse

Antigen	Fluorochrome	Species	Dilution	Company&Catalog number
αSMA	APC	ms	1:200	R&D systems IC1420A
Dead cells	DAPI	/	1:1000	Invitrogen
Dead cells	eFluor780	/	1:1000	eBioscience 65-0865-14

2.2.5 Flow analysis

Cell suspensions were analysed using a BD LSR Fortessa (5 lasers) analyser and the BD FACS Diva v8 software (BD Biosciences), managed by the CRM Flow Cytometry facility.

Voltages were calibrated using unlabelled cell suspensions with the negative peak set over 10^2 units of intensity and checking positive peaks are within the acquisition range using fully stained samples. Compensations were calculated and applied using the software tools using single stained samples (5,000 events recorded when using beads, 10^5 when using cells), and manually checked.

Most common analysis consisted in selecting cells on a side scatter area (SSC-A) vs. forward scatter area (FSC-A) plot, then excluding doublets using a FSC-A and forward scatter height (FSC-H), followed by a dead and lineage positive cells (endothelial, haematopoeitic and myogenic) exclusion. The remaining cells were analysed using a combination of known perivascular cell and novel markers.

2.2.6 Cell sorting

Human cell sorting was performed using a BD FACS Aria III Fusion (BD Biosciences), managed by Fiona Rossi from the CRM Flow Cytometry facility, using the same antibody combination as per the analysis. Mouse cell sorting was performed using a BD FACS Aria II (BD Biosciences), managed by Dr. Claire Cryer from the CRM Flow Cytometry facility. Cells were sorted into microcentrifuge tubes or polyethylene FACS tubes, containing EGM-2 medium. Immunophenotypes corresponding to the total populations sorted are detailed in Table 2.6. Human pericytes were isolated based on CD146 as shown by Crisan *et al.* [16] as the CD146 antibodies were more proficient than the PDGFRβ. Murine pericytes were isolated based on PDGFRβ using a reporter mouse model.

Table 2.6: Sorted immunophenotypes.

Cell population	**Species**	**Immunophenotype**	**Subpopulations**
Adventitial cells	Human	$CD34^{+}CD146^{-}CD31^{-}CD45^{-}CD56^{-}$	$LepR^{+/-}$
Pericytes	Human	$CD146^{+}CD34^{-}CD31^{-}CD45^{-}CD56^{-}$	$LepR^{+/-}$ $NG2^{+/-}\alpha SMA^{+/-}$ $NG2^{+/-}$ $PDGFR\beta^{+/-}PDGFR\alpha^{+/-}$
Pericytes	Mouse WT	$PDGFR\beta^{+}$	$PDGFR\alpha^{+/-}$
Pericytes	Mouse Pbag	$PDGFR\beta$-GFP^{+}	$PDGFR\alpha^{+/-}$
Classical MSC	Human, Mouse	unsorted	-

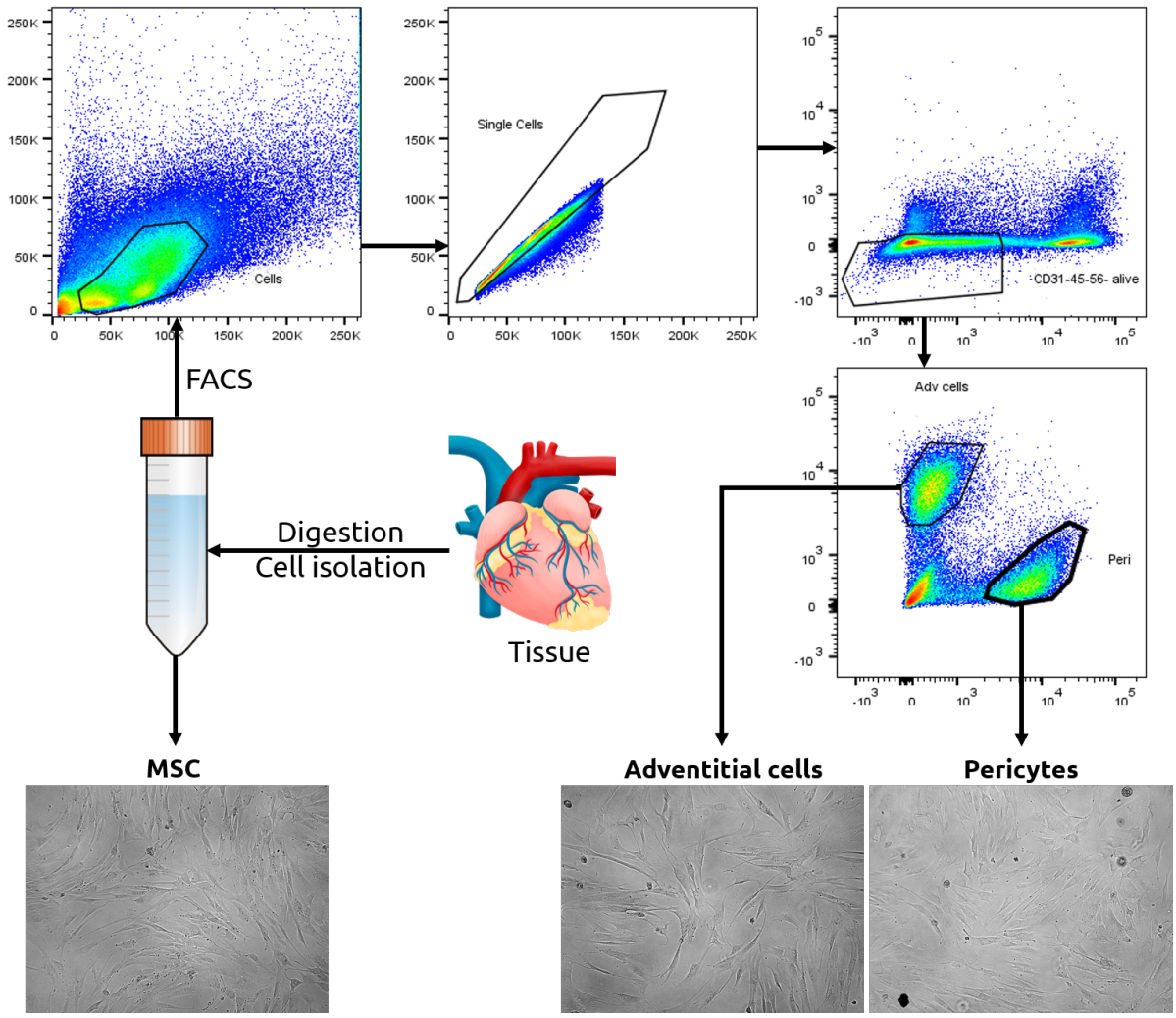

Figure 2.1: **Schematic representation of the method to isolate pericytes, adventitial cells and unsorted classical MSCs.** Sorting strategy to sort $CD146^{+}CD34^{-}CD31^{-}CD45^{-}CD56^{-}$ periytes and $CD34^{+}CD146^{-}CD31^{-}CD45^{-}CD56^{-}$ adventitial cells by FACS, and unsorted classical MSCs.

2.3 Cell culture

2.3.1 Primary culture and cell line establishment

Standard culture conditions

All cells were incubated at 37°C and 5% CO_2 on non-treated tissue culture plastic (Corning) in a humidified atmosphere. Unless stated otherwise, cells were cultured in

standard growth medium (SGM, 20%FCS,1%P/S,DMEM).
Initial passages were used to establish cell lines (P0-3), and intermediate ones were used to expand the cell lines and generate cell banks for additional assays (P2-4).

Perivascular cells

Sorted murine and human perivascular cells were plated on 0.2% (w/v) gelatin coated plates at a density of 20,000 cells/cm^2 in EGM-2. Gelatin coating was performed for 20min at 4°C, with excess of gelatin removed prior to seeding. Medium was refreshed twice a week until near confluence. Cells were trypsinised and transferred onto a new plate with SGM. Cells were expanded into bigger plates and a line was considered established when plated for the first time on a flask.

Mesenchymal stromal cells

Classical MSC lines were established by plating freshly isolated cells in a T75 flask with SGM. When near confluence, cells were trypsinised and passaged using a 1/10 dilution into new flasks.

2.3.2 Cell line maintenance

Maintenance

All cell lines had their medium replaced twice a week until near confluence. Cells were trypsinised using 0.25% (v/v) EDTA-trypsin (Life Technologies) for 5min at 37°C. Trypsin was neutralised by adding the same volume of SGM. Cells were plated in a new flask at a 1/10 dilution, and kept in culture for a maximum of seven passages from

initial seeding.

Cryopreservation

Cells were trypsinised. Once trypsin was neutralised, 13μL of cell suspension was mixed with the same volume of 0.4% trypan blue (BioRad), and cells were counted using a haemocytometer. Cell suspension was centrifuged at 300rcf (relative centrifugal force) for 5 min. Cells were resuspended at 10^6cells/mL in the appropriate volume of freezing medium (10% (v/v) dimethyl sulfoxide (DMSO) in FCS). Cells were transferred in the appropriate number of cryovials (Corning) with 1mL of cell suspension per vial. Immediately, vials were frozen using a Mr. Frosty freezing container (Thermo Scientific) and placed at -80°C. After 24-48h vials were removed from the container and placed into a cryogenic box and stored at -80°C over the short term or in a liquid nitrogen tank over the long term.

Thawing

Frozen vials were warmed up in a water bath until most of the cell suspension was defrosted. The cell suspension was transferred into a 15mL centrifuge tube containing 10mL of SGM. The cryovial was washed twice with 1mL of SGM and added to the centrifuge tube to collect any remaining cell in the cryovial. The tube was centrifuged at 300rcf for 5 min and supernatant was discarded. Cells were resuspended in 10mL of SGM and the whole content was plated into a T75 flask. 24h later, medium was removed, cells washed twice using 5mL of PBS and fresh medium was added. Cells were then passaged as described earlier.

2.3.3 *In vitro* assays

As cell lines are constantly modified in culture, by selection of the cells with high proliferative potential, all *in vitro* assays were performed at similar passage time (P5-6).

Colony forming unit-fibroblast assay

The colony forming unit-fibroblast assay (CFU-f) aims to assess the clonogenic potential of single cells within an MSC-like cell population. Parameters measured are number and size of the colonies formed.
Cells were trypsinised and counted. At least 4 wells of a 6-well plate were seeded with 50, 100 and 500 cells in SGM per well. Cells were incubated for 14d. Plates were washed twice with PBS and cells fixed with ice cold methanol (vWR Chemicals) for 10min. Immediately after, colonies were stained using 0.5% (w/v) crystal violet (Sigma-Aldrich) in 25% (v/v) methanol for 10min at RT. Wells were washed at least 3 times with distilled water until clear and plates were left inverted to dry at RT. Plates were scanned using a Celigo imaging cytometer (Celigo Inc), and colonies manually counted using Fiji/ImageJ software.

Growing chart

The growing chart assay aims to assess the proliferative capacity of a particular cell population. Cell lines grow at an exponential rate until reaching a plateau, allowing to quantify the maximum number of cells and doubling time.
Cells were trypsinised and counted. Two 12-well plates were seeded with 25,000cells/well in SGM. Every two days starting from day 4, 3 wells were trypsinised individually and cells counted, up to d18. Medium was changed every 2-3d.
Doubling time was extracted from the exponential phase of growth using the following

equation:

$$DT = \frac{DaysOfIncubation * log(2)}{log(FinalCellCount) - log(InitialCellCount)} \tag{2.1}$$

Osteogenic differentiation assay

The osteogenic differentiation assay aims to assess whether a cell population contains cells able to produce calcium deposits in the ECM. True osteogenesis should be examined by means of bone nodule formation and supported by means of PCR for the expression of osteogenic genes ALP, RUNX2 or COL1A1 among others. Nevertheless, it is well accepted for pericytes and other perivascular cells to assess osteogenic potential *in vitro* staining differentiated cultures with Alizarin Red for calcium deposits, as shown by previous work in our lab [16].

A total of 28 wells of 4 individual 24-well plates (8 wells per time point, 4 for initial timepoint) were seeded with 40,000cells/well in 10%FCS,1%P/S,DMEM (growth medium, GM). 24h later, medium was removed and replaced with either GM or osteogenic medium (OM: GM supplemented 10mM β-glycerophosphate [Sigma-Aldrich], 0.1μM dexamethasone [Sigma-Aldrich] and 50μM L-ascorbic acid [Sigma-Aldrich]). Medium was replaced twice a week. Plates were collected at days 0, 7, 14 and 21. Phase contrast images were acquired on a Zeiss Observer microscope. Cells were fixed with 4%PFA for 10min at RT, and washed 3 times with PBS. Cells were covered with PBS and stored at 4°C until further use.

Staining

Cells were rinsed with 1mL of distilled water 3 times. Cells were incubated with alizarin red solution (2% (w/v) alizarin red in distilled water, pH=4.1-4.3) for 15min at RT, staining calcium deposits in red. Solution was removed and cells rinsed at least 3 times with distilled water until clear. 1mL of distilled water was added and images were acquired using a Zeiss Observer microscope.

Quantification

Water was removed and cells were incubated with 1mL of 10% (v/v) acetic acid for 30min at RT. Liquid and cells were collected into a microcentrifuge tube and vigorously vortexed for 30s. Tubes were incubated for 10min at -85°C, then cooled for 5min on ice. Tubes were centrifuged for 15min at 16,000rcf. 0.5mL of the supernatant was transferred into a new microcentrifuge tube containing 200μL of 10% (v/v) ammonium hydroxide. Optical density at 405nm was measured using a Promega GloMax Explorer spectrometer to quantify calcium deposits.

Adipogenic differentiation assay

The adipogenic differentiation assay aims to assess whether a cell population contains cells able to produce adipocytes containing intracellular lipid droplets.
A total of 28 wells of 4 individual 24-well plates (8 wells per time point, 4 for initial time-point) were seeded with 40,000cells/well in 10%FCS,1%P/S,DMEM (growth medium, GM). 24h later, medium was removed and replaced with either GM or adipogenic medium (AM: GM supplemented with 0.5mM 3-isobutyl-1-methylxanthine [Sigma-Aldrich], 200μM indomethacine [Sigma-Aldrich], 10μM insulin [Sigma-Aldrich] and 1μM dexamethasone [Sigma-Aldrich]). Medium was replaced twice a week. Plates were collected at days 0, 7, 14 and 21. Phase images were acquired on a Zeiss Observer microscope. Cells were fixed with 4%PFA for 10min at RT, and washed 3 times with PBS. Cells were covered with PBS and stored at 4°C until further use.

Staining

Cells were rinsed with 1mL of distilled water 3 times. Cells were incubated with 60% isopropanol for 5min at RT, then with an Oil red O solution (0.18% (w/v) alizarin red in 60% isopropanol) for 5min at RT, staining lipid droplets in red. Solution was removed

and cells rinsed at least 3 times with distilled water until clear. 1mL of distilled water was added and images were acquired using a Zeiss Observer microscope.

Quantification

Water was removed and cells were incubated with 1mL of 60% isopropanol for 10min at RT. Liquid was collected and absorbance read at 492nm was measured using a Promega GloMax Explorer spectrometer to quantify lipids produced.

Migration assay

The migration, scratch or wound healing assay aims to measure the speed at which the cells can move on the plate. In a near confluent layer of cells, a wound is generated by scraping cells off and images are taken at 0, 3, 6, 12 and 24h following injury. As the doubling time for perivascular cell division has been demonstrated to be higher than 24 hours [16], the wound will be repopulated by migrating cells, rather than by division of the cells at the wound edge. Therefore, and by measuring the time of recovery and the area of damage, migratory speed can be deduced. Relative speed was calculated using the following formula:

$$Velocity_{0-1} = \frac{DamageArea_{Time0} - DamageArea_{Time1}}{2(TimeInHours_1 - TimeInHours_0)} \tag{2.2}$$

A total of 4 wells of a 24-well plate were seeded with 100,000 cells/well in SGM. 24h later, medium was replaced with fresh one and a horizontal scratch was performed on the confluent layer using a p10 pipette tip. Images were acquired on a Zeiss Observer microscope 0, 3, 6, 12 and 24h after scratch.

Using ImageJ/FIJI software, wound area was measured.

Viability assay

The viability assay measures the metabolic activity of cells in culture. Cells were exposed to alamarBlue cell viability reagent (ThermoFisher Scientific), a resazurin-based solution that upon entrance into the cell is reduced by metabolic mechanisms to resorufin, becoming highly fluorescent.
A total of 3 wells of a 96-well plate were seeded with 5,000 cells/well in SGM. 24h later, medium was replaced with fresh one. AlamarBlue reagent was added at a 1:10 dilution. Fluorescence emission at 530nm was measured using a Promega GloMax Explorer spectrometer every hour for 5h.

Table 2.7: Culture media used.

EGM-2	**SGM**	**GM**	**AM**	**OM**
EGM-2	DMEM	DMEM	DMEM	DMEM
	Glutamax	Glutamax	Glutamax	Glutamax
	1% P/S	1% P/S	1% P/S	1% P/S
	20% FCS	10% FCS	10% FCS	10% FCS
			10μM insulin	50μM L-ascorbic acid
			100μM indomethasine	0.1μM dexamethasone
			1μM dexamethasone	10μM β-glycerophosphate
			0.5μM 3-isobutyl-5-methylxantine	

2.4 Histology and imaging techniques

2.4.1 Tissue preparation

With forceps, scissors and scalpels, the tissue of interest was dissected. Soft tissues were washed 3 times by immersion in PBS then transferred into 4%PFA and incubated for 24-48h at 4°C. Bone samples were only washed before the next step.

Snap freezing

Soft tissues were washed 3 times by immersion in PBS and placed in a solution of 10% (w/v) sucrose in PBS. Tissue was incubated for 2h (until the tissue sinks) at 4°C. The same process is repeated with a solution on 20% (w/v) sucrose into PBS and then transferred in a 30% (w/v) sucrose in PBS solution and incubated over night (O/N) at 4°C. Tissue was transferred into a histology cryomould then covered with optimal cutting temperature compound (OCT, Thermo Scientific). Tissue was left to soak for 1-5min then positioned as desired in the cryomould. The cryomould was carefully place in a polysterene box containing dry ice and left to cool for 10min. Carefully, the sample was removed from the cryomould and stored until further use at -80°C.
Bones were cut open to expose the marrow, washed gently with PBS then directly immersed in OCT in a cryomould, and left to soak for 5min. The cryomould was transferred carefully to a recipient containing a mixture of dry ice and 70% ethanol and left to cool for 15min. Carefully, the sample was removed from the cryomould and kept at -20°C until further use.

Gelatin embedding

Adipose tissue was washed 3 times by immersion and placed into a 15% (w/v) sucrose solution in PBS and incubated O/N at 4°C. Tissue was transferred into 15% (w/v) sucrose, 7% (w/v) gelatin solution in PBS and incubated for 5h at 37°C, then at 4°C O/N. Once the gelatin has solidified, sample was carefully placed in dry ice and left to cool for 10min. Samples were stored at -80°C until further use.

Paraffin embedding

Tissues were washed and stored in 70% ethanol. Fixed tissues were dehydrated to 100% ethanol, cleared using xylene, and equilibrated in melted paraffin before mounting in a paraffin block. The whole process was prepared and performed on an automated machine (Leica Biosystems) by the Shared university Research Facility at the Queen's Medical Research Institute, University of Edinburgh. Embedded samples were stored at RT until further use.

2.4.2 Sectioning

Cryosectioning

In dry ice, sample blocks were mounted on a sample holder using OCT and left on dry ice for at least 20min. Using a Leica Brightfield Cryostat (Leica Biosystems) sections were cut at 7μm, or 10μm for bone sections, and mounted on Superfrost Plus microscope slides (Thermo Scientific). Section slides were stored at -20°C or -80°C.

Microtome sectioning

Paraffin blocks were cooled on wet ice for at least 10min. Excess of wax was trimmed using a single blade razor. Using a Leica microtome (RM2035 or RM2135; Leica Biosystems) sections were cut at 5-7μm, floated on a water bath at 45°C and mounted on Polysine microscope slides (Thermo Scientific). Slides were left to dry on a heated rack for 24h. Section slides were stored at RT until further use.

2.4.3 Immunohistochemistry

Paraffin sections preparation

Slides were dewaxed in two changes (5 min) of xylene, and rehydrated through an ethanol series (100%, 100%, 95%, 80%, 70%; 20s each) before immersion in running tap water (5 min). If required, antigen retrieval was performed by boiling the sample in citrate buffer (0.1M pH=6.0) for 8min then sealed and left to cool for 30min at RT. Slides were then washed in running tap water for 5min. Slides were washed 3 times in PBS and tissue was encircled using a wax pen.

Frozen sections preparation

Slides stored at -80°C were left to air dry for 10min at RT. Slides were fixed in ice-cold acetone:methanol (1:1) for 10min, then left to air dry for 10min at RT. This fixation also permeabilises the cells. Slides were washed 3 times with PBS. For staining, one of two methods was used, depending on size of the tissue, number of sections per slides and desired markers. If vertical staining was used, slides were then mounted on a sequenza rack using PBS. If horizontal or flat staining was performed, tissue was encircled using a wax pen.

Non-fluorescent IHC

Slides were first blocked using a BloxAll blocking solution (Vector) for 15min at RT to inactivate endogenous peroxidase activity, washed once with PBS then for 1h with 2.5% (v/v) horse serum (Vector) at RT to block unspecific binding. Immediately after this, the primary antibody with the appropriate dilution in antibody diluent (Invitrogen) was added. Primary antibodies were incubated O/N at 4°C. Slides were washed 3 times with PBS, and incubated with the appropriate Impress HRP secondary antibody

(Horseradish peroxidase, Vector) for 30min at RT. Slides were washed 3 times in PBS and once in distilled water, then incubated 3-6min with a DAB substrate solution (3,3'-diaminobenzidine ,Vector) until desired color appears. Slides were washed 3 times in distilled water.

Sections were counterstained using a Harris haematoxylin solution (Thermo Scientific) for 5min, rinsed for 5min in running tap water and incubated for 1min in Scots tap water (25mM $NaHCO_3$, 150mM $MgSO_4$). Slides were then dehydrated in an ethanol series (70%, 80%, 95%, 100%, 100%; 20 seconds each) then two changes of xylene (5min). Slides were mounted using Pertex and left for vapours to evaporate in a fume hood for 24h.

Primary antibodies used are summarised in Table 2.8.

Fluorescent IHC

Slides were blocked using a 5% (v/v) goat serum (Sigma-Aldrich) in PBS solution to block non-specific staining for 1h at RT. If a biotinylated antibody was used, an additional blocking step was performed by washing 3 times with PBS and using a avidin/biotin blocking kit (Invitrogen) and washing again 3 times with PBS. Primary antibodies were added together in the appropriate dilution in antibody diluent, and incubated O/N at 4°C in the dark. Slide were washed 3 times with PBS. Secondary antibodies were diluted in antibody diluent and incubated for 1h30min at RT. Slides were washed 3 times with PBS. Sections were counterstained by incubating the slides with 0.1 mg/mL DAPI in PBS for 10min at RT. Slides were washed 3 times. Slides were mounted using Fluoromount-G (Southern Biotech).

Alternatively, an amplification signal was performed using the tyramide system (Perkin Elmer). Primary antibody was detected using an Impress HRP secondary, following the non-fluorescent protocol. The fluorescent tyramide reagents covalently bind to nearby proteins when in proximity to HRP, increasing total signal of primary detection

compared to a single detection method using a fluorescent secondary.

Conjugated primary antibodies and secondary used are summarised in Table 2.9 and Table 2.10 respectively.

Table 2.8: Unconjugated primary antibodies. rb=rabbit, hu=human, ms=mouse, p=pig.

Antigen	Species	Used in	Dilution (tyramide)	Company&Catalog number
αSMA	ms	hu, ms, p	1:500	Sigma A2547
aGFP	chicken	hu, ms, p	1:1000	Abcam ab13970
CD34	ms	hu	1:100	BD Pharmingen 550390
CD34	ms	hu	1:100	Abcam ab139551
CD34	rb	hu, ms, p	1:100	Abcam ab81289
CD44	ms	hu, p	1:100	BD Pharmingen 550392
CD73	ms	hu, p	1:100	Invitrogen 41-0200
CD90	ms	hu	1:100	Abcam ab92574
CD90	ms	hu, p	1:100	BD Pharmingen 555593
CD105	ms	hu, p	1:100	Invitrogen MHCD10500
CD146	ms	hu	1:100	BD Pharmingen 550314
CD146	rb	hu, ms, p	1:100	Abcam ab75769
cMHC	ms	hu, ms, p	1:500	Sigma
Collagen I	ms	hu, ms, p	1:500	Sigma
Desmin	rb	hu	1:500	Abcam ab15200
Dystrophin	rb	hu	1:500	Abcam ab15277
LepR	rb	hu	1:200	Abcam ab5593
Mef2c	ms	hu, ms, p	1:100	Abcam ab118406
Nestin	chicken	hu, ms, p	1:500	Abcam ab134017
NG2	ms	hu	1:100	BD Pharmingen 554275
NG2	rb	hu, ms, p	1:100	Abcam ab5320
NG2	rb	hu, ms, p	1:100	Millipore AB5320
PDGFRα	rb	hu, ms, p	1:50 (1:500)	Cell Signalling 3174S
PDGFRβ	rb	hu, ms, p	1:100 (1:500)	Abcam ab32570
SF-MHC	rb	hu, ms, p	1:500	Sigma M4276
Troponin T	ms	hu	1:100	Abcam ab8295

Picrosirius red staining

Picrosirius red (PSR) staining is a counterstaining technique that stains collagen deposits in red, while remaining tissues are stained in yellow. Staining was performed as a counterstaining technique following single non-fluorescent staining.

Table 2.9: Conjugated primary antibodies. hu=human, ms=mouse, p=pig.

Antigen	Label	Species	Used in	Dilution	Company&Catalog number
Dolichos biflorus agglutinin	biotin	plant	p	1:500	Vector B-1035
Griffonia Simplicifolia isolectin B4	biotin	plant extract	ms	1:500	Vector B-1205
Ulex europaeus agglutinin	biotin	plant	hu	1:500	Vector B-1065
von Willebrand Factor	FITC	sheep	hu, ms, p	1:500	Vector B-1065

Table 2.10: Secondary antibodies.

Antigen	Label	Species	Dilution	Company&Catalog number
Anti-mouse IgG	AF488	Goat	1:500	Life technologies A11039
Anti-mouse IgG	AF555	Goat	1:500	Invitrogen A21422
Anti-mouse IgG	AF568	Goat	1:500	invitrogen A11004
Anti-mouse IgG	AF647	Goat	1:500	Invitrogen A21236
Anti-rabbit IgG	AF488	Goat	1:500	Invitrogen A11034
Anti-rabbit IgG	AF555	Goat	1:500	Invitrogen A21428
Anti-rabbit IgG	AF568	Goat	1:500	Life technologies A11011
Anti-rabbit IgG	AF647	Goat	1:500	Invitrogen A21245
Anti-chicken IgG	AF488	Goat	1:500	Life technologies A11039
Anti-chicken IgG	AF568	Goat	1:500	Invitrogen A11041
Streptavidin (anti-biotin)	AF488	Goat	1:500	Life technologies A11039
Streptavidin (anti-biotin)	AF647	Goat	1:500	Life technologies S21374
Anti-mouse IgG	HRP	Horse	as supplied	Vector MP-7402
Anti-rabbit IgG	HRP	Horse	as supplied	Vector MP-7401
HRP	Tyramide Cy3		1:50	Perkin Elmer SAT704B001EA

Stained sections kept in distilled water after the procedure were immersed in PSR solution (0.1% (w/v) Sirius red F3B [Sigma-Aldrich] in saturated (1.3%) aqueous picric acid solution [Sigma-Aldrich]) for 90min. Slides were then washed twice in 0.5% (v/v) glacial acetic acid in distilled water (1min each). Slides were dried and dehydrated in three changes of 100% ethanol (1min each) and two changes of xylene (5 min each) before mounting with glass coverslips using Pertex mounting medium. PSR and mounting was performed by the Shared University Research Facility at the Queen's Medical Research Institute, University of Edinburgh.

2.4.4 Immunocytochemistry

96-well plate

Cells were seeded at 20,000cells/cm^2 in SGM in flat bottom 96-well plates (Corning). 24h later, medium was removed, cells washed 3 times with PBS and fixed with 4%PFA for 10min at RT. Cells were washed 3 times with PBS and unspecific signal blocked with 5% (v/v) goat serum. Primary antibodies were added at the appropriate dilution in 25μL of antibody diluent and incubated at 4°C O/N. Individual stainings were done in triplicates. Cells were washed 3 times with PBS and secondary antibodies were added in 25μL of antibody diluent and incubated for 1h30min at RT in the dark. Cells were washed 3 times with PBS. Cells were counterstained using 0.1 mg/mL DAPI for 15min at RT. Cells were washed 3 times with PBS.

Coverslips/24-well plate

Alternatively, cells were seeded on coverslips. 13 mm glass coverslips were cleaned with 70% ethanol and sterilised by exposure to UV light for 20min. Individual coverslips were placed into individual wells of a 24-well plate (Corning). Cells were seeded into the wells onto the coverslips, and incubated until near confluence. Medium was removed and coverslips washed 3 times with PBS. Unspecific signal was blocked with 5% (v/v) goat serum. Primary antibodies were added at the appropriate dilution in 250μL of antibody diluent and incubated at 4°C O/N. Individual stainings were done in triplicates. Cells were washed 3 times with PBS and secondary antibodies were added in 250μL of antibody diluent and incubated for 1h30min at RT in the dark. Cells were washed 3 times with PBS. Cells were counterstained using 0.1mg/mL DAPI for 15min at RT. Cells were washed 3 times with PBS. Carefully, coverslips were mounted on slides (Thermo Scientific) using Fluoromount-G mounting medium.

2.5 Microscopy, image acquisition and data processing

2.5.1 Macro scripting

This work uses various types of images from which multiple types of informations are extracted. Simple qualitative analysis is easily understood by looking at the image, while more complex quantitative information is extracted by manipulating the images. To manipulate and quantify these images, the Fiji software was primarily used. This software features the ability to automate the image processing by listing the desired commands to execute into a particular file using one of the programming languages from the software. This process is called ”macro scripting” and generates what is called a macro script, macro or script. Scripting enables a more reproducible and unbiased way to analyse images, as the same analysis is performed for every single image.

2.5.2 Widefield fluorescence

Images of stained tissue sections were acquired on an Olympus BX61 microscope (Olympus), with CoolLED p300 light source (CoolLED). Monochromatic fluorescent images were acquired on a Retiga 6000 camera (QImaging), whilst brightfield images were acquired using a Micropublisher 3.3 RTV colour camera (QImaging), utilising either the Volocity v6.3 or MicroManager v1.4 softwares.

Alternatively, images were acquired on a Zeiss Observer microscope with a Colibri7 LED light source (Zeiss). A Hamamatsu Flash 4.0 v3 camera (Hamamatsu Photonics) was used for both tissues and ICC images imaging. Acquisition was controlled using the Zen Pro (blue edition) v2.3 software.

2.5.3 High content imaging

ICC Plates were scanned using an Operetta high content microscope (Perkin Elmer). Images were acquired using the Harmony software and uploaded to a Columbus Image analysis server (Perkin Elmer).

2.5.4 Whole slide scanning

Whole slides were scanned using an Operetta high content microscope (Perkin Elmer). Images were acquired using the Harmony software and uploaded to a Columbus Image analysis server (Perkin Elmer). As the Operetta is not designed to be used as a slide scanner, a macro was scripted to reconstruct the whole section scanned in a single image from the single fields of view using the FIJI software. The full macro can be found in annex .1. Alternatively, a Zeiss Axio Scan.Z1 (Zeiss) using the Zen Pro software was used to scan whole slides.

2.5.5 Bright field

Brighfield and phase images were acquired on a Zeiss Observer microscope with a Zeiss MRc camera (Zeiss). Acquisition was controlled using the Zen Pro (blue edition) v2.3 software.

2.5.6 Image analysis

Images were treated and analysed using mainly the FIJI/imageJ analysis. Alternatively, images were treated using the Zen blue edition software (Zeiss).

Blood vessel quantification and characterisation on IHC

Several FIJI macros were scripted to quantify contents of the whole scan slides. Scripts were designed to quantify tissue area, number of independent blood vessels and their perivascular coverage, in different tissue areas. First, areas of interest were manually dissected from the original image. Then, total tissue area was measured in pixels, followed by an identification of blood vessels using the endothelial marker staining, generating individual regions of interest (ROI). ROIs were counted to quantify total number of blood vessels, then expanded to cover the perivascular cell layer and analysed to assess whether the blood vessel was covered by cells expressing a particular perivascular marker. Specific quantification macro is detailed in annex .2.

Lipid and calcium formation quantification

Similarly, a macro was scripted to quantify lipids or calcium deposits in the differentiation assays, as detailed in annex .3. Colour images acquired where processed by extracting the red signal, corresponding to the staining and the area of lipid/calcium signal over the total image was calculated.

2.6 Statistics

Numeric data was processed in either Excel office (Microsoft) or R studio. Statistics were performed using the Graphpad Prism v7 software. Unless specified, all quantitative data is presented as mean$\pm$standard deviation. Comparisons between the means of two groups were made using paired and unpaired T-test as appropriate. Multiple T-test when required followed the Holm-Sidak method. When more than two groups were compared, One-way ANOVA with Bonferroni's test was performed. P values were

considered significant when less than 0.05. The specific statistics used in each case are indicated in figure legend.

Chapter 3

Identification, isolation and characterisation of leptin receptor positive and negative subtypes of human pericytes and adventitial cells

3.1 Introduction

The leptin receptor (LepR) is a particularly novel marker for PCs. Only pericytes expressing LepR in the haematopoiesis context have been characterised [27, 43, 44], thus little is known on PCs expressing it in other tissues. LepR has been more broadly studied in MSCs. It has been linked to several mesenchymal features including bone formation, hypoxia conditioning and tissue protection but also hypertrophy, arrhythmias and proatherosclerosis [174–184]. Nevertheless, subtypes of PCs based on LepR expression have not yet been characterised.

3.2 Hypothesis and Aims

The working hypothesis for this chapter is that LepR can be used to identify and isolate functionally distinct subtypes of pericytes and adventitial cells. This hypothesis will be articulated in three aims, as follows:

- Identify LepR$^+$ perivascular cells *in situ* in multiple human tissues.
- Isolate subsets of perivascular cells based on LepR expression using FACS and expand them *in vitro*.
- Assess the clonogenic, proliferative and differentiation potentials of the different subsets *in vitro*.

3.3 Results

3.3.1 LepR is expressed on a fraction of pericytes in human bone marrow

Flow cytometry analysis performed on multiple foetal samples, ranging from 14 to 20 weeks of gestation, and adult bone marrow shows a consistent fraction of pericytes and adventitial cells expressing LepR (Foetal pericytes 12.04$\pm$6.32%, adult pericytes 17.49$\pm$6.30%, foetal adventitial cells 8.67$\pm$2.12% and adult adventitial cells 6.44$\pm$2.29%; Figure 3.1a-d). LepR is expressed in the same fraction of pericytes and adventitial cells in both adult and foetal samples (Figure 3.1a-b). In the foetal bone marrow the fraction of pericytes and adventital cells is not significantly different whereas a bigger fraction of pericytes expresses LepR than adventitial cells in the adult bone marrow (Figure 3.1c-d).

Histological analysis confirms the presence of LepR$^+$ pericytes in the adult bone mar-

row (Figure 3.1e). *In situ* identification of adventitial cells was impossible due to the minimal presence of large blood vessels in the processed tissue.

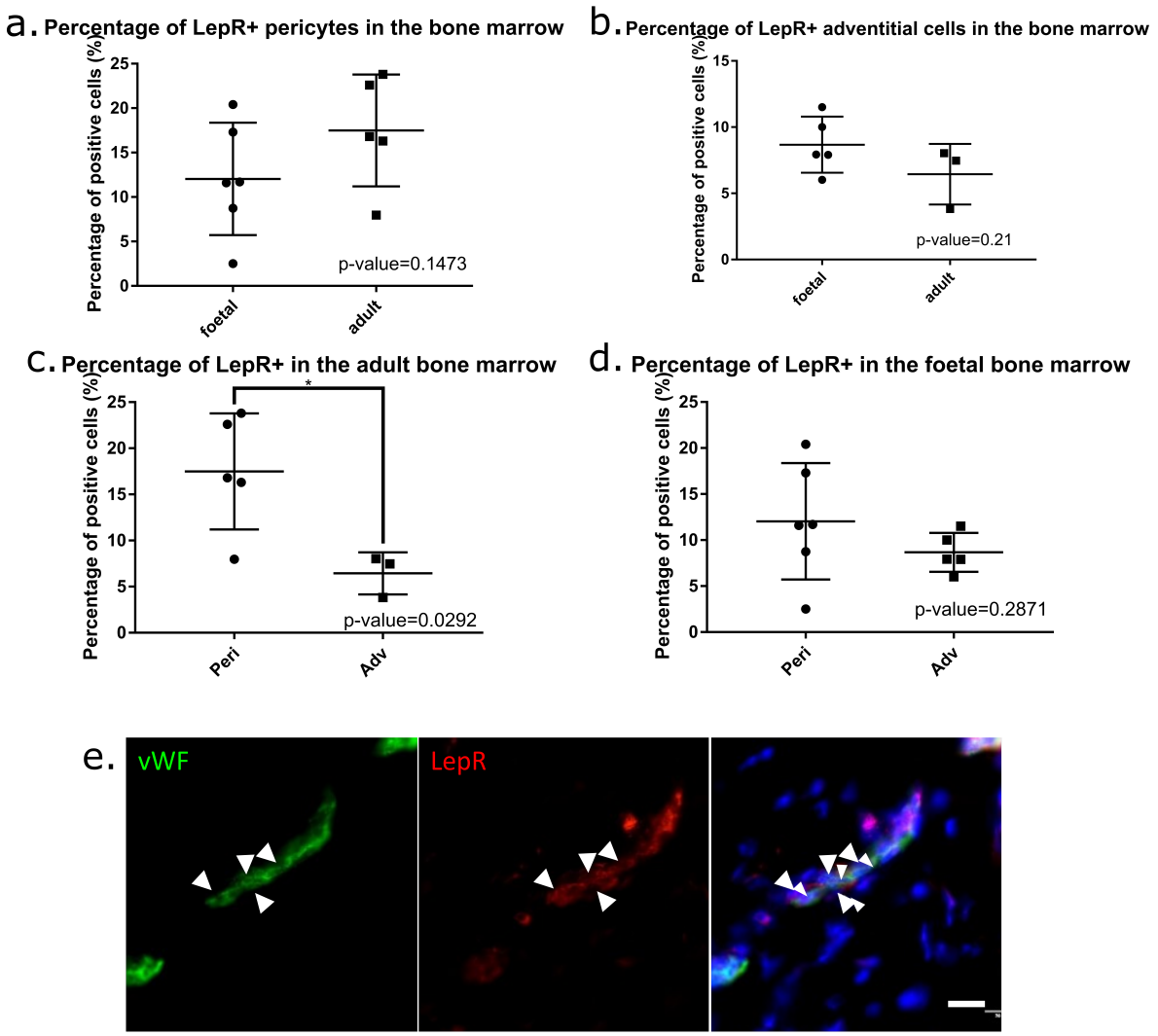

Figure 3.1: **Leptin receptor in the human bone marrow.** Quantifications of pericytes (a) and adventitial cells (b) expressing LepR by flow cytometry, for adult bone marrow (c) and foetal bone marrow (d). Unpaired T-test ($n_{FoetalPericytes}$=6, $n_{FoetalAdvCells}$=5, $n_{AdultPericytes}$=5, $n_{AdultAdvCells}$=3; *,p-value$<$0.05). (e) Immunohistochemistry on adult bone marrow showing LepR$^+$ pericytes surrounding vWF$^+$ endothelial cells (white arrowheads, scale bar=20μm).

3.3.2 LepR is expressed on a fraction of pericytes in human subcutaneous fat

Flow cytometry analysis performed on adult subcutaneous white adipose tissue shows a consistent fraction of PCs expressing LepR (pericytes 21.35±3.04% and adventitial cells 8.27±9.09%; Figure 3.2a). Histological analysis confirms the presence of LepR$^+$ pericytes in the adult fat (Figure 3.2b). *In situ* identification of adventitial cells was impossible due to the minimal presence of large blood vessels in the processed tissue.

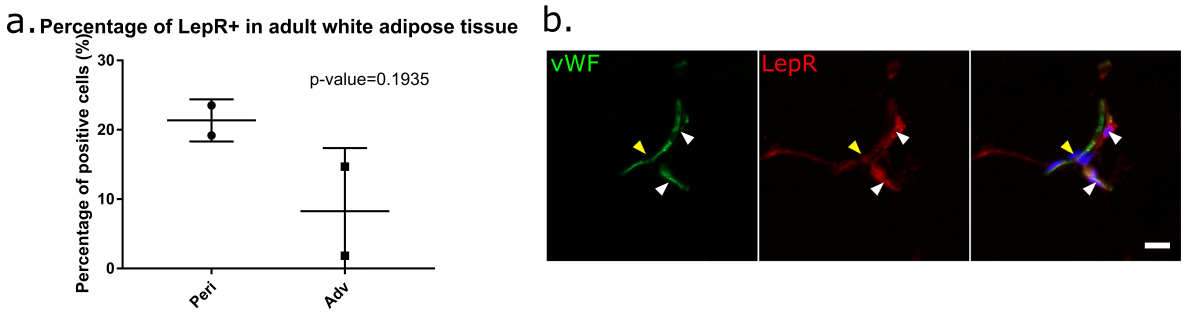

Figure 3.2: **Leptin receptor in the human subcutaneous white adipose tissue.** Quantifications of pericytes and adventitial cells expressing LepR by flow cytometry (a). Unpaired T-test (n=2; *,p-value$<$0.05). Immunohistochemistry on subcutaneous white adipose tissue showing LepR$^+$ pericytes (white arrowheads, scale bar=20μm) and LepR$^-$ pericytes surrounding vWF$^+$ endothelial cells (yellow arrowhead).

3.3.3 LepR is expressed in other human foetal tissues

Other tissues were also explored for LepR expression in PCs. Flow cytometry analysis confirms LepR expression on pericytes and adventitial cells in foetal hearts (figure 3.3a) although expression is very variable. Expression was also confirmed in skeletal muscle (figure 3.3b).

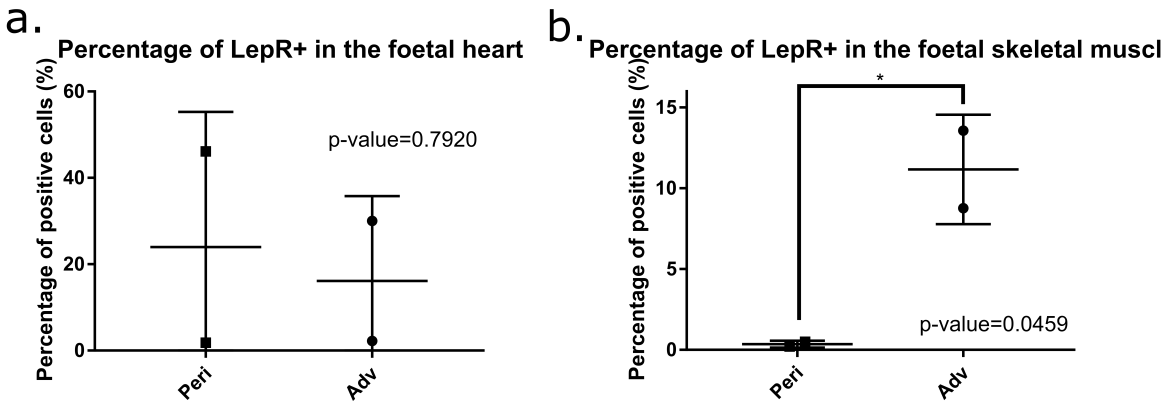

Figure 3.3: **Leptin receptor in the human foetal heart and skeletal muscle.** Quantifications of pericytes and adventitial cells expressing LepR by flow cytometry in heart (a) and skeletal muscle (b). Unpaired T-test (n=2; *,p-value$<$0.05).

3.3.4 Do LepR$^{+/-}$ perivascular cells exhibit different potential *in vitro*?

Pericytes and adventitial cells both positive and negative for LepR were sorted by FACS (Figure 3.4) from bone marrow (FBM) and skeletal muscle (SkM) from two foetal biological samples (sample 378, 15 weeks of gestation; sample 379, 17 weeks of gestation). Unsorted cells were placed in culture and considered as standard MSCs. All cell lines were successfully established (except for the LepR^{+} pericyte population from the FBM sample 378, where cell cultures were not successfully established) and tested *in vitro* for clonogenic potentials, growth and differentiation potential. The unsorted cells (considered classical MSCs) from these tissues were also tested.

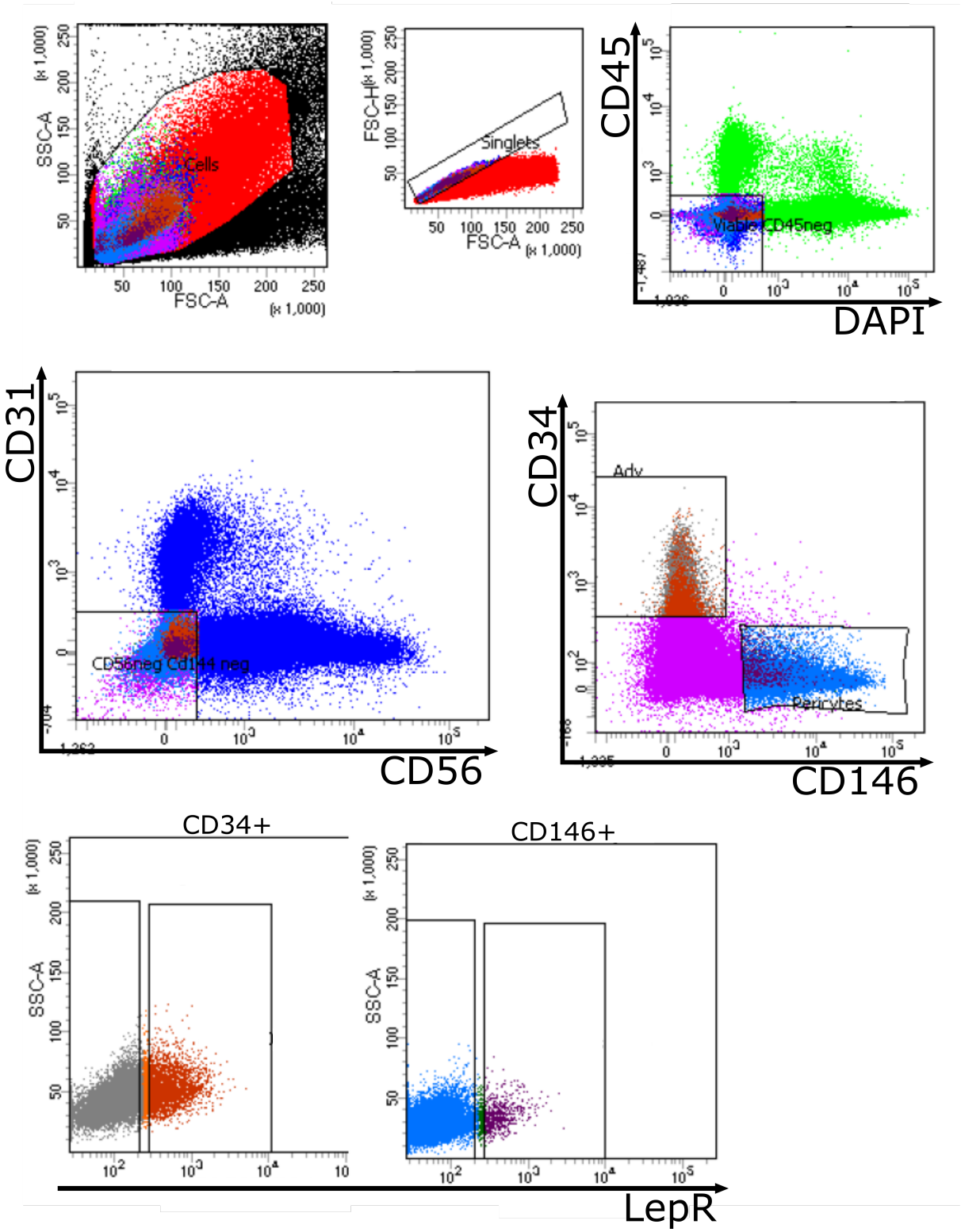

Figure 3.4: **FACS plots for foetal human perivascular LepR subset sorting.** Sorting strategy to isolate LepR$^{+/-}$ pericyte and adventitial cell subsets from human tissues.

Colony forming unit-fibroblast (CFUf) assay does not reveal consistent differences between subtypes based on LepR expression

Tested subtypes display very different clonogenic potentials (Figure 3.5). Overall, LepR$^+$ pericytes perform equally well or worse than the negative subtype for all samples. Adventitial cells' performance is less consistent, with one subtype performing better for one sample, inversed results for another sample and no differences for the last two. When comparing samples, high donor diversity was observed: sample FBM379 performs overall better than sample FBM378 and skeletal muscle samples perform equally well when observing the wells, but proper counting of colony formation reveals differences among cell lines for only one sample (Figure 3.5c-d); the unsorted classical MSCs perform differently among the different samples (Figure 3.5f). Thus this assay has not conclusively revealed functional differences in terms of clonogenic potential when comparing subtypes of PCs based on LepR.

Growth chart does not reveal consistent differences between subtypes based on LepR

Tested subtypes display very different clonogenic potentials. No consistent differences were observed when comparing across samples or cell lines, similar to the CFU-f assay. No differences can be observed when comparing LepR$^+$ adventitial cells from different donors (Figure 3.6a). For the rest of cell lines, some differences can be observed but remain inconsistent. These include significant differences within the same donor but different tissue, same tissue from different donor or both (Figure 3.6b-e). When comparing samples, high donor diversity was observed: sample FBM378 exhibits significant differences between multiple cell lines (Adv+ vs. Adv-, Adv+ vs. Uns and Peri- vs. Uns; Figure 3.6f) while sample FBM379 shows no differences between any line (Figure 3.6g). As only one of the LepR$^+$ pericyte cell culture were success-

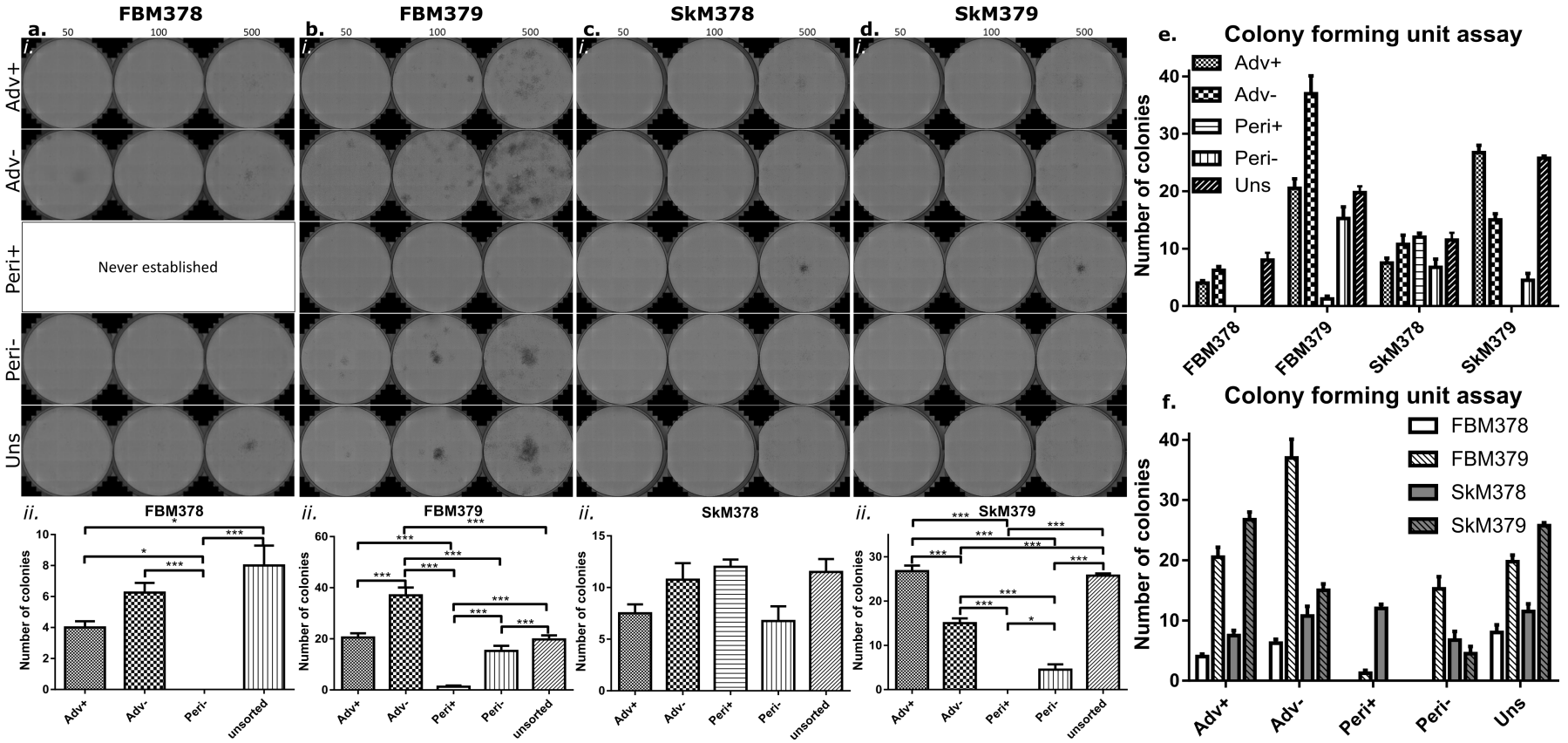

Figure 3.5: **CFUf assay reveals no conclusive differences when comparing subtypes of PCs based on LepR.** CFUf assay on LepR$^+$ adventitial cells (Adv+), LepR$^-$ adventitial cells (Adv-), LepR$^+$ pericytes (Peri+), pericytes LepR$^-$ (Peri-) and classical MSCs (Uns) isolated from foetal samples FBM378 (a; bone marrow, 15 weeks of gestation), FBM379 (b; 17 weeks of gestation), SkM378 (c; skeletal muscle) and SkM379 (d). Representatives images of the wells seeded with 50, 100 and 500 cells are displayed ($_i$), and quantifications ($_{ii}$) of the number of colonies in the wells seeded with 100 cells. Quantifications show mean$\pm$SD (n=4 wells). Statistical analysis consisted of a one-way ANOVA followed by Bonferroni's multiple comparison test (*, p-value$<$0.05; **, p-value$<$0.01; ***, p-value$<$0.001; no indication, non-significative, p-value$>$0.05). General overview per subtype tested (e) and per sample (f). No statistical analysis shown for subfigures e-f.

fully established, no statistical comparisons could be made. Thus this assay has not revealed a functional difference in terms of growth potential when comparing subtypes of PCs based on LepR.

Adipogenesis assay does not reveal consistent differences between subtypes based on LepR

When placed in adipogenic differentiation medium, significantly higher lipid coverage was observed in LepR$^+$ adventitial cells derived from the skeletal muscle (Figure 3.7e) while this observation does not match the lipid production observed by spectrophotometry (Figure 3.7k). LepR$^-$ adventitial cells from one of the bone marrow samples have significantly higher lipid coverage, as well as lipids detected by spectophotometry, while there are no significant differences observed on the second foetal sample (Figure 3.7e,k). Pericytes derived from skeletal muscle exhibit opposite differences with the LepR$^+$ subtype presenting significantly higher lipid coverage for one sample and lower for the other, with no significant differences detected by spectrophotometry for either (Figure 3.7f,l). LepR$^+$ pericytes exhibit much higher coverage for the sample where the cell line was successfully established, although no differences can be observed by spectrophotometry (Figure 3.7f,l). Overall, adventitial cells exhibit much higher adipogenic potential than pericyte populations derived from the same donor (Figure 3.7a-e,g-j), while there are still differences when same cell populations are compared between samples.

LepR$^+$ adventitial cells and LepR$^-$ pericytes exhibit higher osteogenic potential

When placed in osteogenic differentiation medium, significantly higher calcium deposition was observed in LepR$^+$ adventitial cells derived from the foetal bone marrow. This same difference is observed for one of the skeletal muscle samples while the second

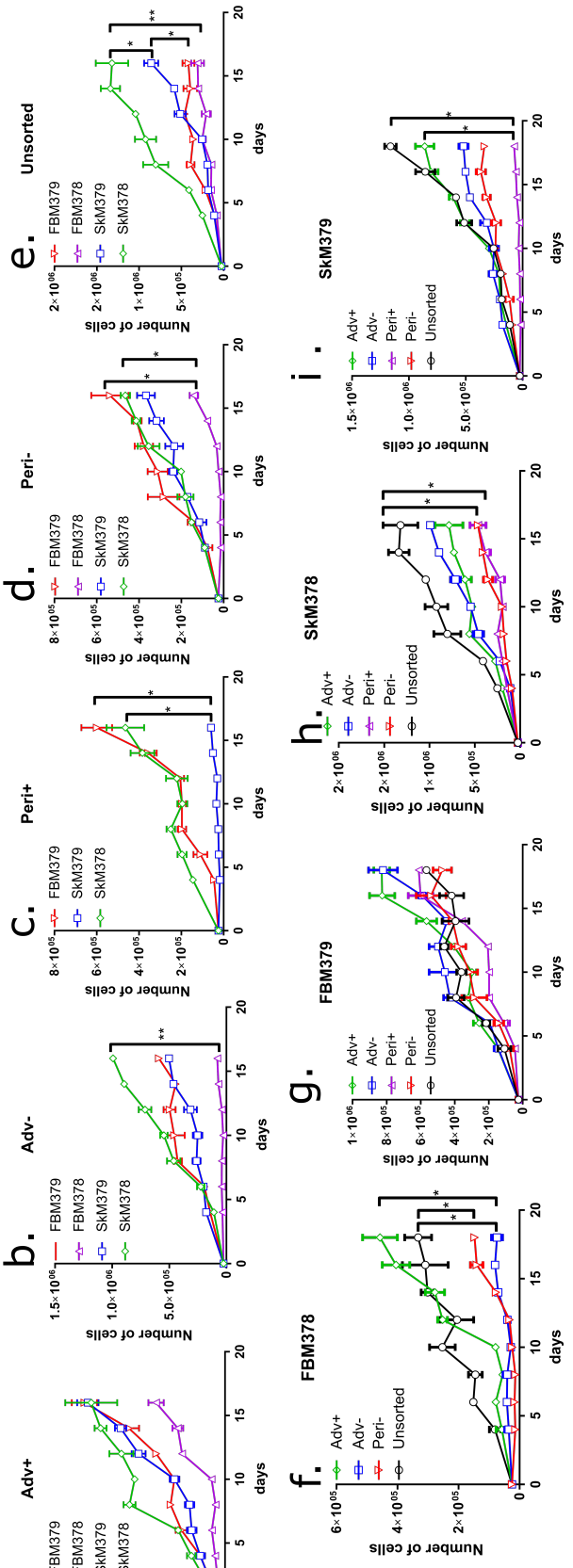

Figure 3.6: **Growth in culture reveals no conclusive differences when comparing subtypes of PCs based on LepR.** Growing charts assay for LepR$^+$ adventitial cells (Adv+; a), LepR$^-$ adventitial cells (Adv-; b), LepR$^+$ pericytes (Peri+; c), LepR$^-$ pericytes (Peri-; d) and classical MSCs (Unsorted; e) isolated from foetal samples FBM378 (f; bone marrow, 15 weeks and 3 days of gestation), FBM379 (g; 17 weeks and 5 days of gestation), SkM378 (h; skeletal muscle) and SkM379 (i). Quantifications show mean±SD (n=4). Statistical analysis consisted of a one-way ANOVA followed by Bonferroni's Multiple comparison test (*, p-value$<$0.05; **, p-value$<$0.01; no indication, non-significative, p-value$>$0.05).

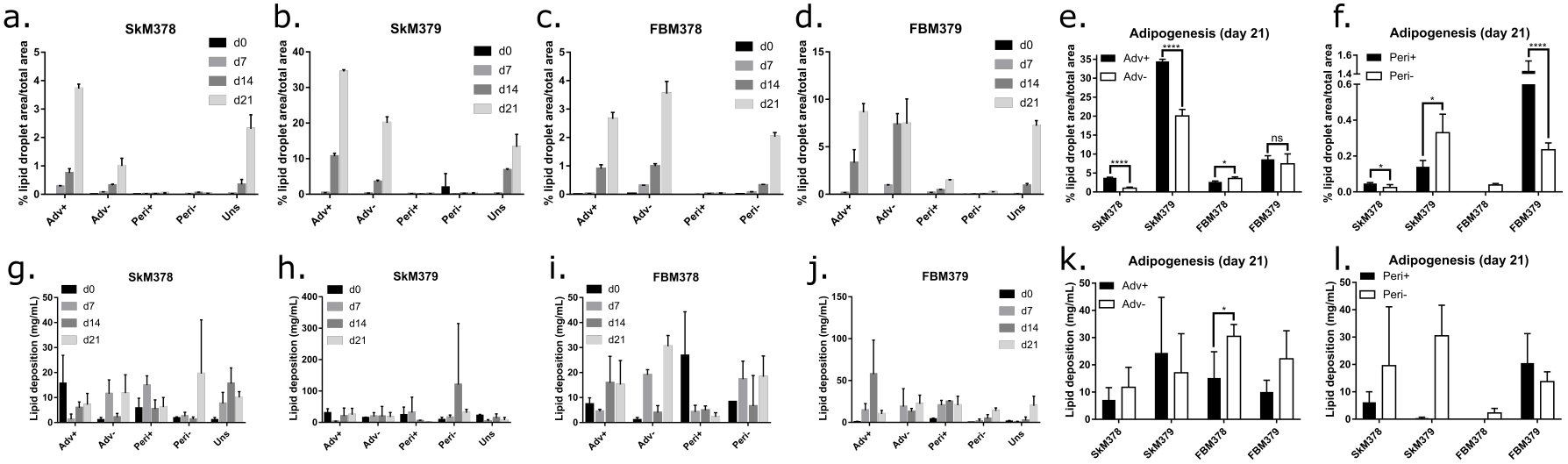

Figure 3.7: **Adipogenesis assay does not reveal consistent differences between subtypes based on LepR.** Quantifications of Oil red O staining coverage on scanned wells (a-f) and lipid formation via spectrophotometric measurements (g-l) after culture in adipogenic medium of adventitial cells (Adv) and pericytes (Peri), both positive and negative for LepR, and classical MSCs (Uns) cell lines derived from samples 378 and 379 of foetal bone marrow (FBM) and skeletal muscle (SkM; a-d, g-j; n=4, no statistical analysis). Quantifications at d21 for Adv (e,k) and Peri (f,l; unpaired T-test, n=4; *, p-value$<$0.05; **, p-value$<$0.01; ****, p-value$<$0.0001).

exhibits no differences (Figure 3.8e). Very little calcium deposition was observed for pericytes in general, while LepR$^-$ pericytes for the sample where both pericyte subtype lines were successfully established produced more calcium deposits.

3.3.5 Brief summary

This work shows the existence of subtypes based on LepR in pericytes and adventitial cells in foetal and adult bone marrow, adult white adipose tissue and foetal skeletal muscle and heart by histological analysis and flow cytometry. When cultured, subpopulations show different behaviours depending on the donor sample.

3.4 Discussion

3.4.1 LepR is expressed by a fraction of pericytes and adventitial cells in adult and foetal tissues

The work here presented shows the existence of subtypes of both pericytes and adventitial cells based on LepR. LepR is found expressed on pericytes in adult tissues such as the bone marrow and subcutaneous white adipose tissue, and in foetal samples that include skeletal and cardiac muscle and bone marrow. High variability can be observed via flow cytometry, but interestingly both subtypes are maintained from foetal stage to adulthood, as evidenced by the analysis on the bone marrow. *In situ* characterisation of these cells is particularly difficult due to the ubiquitous presence of LepR. As many cells types express LepR, it is not obvious whether the observed perivascular cells express LepR when analysed by imaging techniques on histological sections.

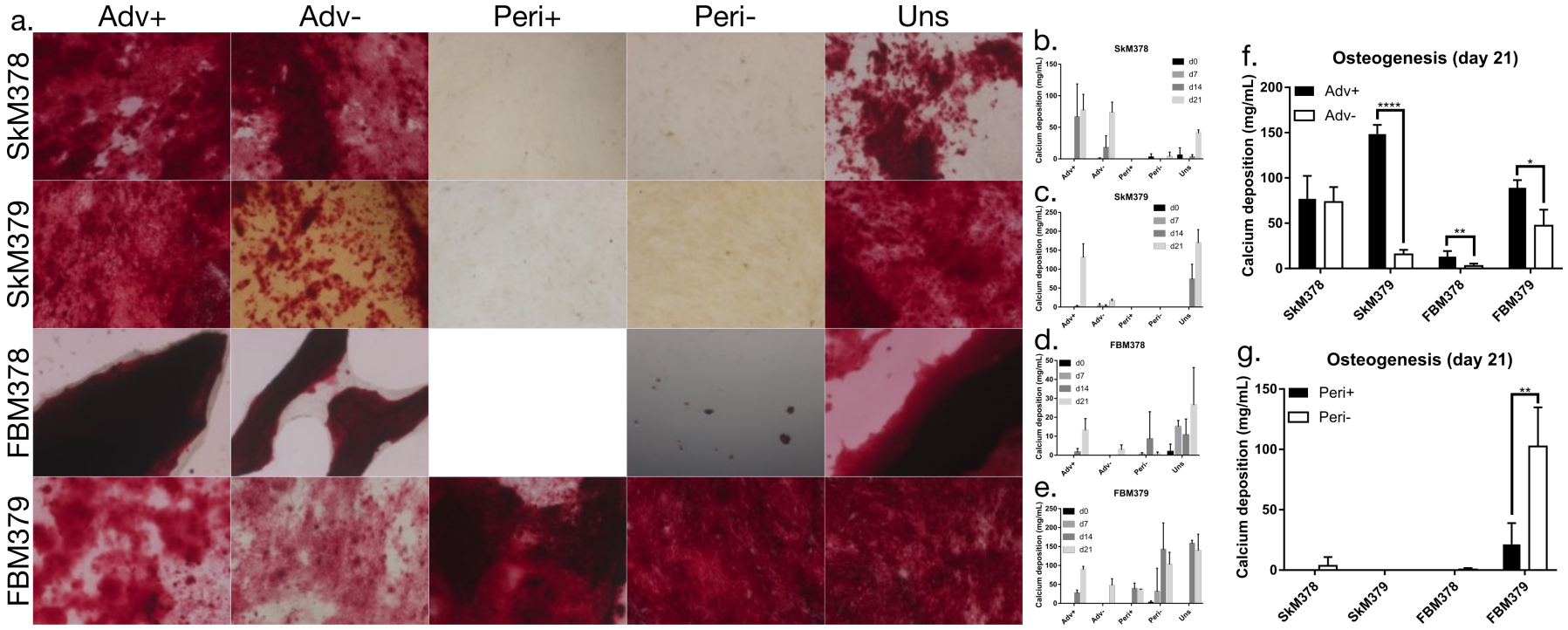

Figure 3.8: **LepR$^+$ adventitial cells and LepR$^-$ pericytes exhibit higher osteogenic potential.** (a) Representative images for calcium depositions stained with Alizarin Red at day 21 of differentiation. (b-e) Quantifications of calcium deposition via spectrophotometric measurements after culture in osteogenic medium of adventitial cells (Adv) and pericytes (Peri) positive and negative for LepR and classical MSCs (Uns) cell lines derived from samples 378 and 379 of foetal bone marrow (FBM) and skeletal muscle (SkM; n=4, no statistical analysis). (e-f) Quantifications at d21 for Adv and Peri (unpaired T-test, n=4; *, p-value$<$0.05; **, p-value$<$0.01; ****, p-value$<$0.0001).

3.4.2 LepR does not functionally discriminate subtypes of PCs based on the assays performed

The assays here performed do not reveal any major functional differences between $LepR^+$ adn $LepR^-$ cell populations. Growth potential exhibited no consistence and clonogenic potential seemed to favour the $LepR^-$ subtypes. The only consistent result is a higher osteogenic potential in $LepR^+$ foetal bone marrow adventitial cells. Nevertheless, the assays here performed are not sufficient to prove that these cell populations do not present any sort of functional differences.

It should be of particular interest to investigate if there are any functional differences concerning haematopoiesis support. Studies performed in mice revealed that $LepR^+$ pericytes, located around sinusoids, regulate HSC quiescence [43]. It has been previously described by our group that human pericytes support HSC maintenance *in vitro* and that $LepR^+$ pericytes were present in the tissue of origin [27], nevertheless, subtypes of pericytes based on this marker were not tested then. Assays were indeed considered, but experiments focused on haematopoiesis characterisation are especially long, exceeding the time left for the completion of the experimental phase of the PhD. Similarly interesting would be to examine the modulatory effects of these populations over the immune system, as well as their secretory activity.

3.4.3 Foetal samples exhibit dramatic donor dependent differences

It is interesting to note that there are dramatic differences over the behaviour of the same cell populations isolated from distinct donor samples. Whereas it is somehow expected to find differences between tissues, the same cell populations isolated from the same tisse of origin exhibited different potentials when compared between donors, as here shown by cells derived from samples FBM378 and FBM379. In the particular case of the bone marrow, we observe a consistent expression of LepR in pericytes

and adventitial cells in both foetal and adult samples, but when assessed *in vitro* the sorted populations behave differently. Thus an interesting question is: where is this variability originating?

As some trends seem to be similar when comparing the overall behaviour of the cell populations, it is likely that the origin of the variation is in the donor itself. As foetal samples are procured by delivery (as opposed to surgery), samples could be damaged during collection and could affect later on when cells are isolated and tested.

Additionally, foetal samples seem to trend differently from adult samples, suggesting possibles differences in distribution of these perivascular subpopulations when comparing developing and adult tissues.

It is also possible that differences are due to the genetic background of the donors and cell populations only behave differently because of natural variations within the human populations.

The data her shown provides interesting preliminary data, but more samples should be analysed.

Chapter 4

Identification, isolation and characterisation of NG2$^{+/-}$ and αSMA$^{+/-}$ subtypes of human and porcine pericytes

4.1 Introduction

NG2 and αSMA are two of the major markers to identify perivascular cells, in particular pericytes. Both of these markers are expressed in other cell types, and in particular αSMA is also found in VSMCs and fibroblasts. In mouse, it has been demonstrated that although being major markers widely expressed among pericytes there are substantial differences in distribution. In particular, NG2 is not found on veins and venules. Nevertheless, pericyte subtypes based on NG2 and αSMA have not yet been tested for differences *in vitro* nor *in vivo*.

4.2 Hypothesis and Aims

The working hypothesis for this chapter is that αSMA and NG2 can be used to identify and isolate functionally distinct subtypes of pericytes. This hypothesis will be articulated in four aims, as follows:

- Identify NG2$^+$ and αSMA$^+$ perivascular cells *in situ* in multiple human tissues.
- Isolate subsets of pericytes based on αSMA and NG2 expression using FACS.
- Isolate subsets of pericytes based on NG2 and expand them *in vitro*.
- Assess clonogenic, proliferative and differentiation potentials of the different subsets *in vitro*.

4.3 Results

4.3.1 Different vessels in close proximity to each other possess distinct perivascular layers

Foetal heart cryosections were stained for the canonical markers αSMA, NG2, CD146, CD34 and the endothelial lectin *Ulex europaeus* (Ulex). Multiple types of blood vessels could be identified in close proximity to each other. Perivascular layers differently expressed the markers αSMA and NG2 (Figure 4.1).

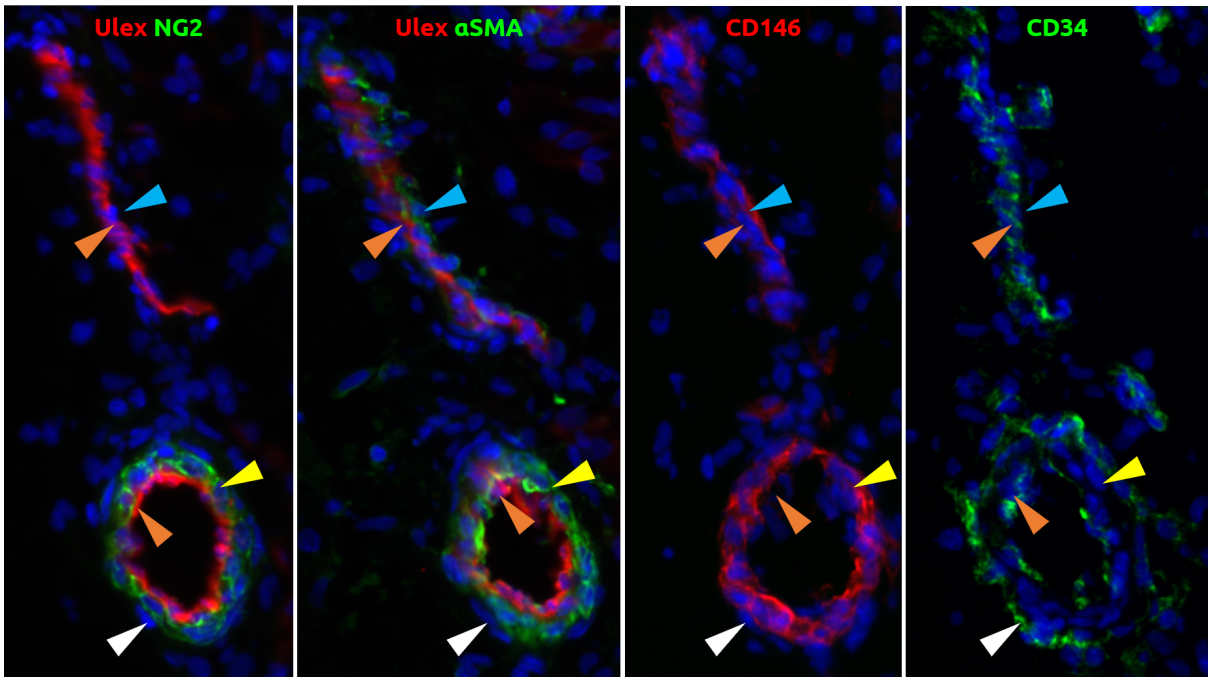

Figure 4.1: **Different vessels in close proximity to each other possess distinct perivascular layers.** Two human cardiac blood vessels are found in close proximity but exhibit different perivascular layers in consecutive sections. The top blood vessel -a vein- shows an endothelial layer positive for Ulex and CD34 (orange arrowhead), and a perivascular layer positive for CD146 and αSMA, while negative for NG2 (blue arrowhead). The bottom blood vessel -an artery- also shows an endothelial layer positive for Ulex and CD34 (orange arrowhead), but displays an inner perivascular layer positive for CD146, αSMA and NG2 (yellow arrowhead), and an outer layer positive for CD34 (white arrowhead).

4.3.2 Mef2c is exclusively expressed on CD146$^+\alpha$SMA$^+$NG2$^+$ cells in a transient fashion.

To examine whether any of these cardiac pericyte subpopulations hold cardiomyogenic potential, consecutive sections of foetal cardiac tissues were stained for the developmental cardiac markers GATA4, Mef2c and c-kit (Figure 4.2). Interestingly, expression of Mef2c is detected on pericytes, but restricted to pericytes expressing CD146, αSMA and NG2 (Figure 4.2e-h).

However Mef2c expression was only detected in a single foetal sample aged 19 weeks of gestation among multiple samples of different gestation stage that were tested, indi-

cating a transient expression of Mef2c in a particular subset of pericytes (Figure 4.3). This evidence points to the existence of a distinct subtype of pericytes in the heart during foetal development, being CD146$^{+}\alpha$SMA^{+}NG2^{+}.

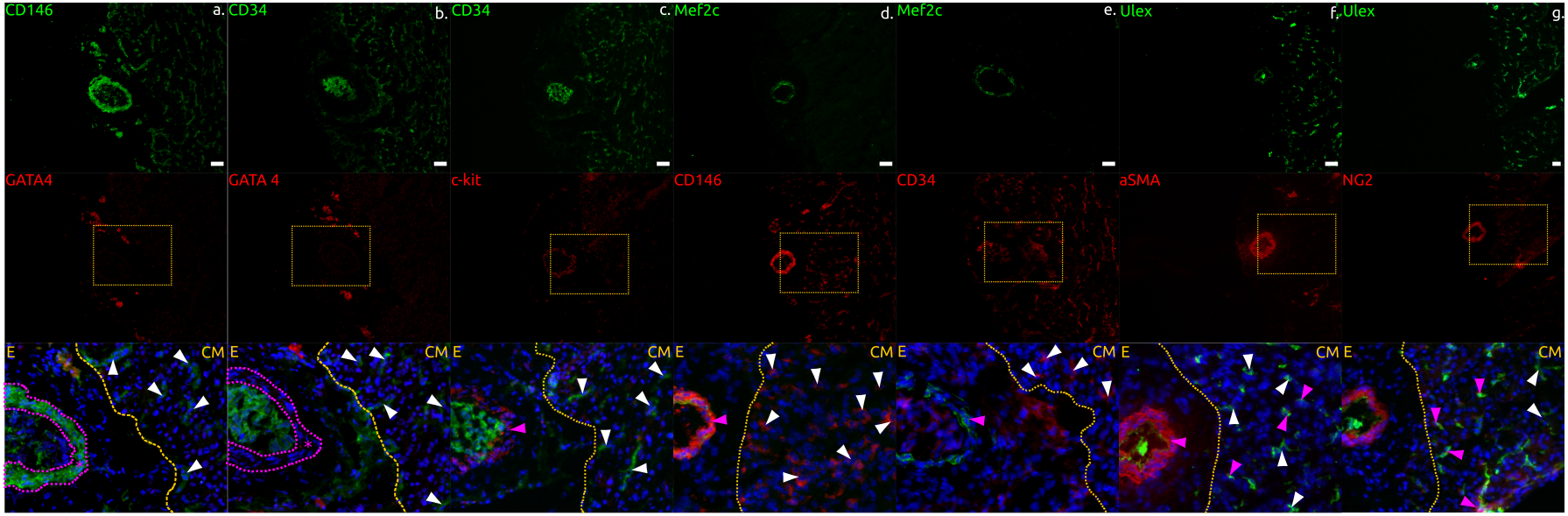

Figure 4.2: **Foetal perivascular cells differently express developmental cardiac markers.** Immunostaining on foetal human heart (a-g, 19 weeks gestation) for pericyte markers CD146, αSMA and NG2, endothelial cell markers CD34 and *Ulex europaeus* and cardiac related markers GATA4, c-kit and Mef2c shows that: (i) cardiac pericytes do not express GATA4 (a-b; white arrow, negative pericyte; magenta asterisk, negative perivascular layer); (ii) a fraction of CD146$^+$ pericytes exclusively express cardiac related markers Mef2c and c-kit (c-e; orange arrowhead, positive pericyte; magenta arrowhead, positive perivascular layer) surrounding arteries like in the epicardium (Ep) and the compact myocardium (CM); (iii) these Mef2c$^+$ pericytes also express αSMA and NG2, while not all CD146$^+\alpha$SMA$^+$NG2$^+$ express Mef2c revealing a specific subpopulation within this triple positive subset of pericytes (f-g); (iv) CD146$^+\alpha$SMA$^+$NG2$^+$ arteriolar pericytes only express Mef2c at 19 weeks of gestation; (v) only fractions of human cardiac pericytes express most common markers αSMA and NG2 (f-g) clearly showing the heterogeneity of pericytes.

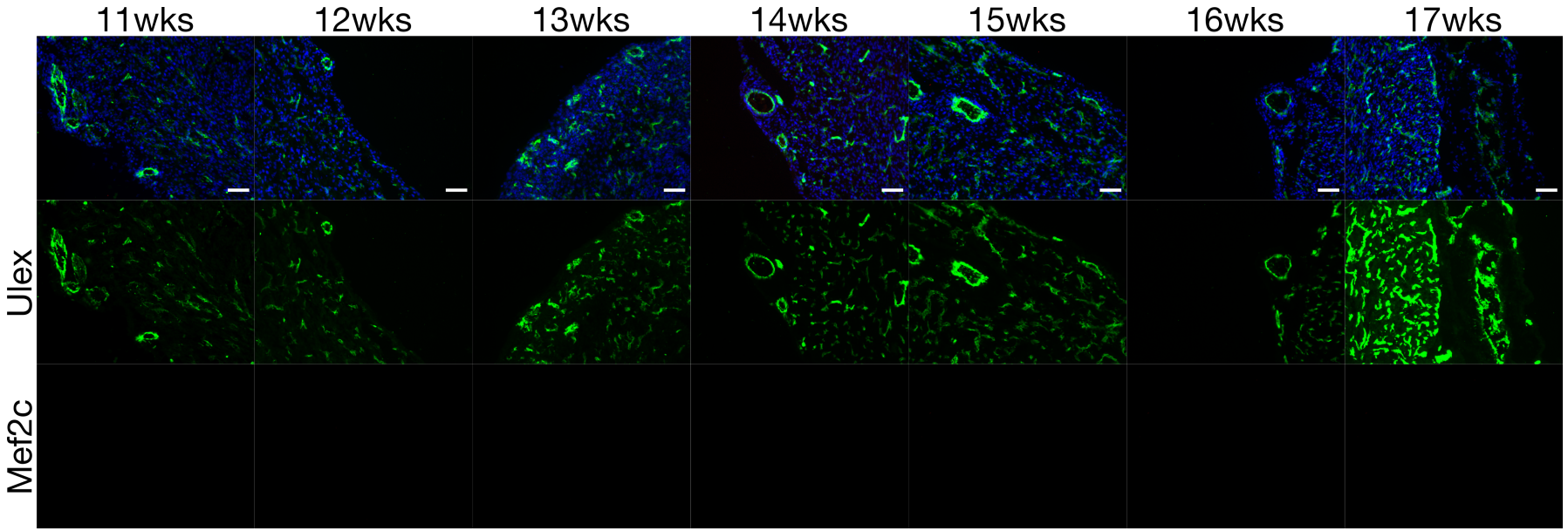

Figure 4.3: **Mef2c is not expressed on cardiac tissues ranging 11 to 17 weeks of development.** Immunostaining on foetal human heart ranging 11 to 17 weeks of gestation endothelial cell marker *Ulex europaeus* and cardiac related marker Mef2c shows no expression of Mef2c in the cardiac tissue at these developmental stages. Scale bar = 50μm.

4.3.3 Different cardiac compartments have significantly different vascularisation levels, while constant during development

Whole foetal heart sections were stained and scanned. Different heart compartments were dissected out during the imaging analysis and the epicardium and compact myocardium were separately quantified for total number of blood vessels as shown in Figure 4.4.

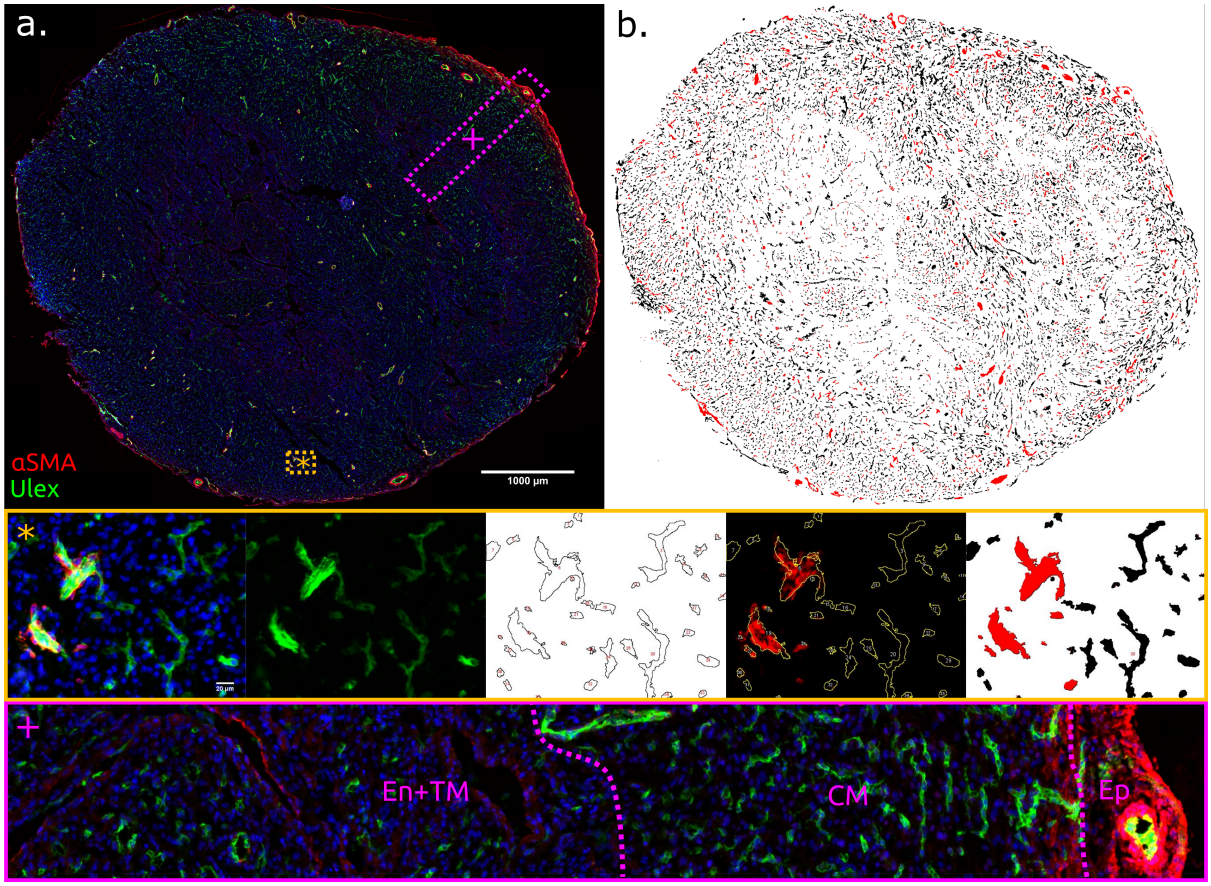

Figure 4.4: **Blood vessel quantification on foetal cardiac whole sections.** Frozen cardiac sections were stained for an endothelial cell marker and a perivascular cell marker, then whole scanned (a). Using the FIJI software, the epicardium (Ep), compact myocardium (CM) and endocardium+trabecular myocardium (En+TM) were dissected out (+). A specific computer script was coded to automatically isolate individual blood vessels and characterise them according to whether their perivascular layer is positive or negative for the tested marker. This script takes the whole image, isolated the channel with the endothelial marker (here green), indentifies individual blood vessels, overlays the perivascular marker channel and identifies with blood vessel have a positive and negative perivascular layer, as shown in close view in (*) and overall in (b).

Histological measurements of the tissue area (Figure 4.5a) and total blood vessel quantification (Figure 4.5b) allowed the calculation of the total coverage of blood vessels in the different heart compartments on the developing human heart. This analysis revealed higher vascularisation of the compact myocardium compared to the epicardium (Figure 4.5c).

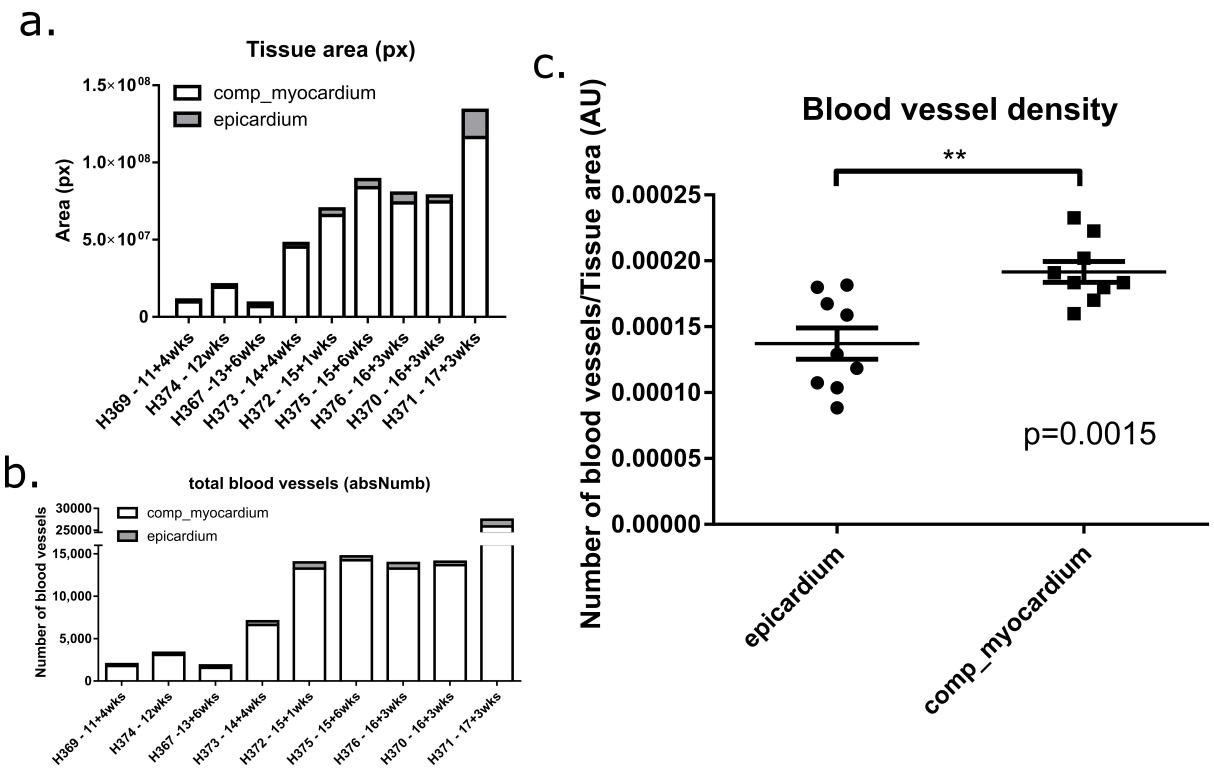

Figure 4.5: **Human foetal epicardium is less vascularised than the compact myocardium.** Histological image analysis allowed to measure: (a) section area on the tissue in pixels for the epicardium (black) and compact myocardium (comp_myocardium, white); and (b) number of distinguishably different blood vessels. The ratio between number of blood vessels quantified and tissue area calculated (c) the blood vessel density. Analysis reveals that: (i) Epicardium maintains its total area while compact myocardium dramatically increases in size during development; (ii) Number of blood vessels increases in proportion to the tissue area; and (iii). Overall vascularisation remains homogeneous within regions during development, with the compact myocardium being more vascularised than epicardium (Unpaired t-test, n=9, mean±SD, p-value=0.0015).

4.3.4 The epicardium is enriched in vessels with an αSMA$^+$ perivascular layer compared to the compact myocardium

Quantification of the perivascular layer revealed that, while less vascularised, the epicardium contains a higher percentage of αSMA$^+$ blood vessels compared to the compact myocardium (Figure 4.6a-b). Similar analysis was performed for NG2, but stainings contained excessive background impeding a whole section image analysis.

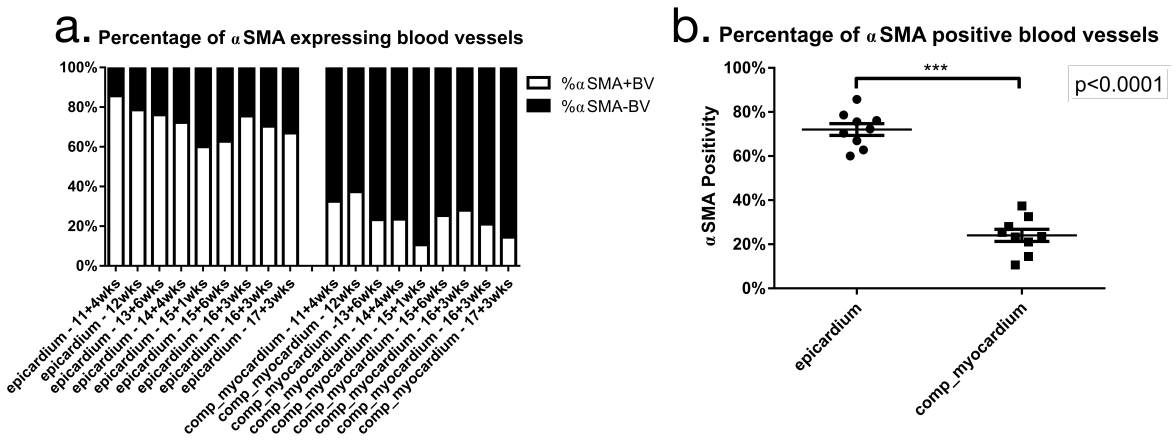

Figure 4.6: **The human foetal epicardium contains a higher percentage of αSMA$^+$ perivascular layered blood vessels than the compact myocardium.** Quantifications, shown per sample (a) and grouped (b), of the totality of the blood vessels reveals that: (i) only a fraction of blood vessels are covered by pericytes positive for αSMA; and (ii) the epicardium contains more αSMA$^+$ PC-associated blood vessels, in percentage, than the compact myocardium (Unpaired t-test, n$=$9, mean$\pm$SD, p-value$<$0.0001).

4.3.5 Native response of cardiac pericyte subsets to myocardial infarction in a large animal

The pig is an excellent model of human cardiac ischaemia, as the porcine heart is anatomically and physiologically similar to the human [185, 186]. The mouse has been widely used to study native perivascular cell behaviour following cardiac injury, but the adult mouse heart is too small to properly mimic the human heart. In fact, the adult mouse heart is smaller than a human foetal heart older than 12 weeks of gestation, while the porcine heart is physiologically equal to the adult human heart. Porcine histological samples after acute cardiac ischaemia by left anterior descending coronary artery ligation were provided by Dr. Montse Rigol. Sections were stained for perivascular cell markers.

4.3.6 Porcine pericytes can be detected *in situ* using human pericyte markers

There were no published studies looking at the perivascular cell compartment in porcine tissues, thus the same antibodies as used for human tissues were tested against pig antigens. After multiple antibodies were tested, proper identification of perivascular cells was achieved using CD146, αSMA and NG2 on subcutaneous white adipose tissue (Figure 4.7).

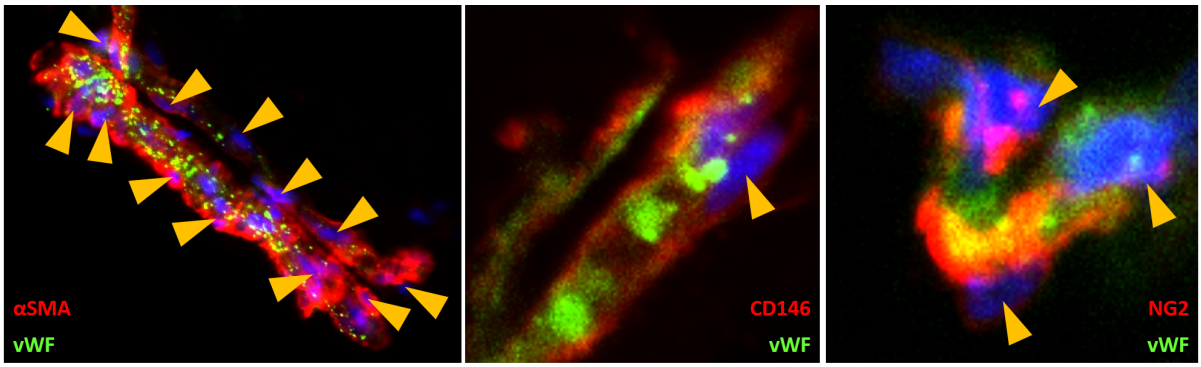

Figure 4.7: **Porcine adipose-resident pericytes express the same markers as human pericytes.** IHC on pig subcutaneous fat for pericyte markers CD146, αSMA and NG2, negative for endothelial marker vWF. Positive pericytes (orange arrowhead). 20x magnification.

Similarly, immunohistochemistry was performed on adult porcine ventricle in healthy and infarcted areas, 2 and 60 days post myocardial infarction (MI). In the healthy area 2 days postMI, the vast majority of blood vessels are covered with a CD146$^{+}\alpha$SMA^{+} perivascular cell layer, while only some large vessels and fewer microvessels are covered with NG2^{+} perivascular cells (Figure 4.8).

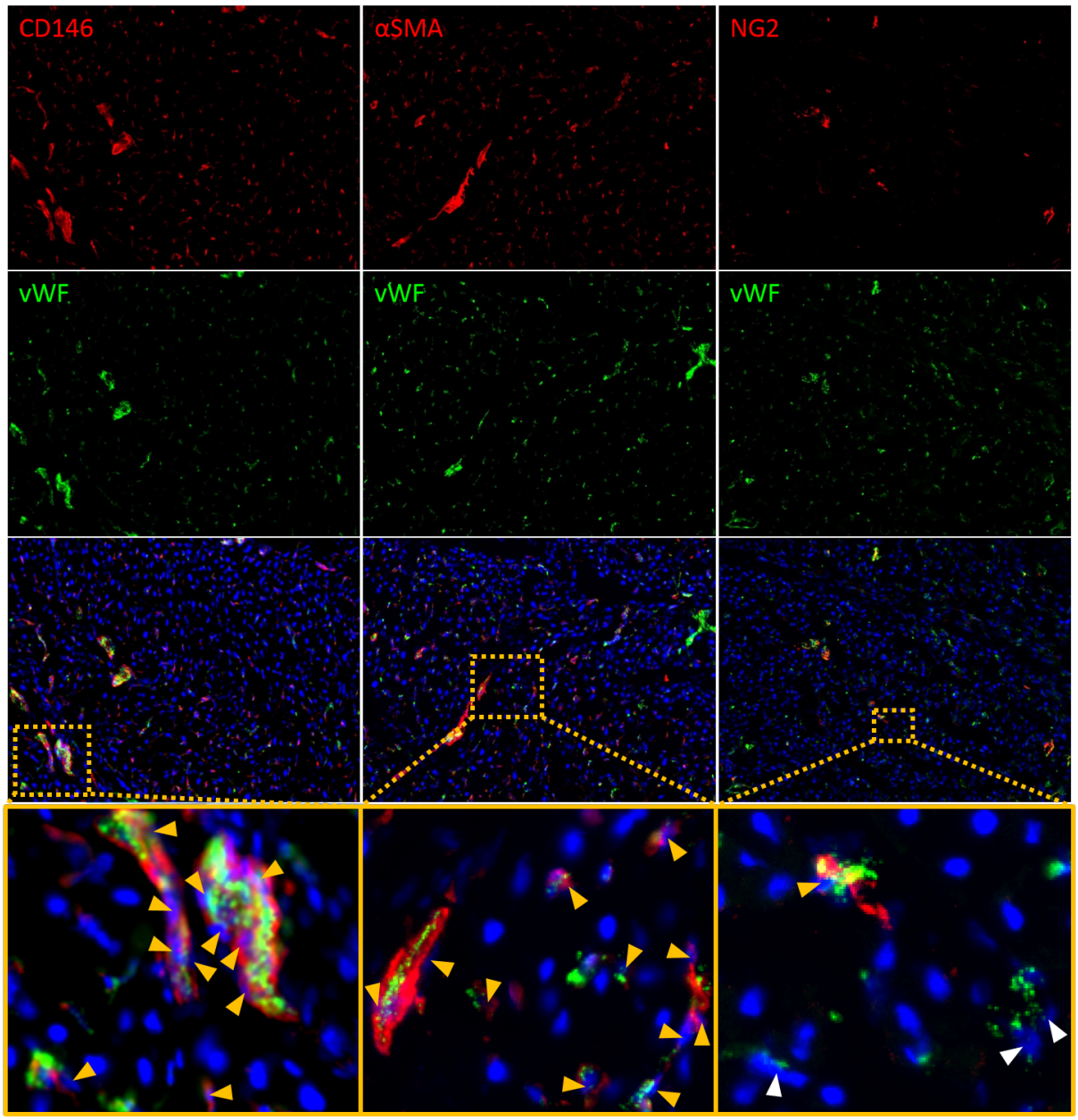

Figure 4.8: **Porcine cardiac pericytes express the same markers as human pericytes.** Immunofluorescence staining on a healthy area of adult porcine left ventricle 2 days after acute myocardial infarction for the pericyte markers CD146, αSMA and NG2, negative for the endothelial marker vWF. Positive pericytes (orange arrowhead), negative pericytes (white arrowhead). 20x magnification.

4.3.7 Pericyte markers are detected in non-perivascular areas following acute myocardial infarction

Following acute myocardial infarction, an important decrease in the microvasculature can be appreciated after two days whereas larger vessels remain. As the perivascular layer remains intact, cells expressing αSMA or CD146 can be found not associated to any endothelial cell (Figure 4.9).

60 days following acute myocardial infarction, the tissue in the remote area remains unchanged when compared to a 2 day post MI heart (Figure 4.10).

60 days following the infarction, no microvasculature could be detected with few large vessels present. Most of these large blood vessels had an abnormal perivascular layer: a large number of cells positive for NG2, CD146 and αSMA were found surrounding large vessels, while not in contact with the endothelial layer (Figure 4.11). These cells seem to be migrating out of the perivascular layer, possibly originated from perivascular cells. Nevertheless some vessels maintain normal perivascular coverage suggesting again functionally distinct subsets of pericytes with specific roles during cardiac remodelling.

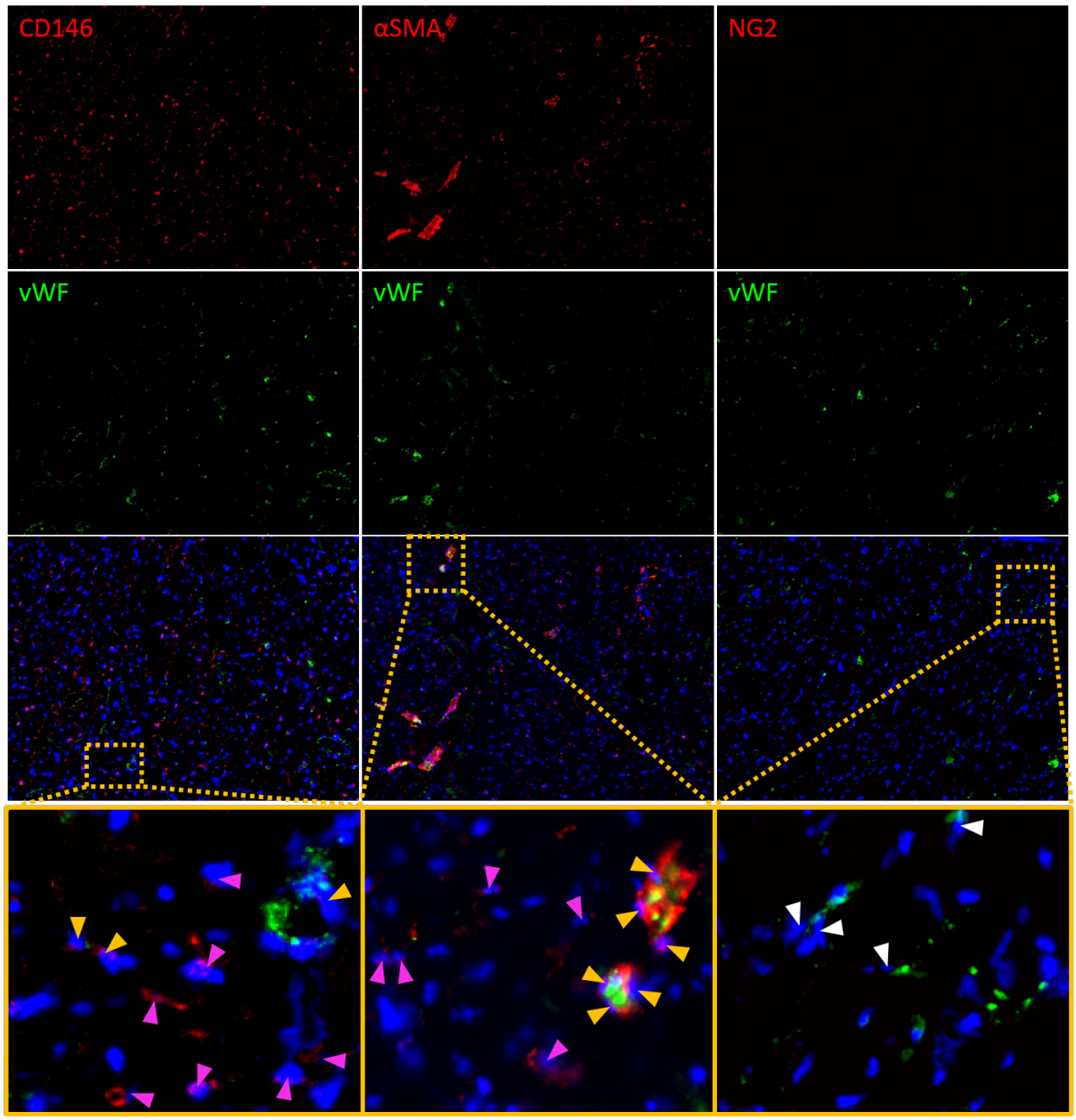

Figure 4.9: **Porcine pericytes in a 2-day post-myocardial infarction heart.** Immunofluorescence staining on an infarcted area of adult porcine left ventricle 2 days after acute myocardial infarction for pericyte markers CD146, αSMA and NG2 and endothelial marker vWF. Endothelium-associated positive pericytes (orange arrowhead), endothelial non-associated positive pericytes (magenta arrowhead), negative pericyte (white arrowhead). 20x magnification.

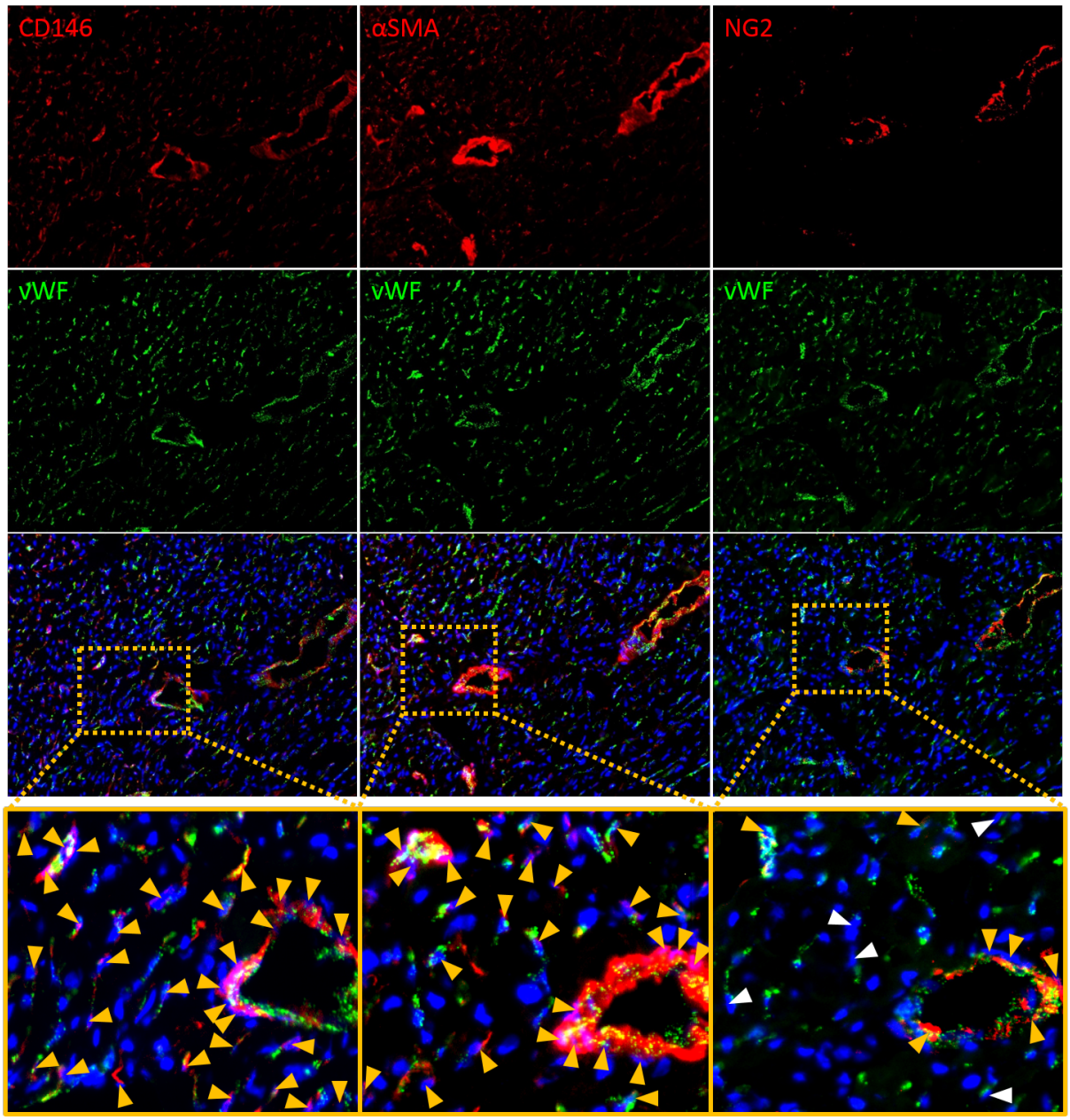

Figure 4.10: **Pericytes in a non-infarcted area of the pig heart.** Immunofluorescence staining on a healthy area of adult porcine left ventricle 60 days after acute myocardial infarction for pericyte markers CD146, αSMA and NG2 and endothelial marker vWF. Positive pericytes (orange arrowhead), negative pericytes (white arrowhead). 20x magnification.

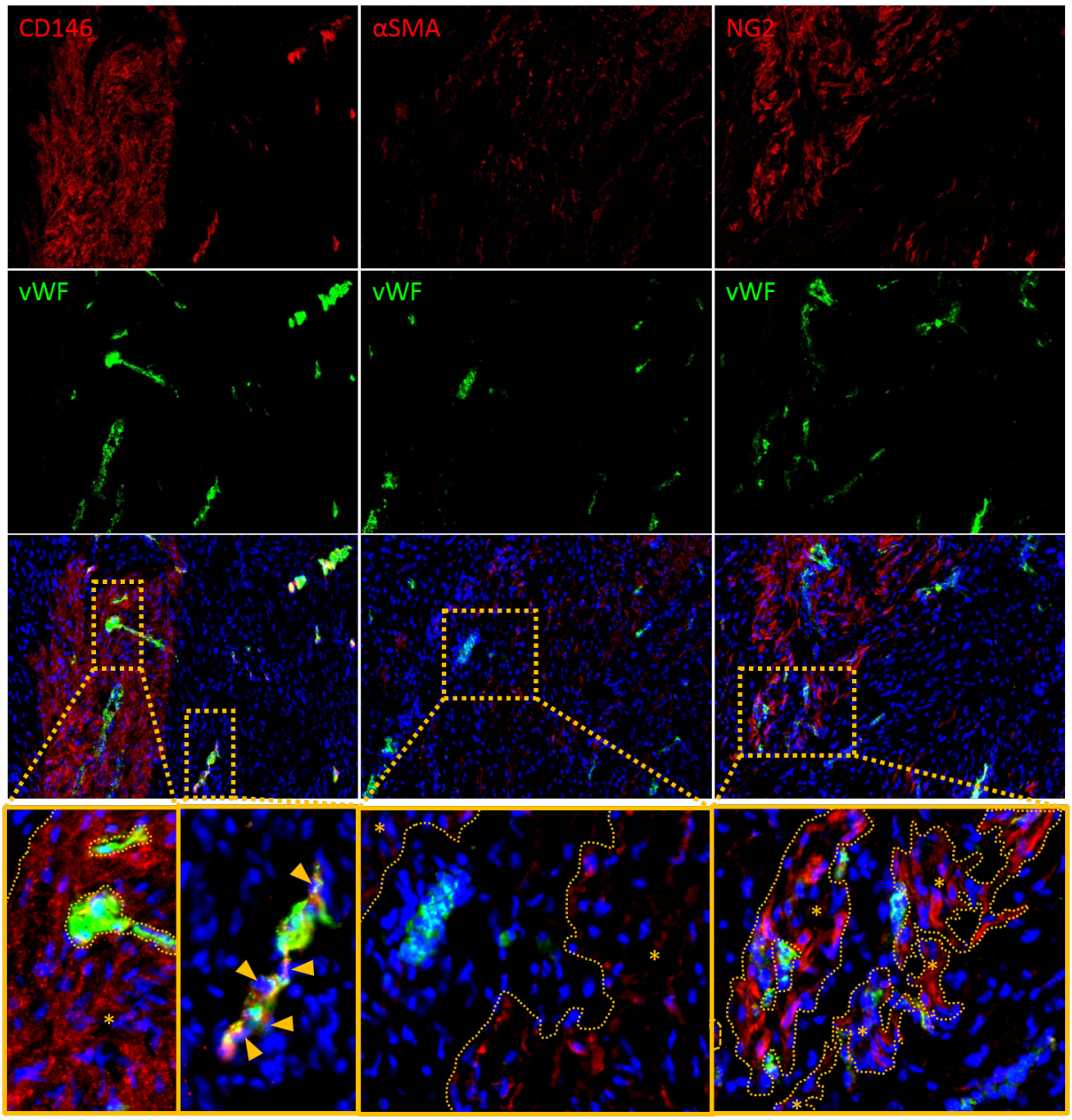

Figure 4.11: **Pericytes in a 60 days post-myocardial infarction pig heart.** Immunofluorescence staining for pericyte markers CD146, αSMA and NG2 and endothelial marker vWF. Positive pericytes (orange arrowhead), positive non-pericytes cells (orange asterisk). 20x magnification.

4.3.8 αSMA can be detected by intracellular flow cytometry in human tissues

As αSMA is an intracellular protein, the conventional cell staining method used in the laboratory was no longer effective to quantify by FACS expressing cells in suspensions of whole organs and a new method was designed to stain intracellular markers in the perivascular fraction of the isolated cell suspension (see section 2.2.4). This protocol involves cell permeabilisation that results in cell death, thus preventing the use of this technique for cell sorting with the intent to establish cell cultures. The newly designed and optimised protocol successfully stains perivascular cells and allows detection of subsets based on CD146 in multiple tissues (Figure 4.12a). Interestingly, the percentage of CD146$^+\alpha$SMA$^+$ pericytes is rather homogeneous in the foetal skeletal muscle, but much more variable in the foetal heart (Figure 4.12b). This is likely due to bigger variations in the developing heart not present in the skeletal muscle, affecting the total distribution of subtypes.

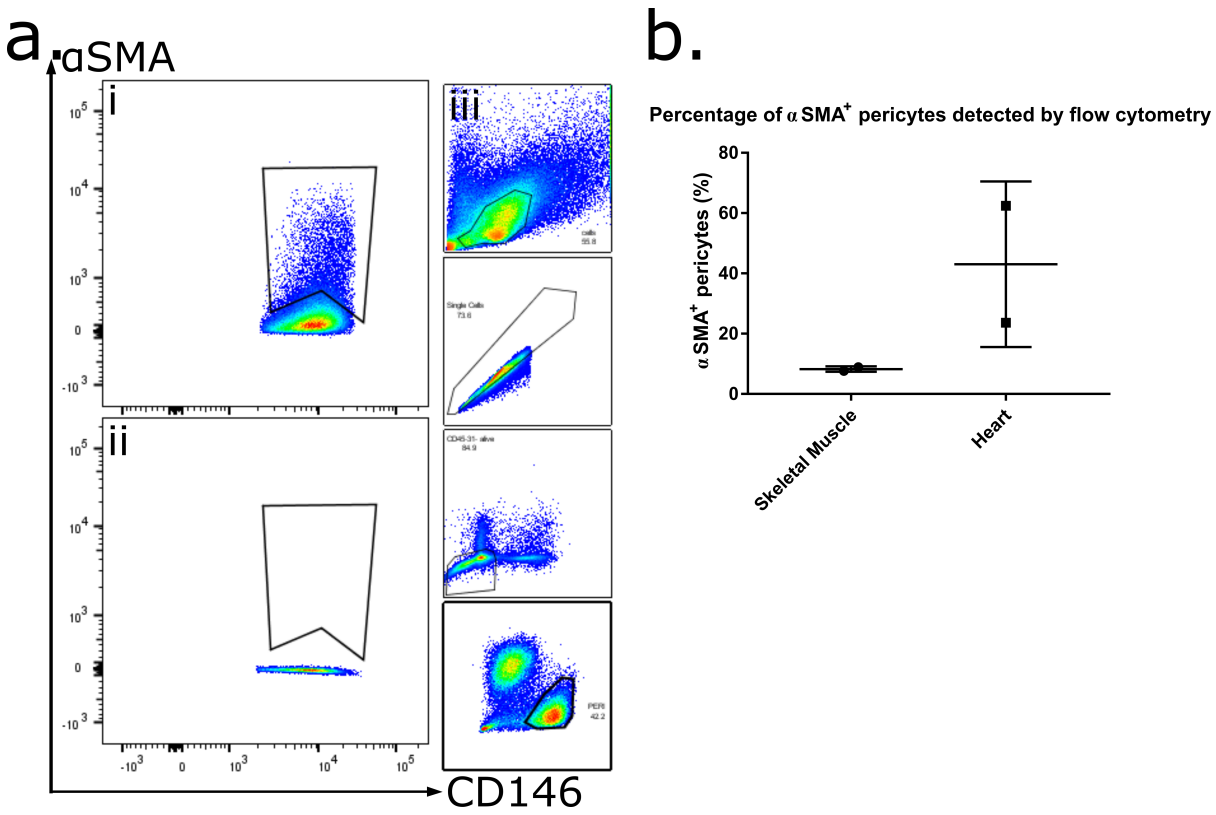

Figure 4.12: **Subsets of CD146$^+$ pericytes based on αSMA expression can be detected by intracellular flow cytometry.** The newly generated protocol successfully stains subsets of perivascular cells based on CD146 and αSMA in foetal heart and skeletal muscle. Flow plot (a) is representative of the αSMA distribution (a_i) compared to the isotype control (a_{ii}) on gated pericytes (a_{iii}). Percentages of CD146$^+\alpha$SMA$^+$ pericytes was rather homogeneous in skeletal muscle, but much more variable in heart (b; n=2, no statistical analysis).

4.3.9 Subsets of human pericytes based on CD146, αSMA and NG2 can be detected by intracellular flow cytometry

When used in combination with NG2, this protocol enabled the identification and quantification of subsets of pericytes based on CD146, αSMA and NG2 (Figure 4.13).

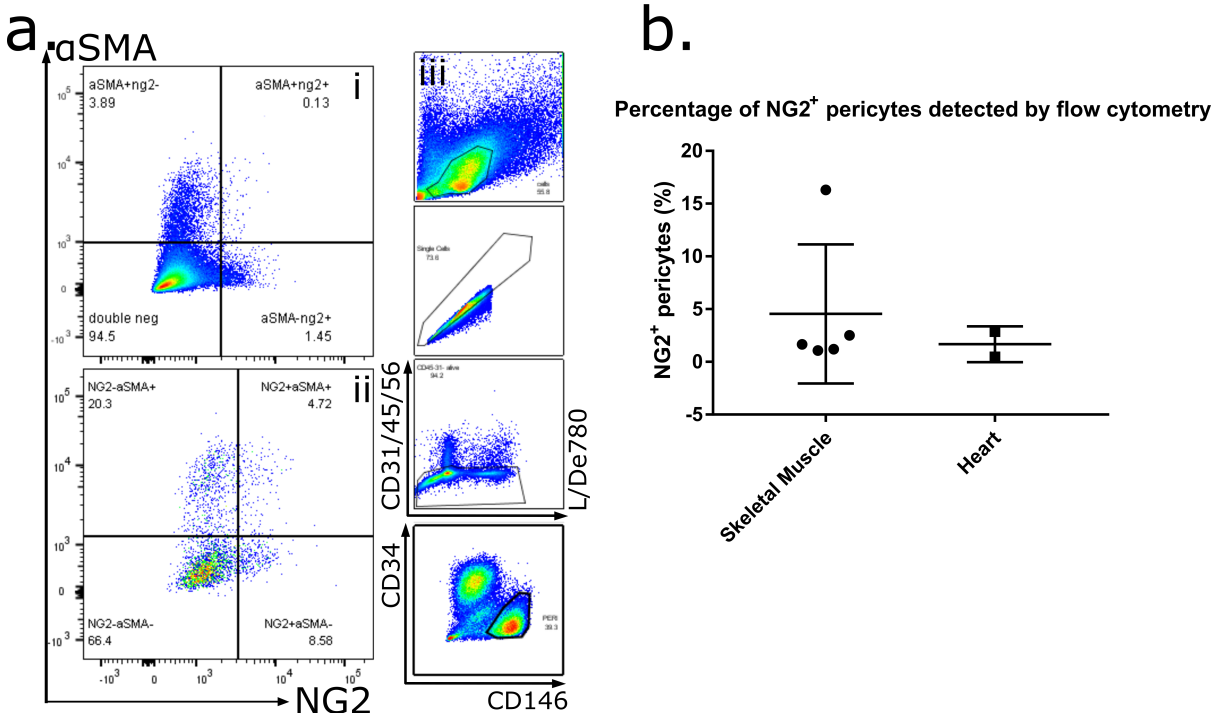

Figure 4.13: **Subsets of pericytes based on CD146, αSMA and NG2 can be detected by intracellular flow cytometry.** Intracellular staining identifies subsets of CD146$^+$ pericytes based on αSMA and NG2 in skeletal muscle (a$_i$) and foetal heart (a$_{ii}$) based on the standard gating strategy including the dead cells (a$_{iii}$). Percentages of CD146$^+$NG2$^+$ pericytes was homogeneous in both tissues (b; n$_{heart}$=2, n$_{skeletalmuscle}$=5, no statistical analysis).

4.3.10 CD146$^+$NG2$^+$ pericytes exhibit high mortality rate while undergoing cell isolation

When NG2 was included in the intracellular staining protocol, elevated cell death was observed in the CD146$^+$NG2$^+$ subset (Figure 4.14). While autofluorescence in multiple channels is frequent in dead cells, these cells have a very specific immunophenotype CD146$^+$ CD34$^-$CD31$^-$CD45$^-$CD56$^-$NG2$^+$ αSMA$^{+/-}$, therefore having been negatively selected for at least two other fluorescence channels. These results might indicate that the cells have died very recently prior to the fixation step of the new protocol (about 1h20min into the protocol), possibly during cell isolation.

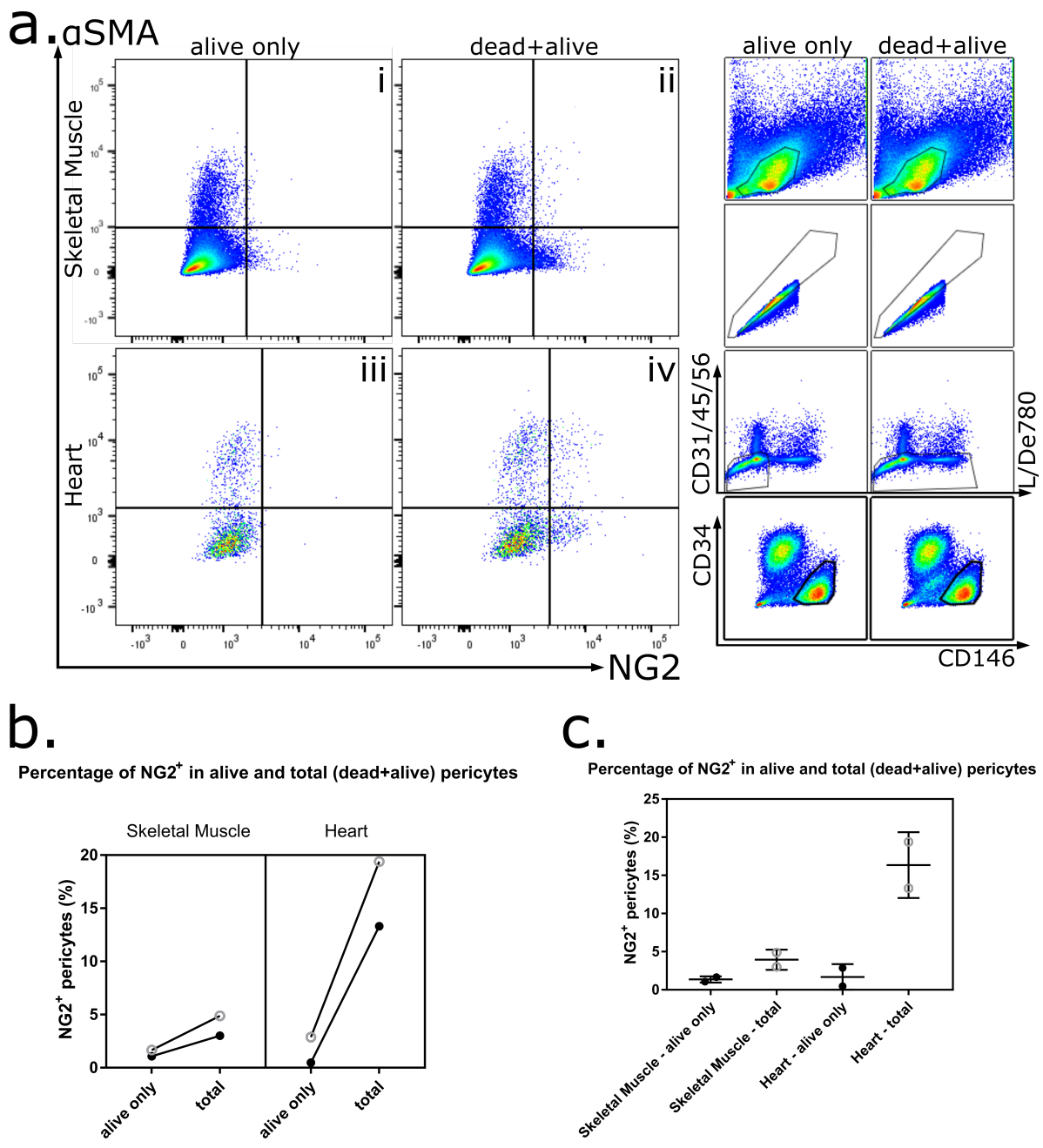

Figure 4.14: **The majority of NG2$^+$ pericytes are positive for the cell death marker live/death e780.** While αSMA$^+$NG2$^+$ subsets of CD146$^+$ pericytes are detected, the NG2$^+$ subtype is expressed in low percentages in both skeletal muscle (a_i) and heart (a_{iii}). When L/De780$^+$ dead cells are included in the analysis there is an increase in the percentage within the NG2$^+$ subset, while the αSMA$^+$ subsets remain the same (a_i,a_{iv}). These CD146$^+$NG2$^+$ pericytes are negative for CD31, CD34, CD45 and CD56, and a fraction also negative for αSMA, indicating the signal detected is not autofluorescence commonly found in dead cells but true NG2 fluorescent labelling. Thus a majority of CD146$^+$NG2$^+$ pericytes appear to be dead. (b-c) shows the quantifications (n=2, no statistical analysis).

Sequential digestion did not improve cell survival.

It was suspected that low cell viability could be due to a long exposure to the digestion enzymes used to dissociate the tissues. Sequential dissociation was performed to ensure a maximal tissue exposure of 5 min to active enzymes immediately quenched. The survival rate of the $CD146^{+}NG2^{+}$ subset of pericytes was similar (Figure 4.15), indicating that long exposure to enzymatic action is not compromising the viability of this particular cell subset.

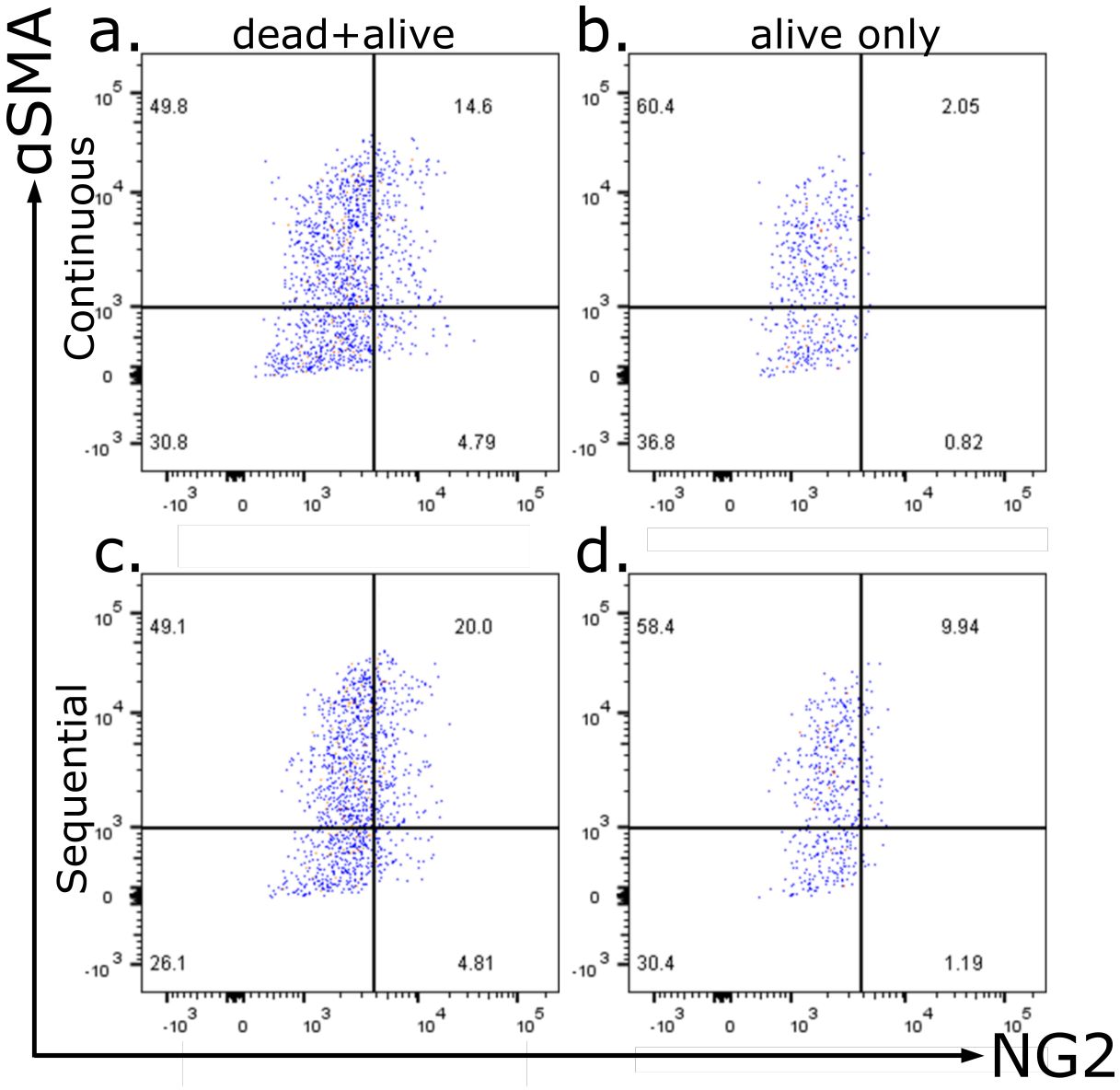

Figure 4.15: **Sequential digestion did not improve NG2$^+$ survival.** Foetal heart was digested using a continous digestion (a-b) or a sequential one with a maximum exposure time to active enzymes of 5 min (c-d). Plots a and c show total gated CD146$^+$ pericytes, while plots b and d show the same gated pericytes with cells dead excluded in the gating process. In both digestions, the NG2$^+$ percentage is extremely low within alive pericytes thus indicating the sequential digestion did not improve the amount of cells isolated.

Alternative protocols using other digestion enzymes and apoptosis inhibitors did not improve cell survival.

Two more elements of the standard isolation protocol were tested: the presence of FCS during the dissociation and the lysis of red blood cells following filtration. Some studies use FCS to provide nutrients to the cells while the tissue is being digested, while our standard protocol adds serum following digestion for the same reason, as well as to quench active enzymes thus protecting the cells from longer exposure. When FCS was added to the digestion mix tissue dissociation remained inaccurate even when extended from 45 min to 1h30, at which point cell viability decreased dramatically. When digested for 45 minutes, a higher cell death was observed when dissociated with FCS thus it was determined that this modification reduced the efficiency of the current protocol.

The second factor from the current protocol tested was the lysis buffer included to eliminate red blood cells from the cell suspension to clear and avoid unspecific cell labelling for analysis with the flow cytometer. Nevertheless, as lysis works based on osmotic pressure, it was considered that this could not only affect red blood cells but also somehow more fragile populations of stromal cells such as $NG2^+$ pericytes. When the lysis step was removed from the protocol, not only did cell suspension become dirtier from red blood cells as predicted, but a higher proportion of dead $NG2^+$ cells appeared to be present in the cell suspension, thus again the current isolation protocol was deemed better.

The cell surface part of the NG2 proteoglican is linked to the process of anoikis, a specific apoptosis program triggered by an abrupt separation of the cell from the rest of the tissue and the ECM [187, 188]. Theorising that NG2 was mediating anoikis in isolated perivascular cells, novel digestion cocktails were tested that included apoptosis inhibitors and metalloproteases that should inhibit anoikis. A commercially available caspase inhibitor, Z-vad-FMK, was tested, as was a collagenase III metalloprotease, described to cleave NG2 thus inhibited the subsequent anoikis process. Neverthe-

less, none of these seemed to increase the effectiveness of the cell isolation to obtain a higher amount of NG2^{+} cells (Figure 4.16).

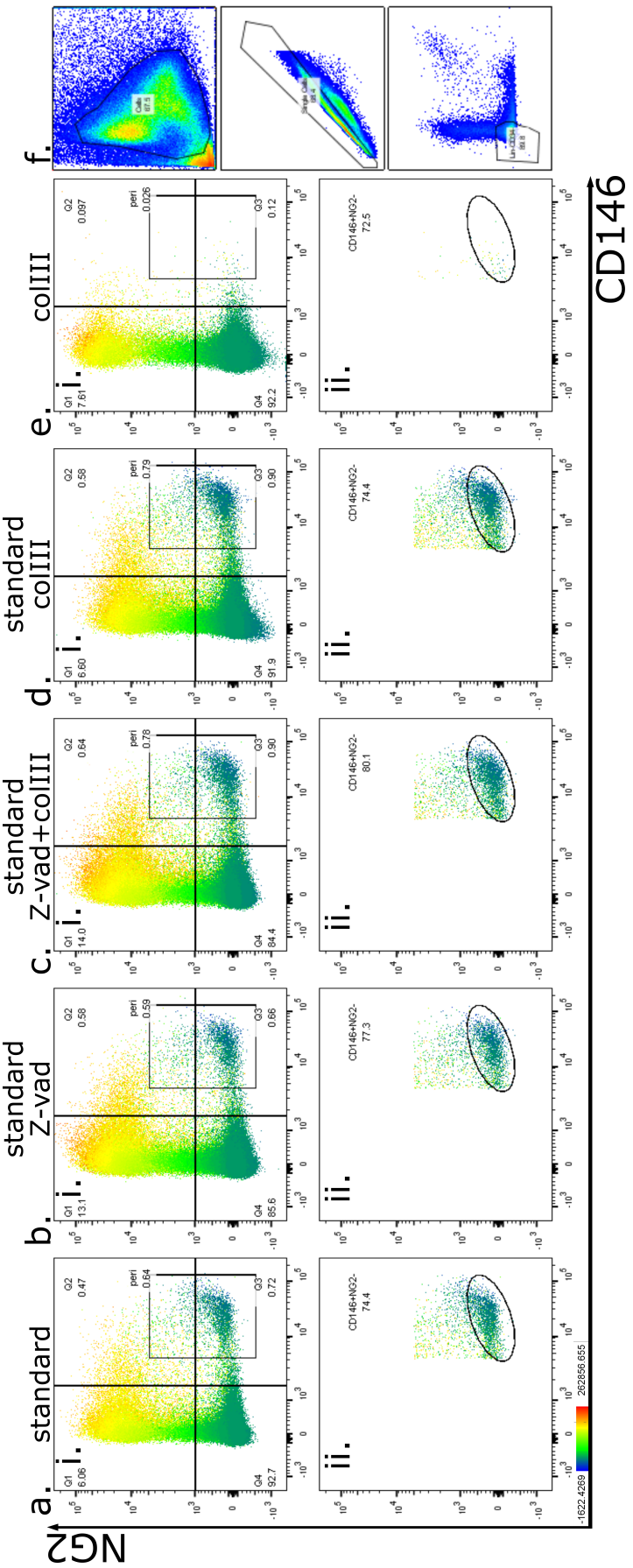

Figure 4.16: **Apoptosis inhibitors and metalloproteases did not improve NG2 yield.** Foetal skeletal muscle was digested using 5 different digestion mixes: (a) standard mix containing collagenases I, II and IV, (b) standard mix supplemented with caspase inhibitor Z-Vad-FMK (BD), (c) standard mix supplemented with Z-Vad-FMK and collagenase III (Stem Cell technologies), a specific metalloprotease, (d) standard mix supplemented with collagenase III, (e) collagenase III only. Stromal cells were gated $CD31^{-}CD45^{-}CD56^{-}$ and $CD34^{-}$ as shown in (f), and shown in (i). Specific $CD146^{+}$ pericytes were gated and shown in (ii). Heatmap coloring represents the intensity of the live/dead marker, where less intensity translates in more alive cells.

4.3.11 Do surviving CD146^{+}NG2$^{+/-}$ pericytes exhibit a different potential *in vitro*?

While the CD146^{+}NG2^{+} pericyte overall survival rate was not successfully increased, remaining living CD146^{+}NG2^{+} pericytes (0.145$\pm$0.15% of the total cells) and their CD146^{+}NG2^{-} pericyte counterpart (1.73$\pm$0.37% of the total cells) were sorted from 3 foetal skeletal muscle samples (Figure 4.17). As the live/dead marker DAPI is used in the same excitation channel as CD31 and CD45, quantification of living and dead cell was not possible. Sorted cells were analysed to confirm the purity of the sorted subpopulations. Successful cultures were established for all 6 sorted cell populations despite low cell yields for the NG2^{+} subset (Table 4.1).

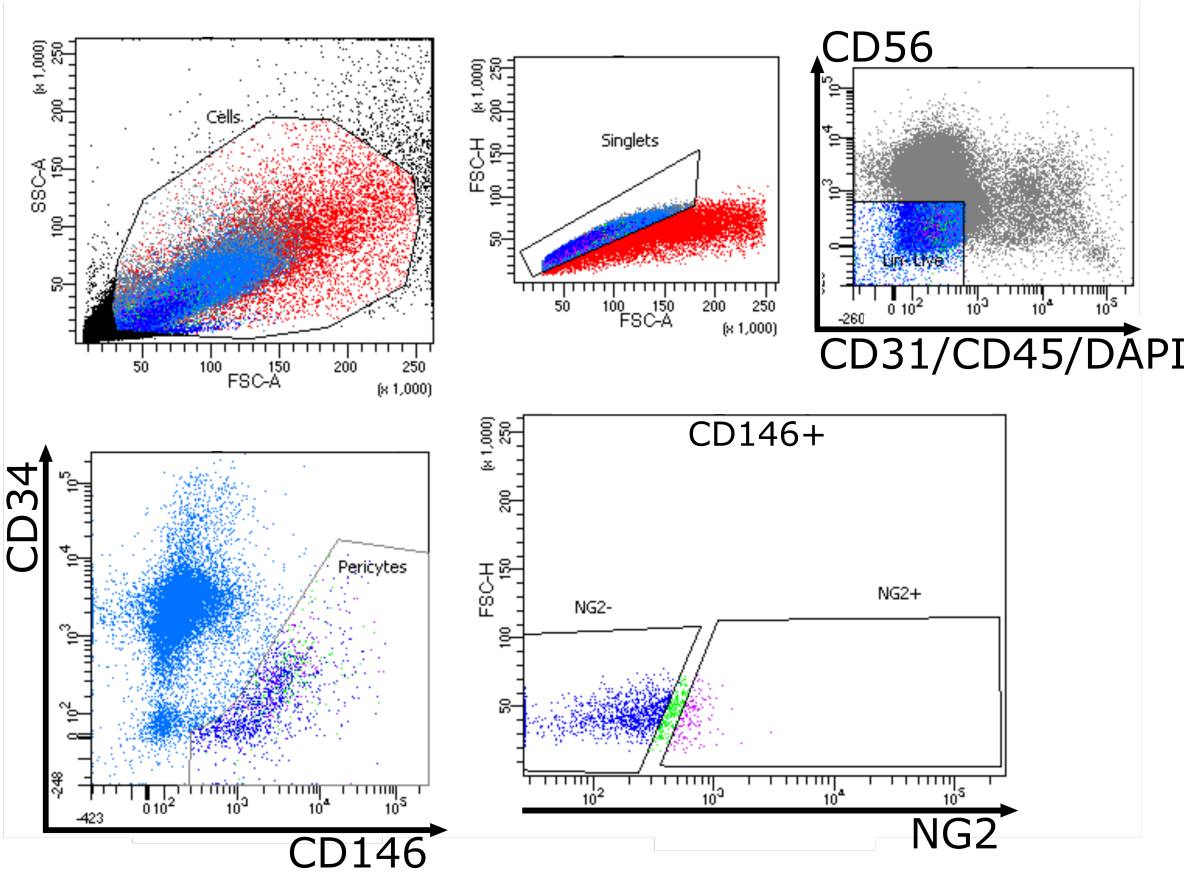

Figure 4.17: **Foetal pericyte subset sorting.** Example of dot plots showing the sorting strategy to isolate living CD146^{+}NG2$^{+/-}$ pericyte subsets, here shown foetal skeletal muscle. Gates were set using FMOs with isotypes controls.

Table 4.1: FACS sorting of CD146^{+}NG2$^{+/-}$ pericyte subsets.

Sample	Subset	Cell yield
SkM397	NG2^{+}	1,062
gestation: 17 weeks	NG2^{-}	88,000
SkM398	NG2^{+}	300
gestation: 14 weeks	NG2^{-}	15,000
SkM399	NG2^{+}	12,100
gestation: 16 weeks	NG2^{-}	118,000

Cell cultures derived from CD146$^+$NG2$^-$ pericytes contain a higher fraction of PDGFRα^+ cells than cultures derived from CD146$^+$NG2$^+$ pericytes

After 4 passages, cell numbers for each cell line were sufficient to plate all assays. Immunocytochemistry revealed only a higher percentage of cells expressing PDGFRα on the cell lines derived from NG2$^-$ pericytes (Figure 4.18). NG2 is acquired by the NG2$^-$ pericyte derived cell line (Figure 4.18c,j), and both cell lines contain a fraction of cells expressing CD56 and CD34 (Figure 4.18f-g,j). None of the cell lines express CD31 (Figure 4.18h,j).

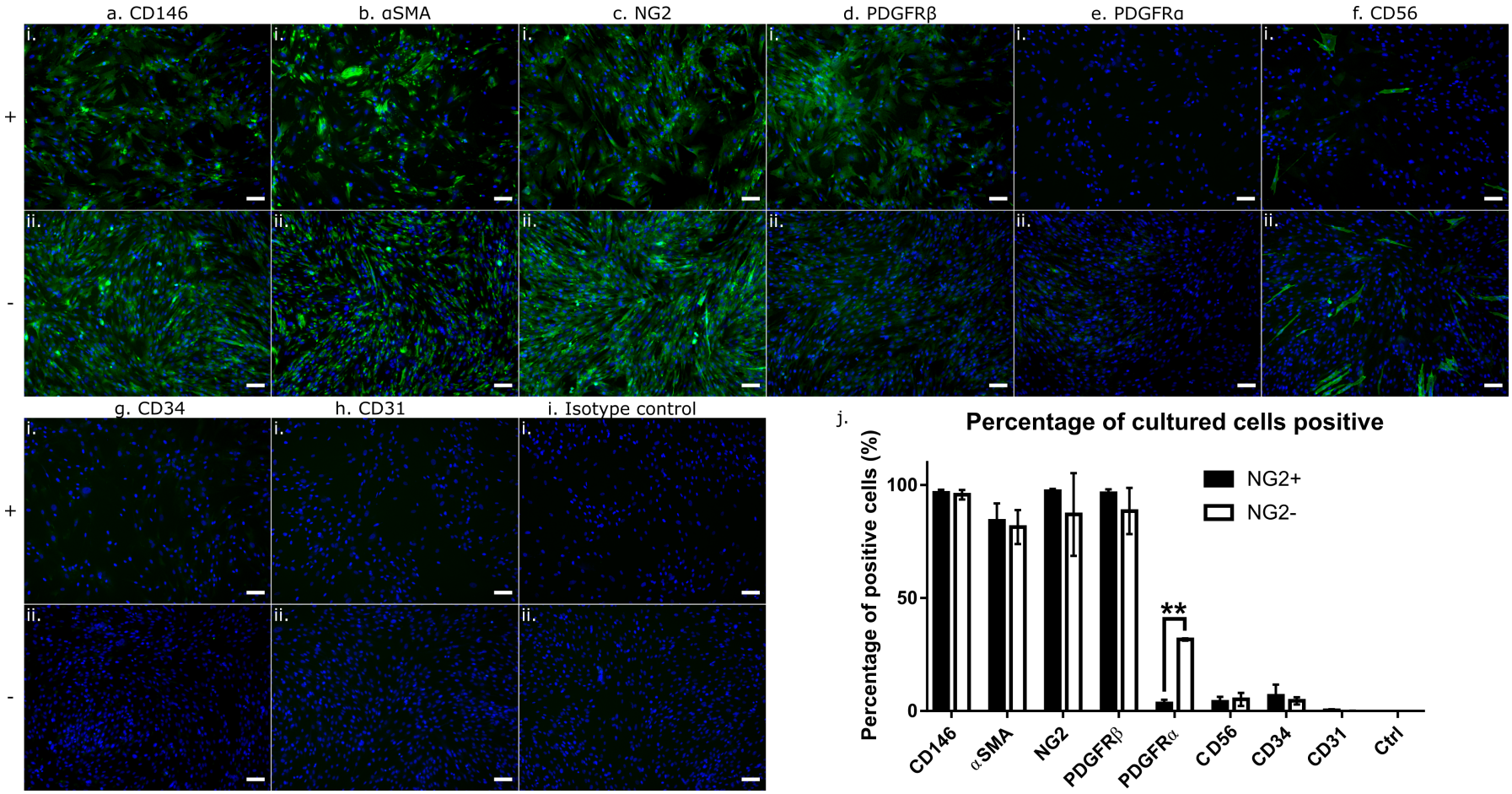

Figure 4.18: **NG2$^-$ pericyte derived populations contain a higher proportion of PDGFRα than the NG2$^+$ after 5 passages.** Immunocytochemistry on ($_{i.}$)NG2$^+$ and ($_{ii.}$)NG2$^-$ pericytes for (a) CD146, (b) αSMA, (c) NG2, (d) PDGFRβ, (e) PDGFRα, (f) CD56, (g) CD34, (h) CD31 and (i) isotype control. (j) Quantification of the postive cells for the three cell lines pooled by subtype (showed mean$\pm$SD, n=3, multiple t-test using Holm-Sidak method. **=p-value$<$0.01 Scale bar$=$50μm).

NG2$^-$ pericytes exhibit higher metabolic activity than NG2$^+$ pericytes

Viability assay revealed that from two donors the NG2$^-$ subtype was more metabolically active, processing more AlamarBlue reagent (Figure 4.19a,c), whereas for one of the donors, the NG2$^+$ subtype was marginally more active (Figure 4.19b). Interestingly, when put together, both subtypes from one of the donors were less active than the other two, pointing out to donor dependent variations (Figure 4.19d).

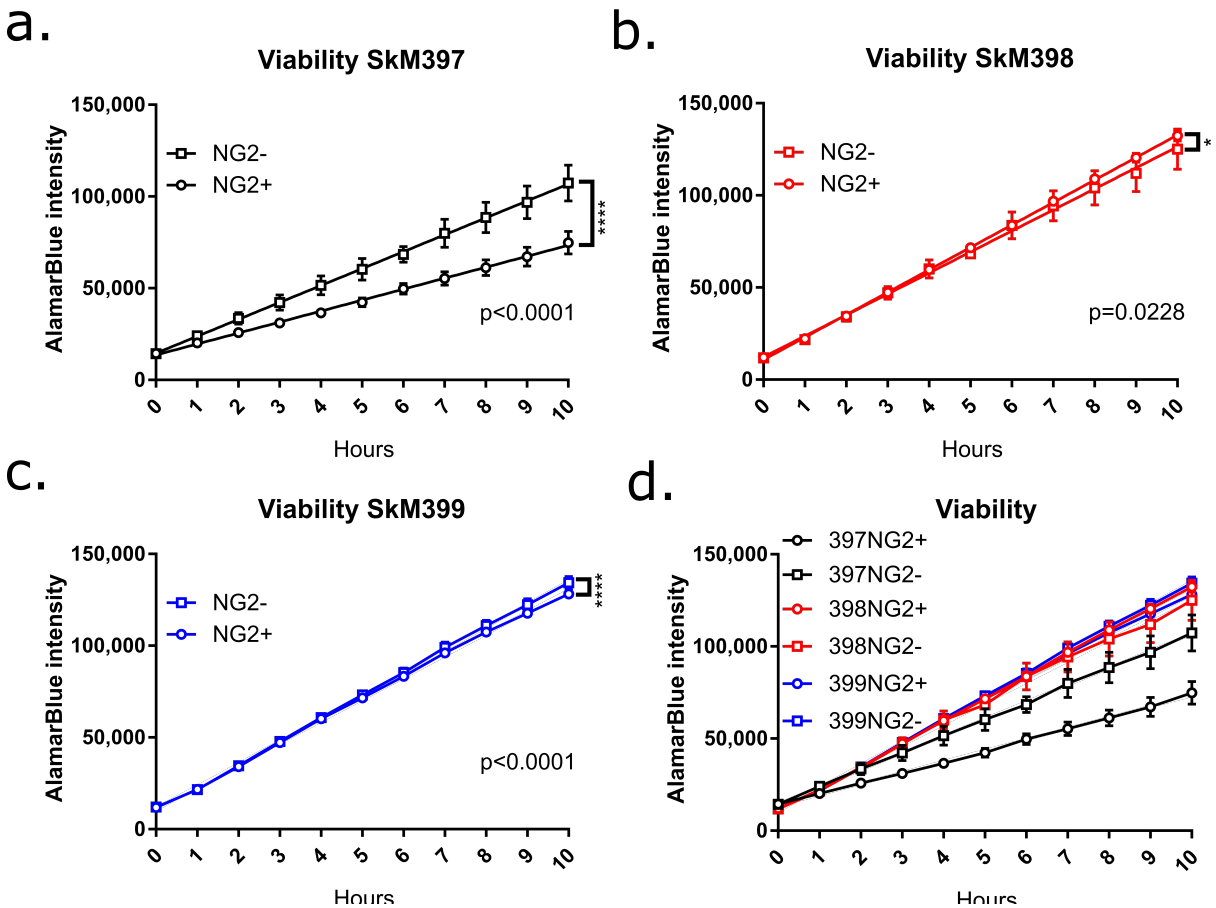

Figure 4.19: **NG2$^-$ pericytes exhibit higher metabolic activity.** NG2$^{+/-}$ pericyte subtypes from the three foetal samples tested SkM397 (a; 17 weeks old), SkM398 (b; 14 weeks old) and SkM399 (c; 16 weeks old). Linear regression curves of the intensity of AlamarBlue reagent in the well revealed significant differences when comparing NG2$^{+/-}$ pericyte subtypes (a-c, mean±SD, n=3, *=p-value$<$0.05, ****=p-value$<$0.0001). Same plots are displayed together revealing differences between donors (d, mean±SD, n=3, no statistical analysis showed).

Migration assay does not reveal consistent differences between sorted cell populations

Tested subtypes displayed different migration potentials in a donor dependent manner. Among the three donors tested, one displayed higher migration ability of the $NG2^-$ cell line (Figure 4.20a-e), one displayed no significant difference between cell lines (Figure 4.20f-j) and one displayed higher migration ability of the $NG2^+$ cell line (Figure 4.20k-o). Thus, this test remains inconclusive to describe whether one of the subtypes migrates faster than the other.

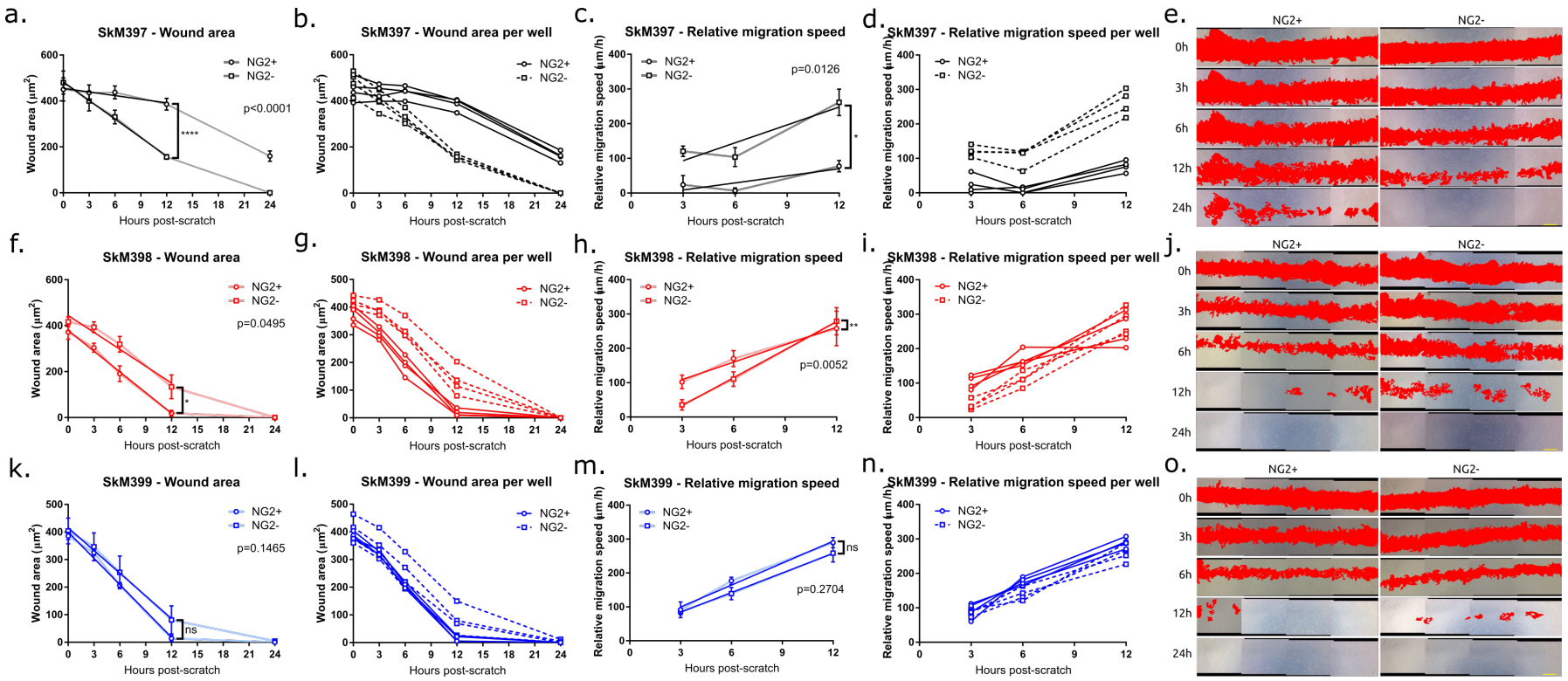

Figure 4.20: **Scratch assays revealed donor dependent differences in cell cultures when tested for their migration ability.** Pericyte NG2$^{+/-}$ subtypes from the three foetal samples tested SkM397 (a-e, 17 weeks old), SkM398 (f-j, 14 weeks old) and SkM399 (k-o, 16 weeks and 5 days old). Quantifications of the wound area (a,f,k) and relative speed migrations (c,h,m) show different behaviours within donors (linear regression, showed mean±SD, n=4; *=p-value$<$0.05, **=p-value$<$0.01, ****=p-value$<$0.0001). Representative images of the wound healing time points (e,j,o) show the wound area quantified (false colored in red, yellow bar = 500μm).

NG2$^-$ pericytes exhibit higher proliferation potential than NG2$^+$ pericytes

When plated for a growth assay, all three NG2$^-$ pericyte lines exhibited higher proliferation potential than their NG2$^+$ counterparts (Figure 4.21a-c), while the doubling time was only significantly different for one of the donor lines tested (Figure 4.21d-f). Despite the NG2$^-$ subtype showing greater ability within the same donor, when compared across donors, lines exhibit differences in a donor dependent manner, with NG2$^+$ lines displaying higher growth potential than NG2$^-$ lines from another donor: for instance NG2$^+$ pericytes from sample SkM399 perform better than NG2$^-$ pericytes from sample SkM398 (Figure 4.21g). Similarly, differences in doubling times are not the same when compared across donors (Figure 4.21h).

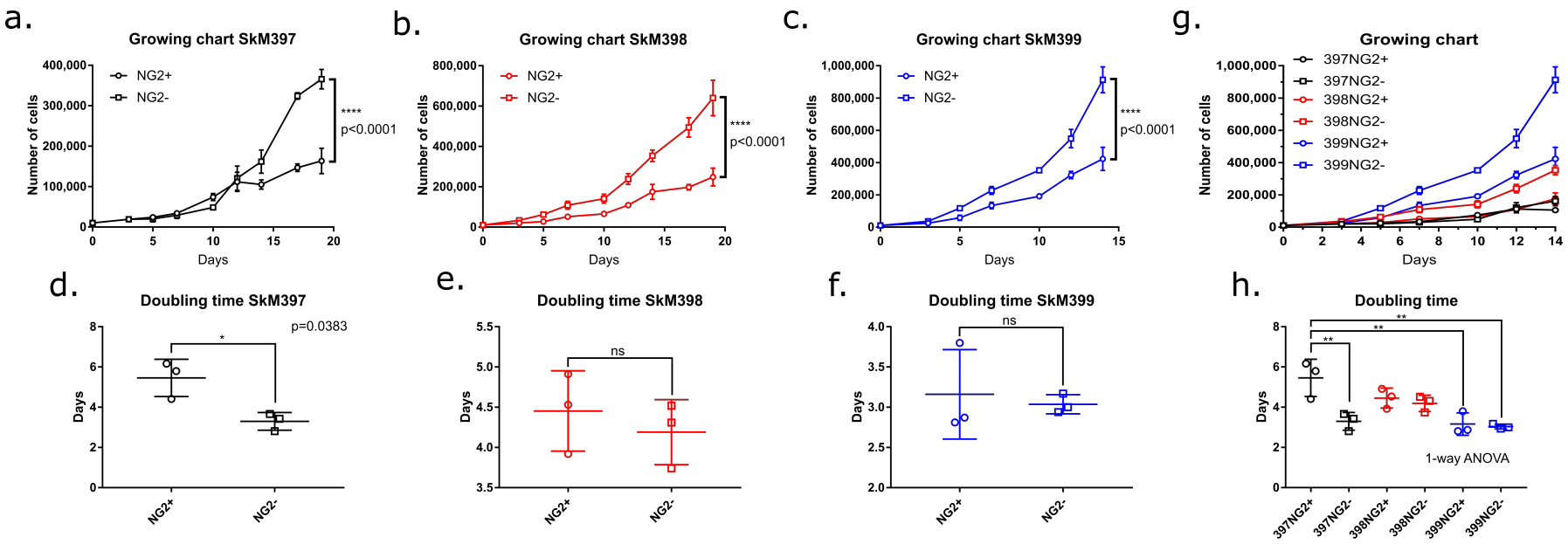

Figure 4.21: **NG2^{-} pericytes exhibit higher proliferation potential than NG2^{+} pericytes.** NG2$^{+/-}$ pericyte subtypes from the three foetal samples tested. Linear regression curves from day 7 to d14 (not shown) of growth in standard conditions revealed significant differences when comparing NG2$^{+/-}$ pericyte subtypes (a-c, mean±SD, n=3, p-value$<$0.0001). Doubling times from day 7 to d14 (d-f) were calculated using an unpaired T-test with Welch correction (mean±SD, n=3, ns=non significant). Growth charts are displayed for all three donors (g) and their doubling times (h) compared using a 1-way ANOVA (mean±SD, n=3, ns not shown).

Clonogenicity assay does not reveal consistent differences between sorted populations

Tested subtypes displayed different clonogenic potentials in a donor dependent manner. Among the three donors tested, one displayed higher clonogenic ability of the $NG2^+$ cell line (Figure 4.22a,d), one displayed no significant difference between cell lines (Figure 4.22c,f) and one displayed higher clonogenic ability on the $NG2^-$ cell line (Figure 4.22b,e). Thus, this test remains inconclusive to describe whether one of the subtypes holds higher clonogenic potential than the other.

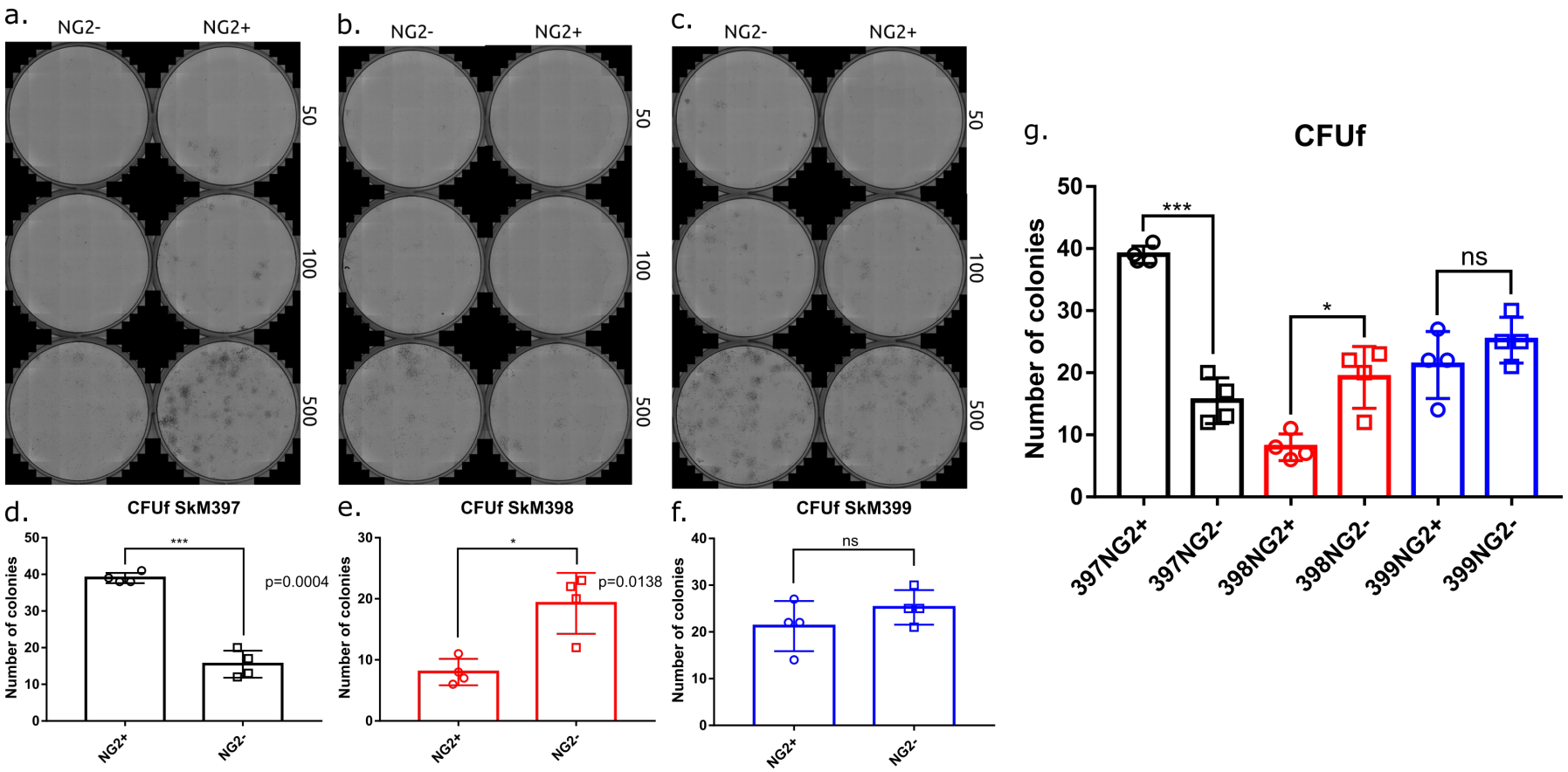

Figure 4.22: **Tested subtypes behaved in a donor dependent manner when tested for their clonogenic ability.** Pericyte NG2$^{+/-}$ subtypes from the three foetal samples tested. Colonies formed after 14d of culture when plating 50, 100 and 500 cells (a-c). Colony numbers in wells initially seeded with 100 cells (d-f) were compared using an unpaired T-test followed by Welch correction (showed mean±SD, n=4). All three quantifications are displayed together (g), comparing subtypes within the same donor sample.

NG2$^-$ pericytes exhibit higher osteogenic potential than NG2$^+$ pericytes

Cell lines were tested for osteogenic differentiation potential. All cell lines were able to differentiate into osteoblasts and produce calcium depositions that were detected by alizarin red staining (Figures 4.23-4.25). In all three donors, NG2$^-$ pericytes exhibited higher osteogenic potential, but as per growth potential, differences across donors could be observed. In particular, one of the donor's derived lines deposited close to no calcium, which was primarily detected by the imaging analysis rather than the spectophometric analysis (Figure 4.23a-c). Another sample exhibited such a huge osteogenic potential in both subtypes that imaging analysis resulted useless as the whole well was covered by mineral depositions, thus differences among subtypes could only be observed via spectrophotometric analysis (Figure 4.25a-c). These results indicate that while NG2$^-$ pericytes are potentially more interesting for bone regeneration purposes, huge differences among donors are still present and must be considered (Figure 4.26a-b).

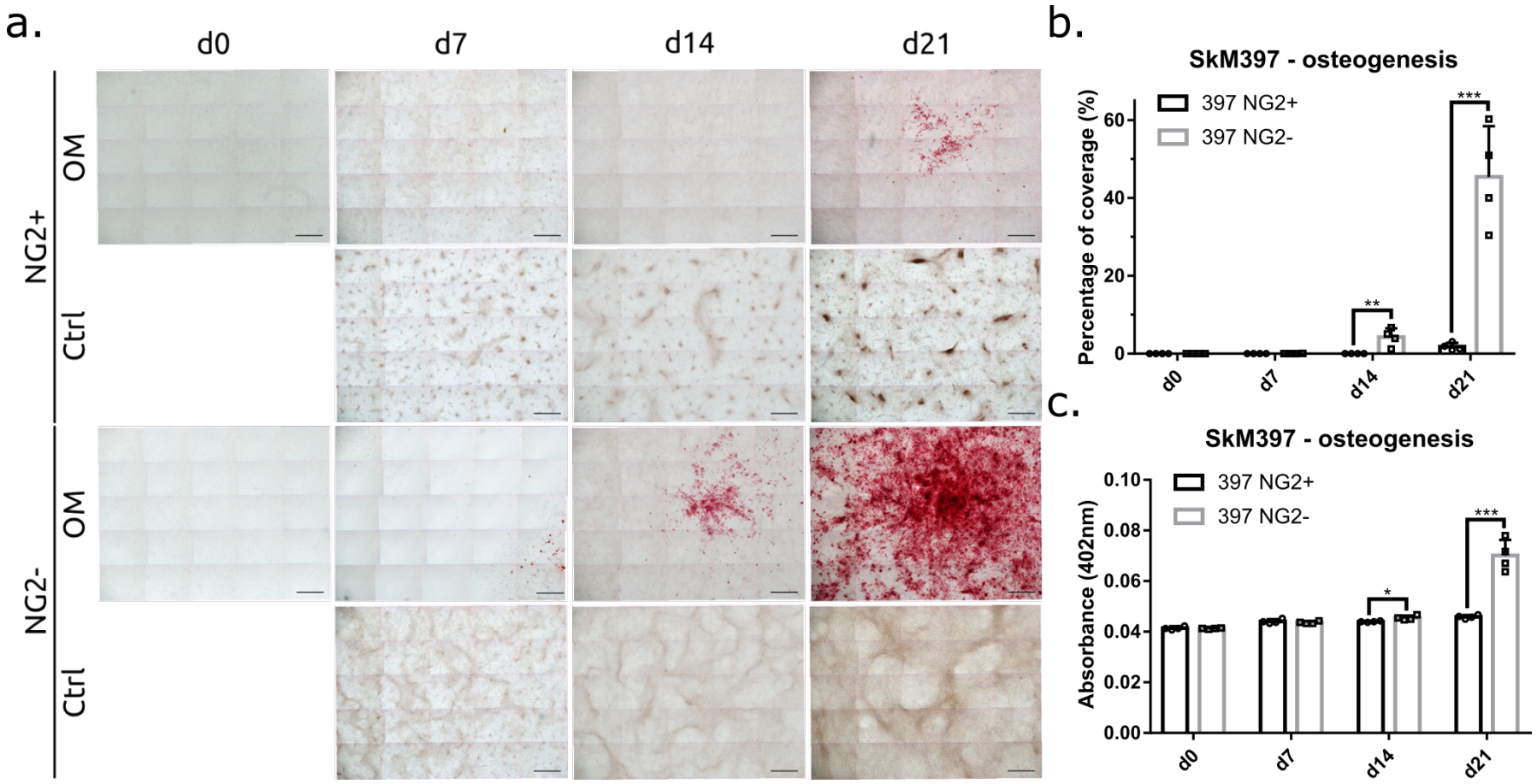

Figure 4.23: **NG2^{-} pericytes exhibit higher osteogenic potential.** Osteogenesis assay *in vitro* performed on foetal sample SkM397 (17 weeks old) NG2$^{\pm}$ pericytes derived populations. Alizarin red staining for calcium deposition (a, scale bar=1mm) after culture in osteogenic medium (OM) or standard growth medium (Ctrl). Alizarin red coverage (b) and calcium detection by spectrophotometry (c) revealed that the NG2^{-} subtype exhibits higher osteogenic potential than the NG2^{+} counterpart (mean$\pm$SD, n=4, multiple T-test, *=p-value$<$0.05,**=p-value$<$0.01,***=p-value$<$0.001).

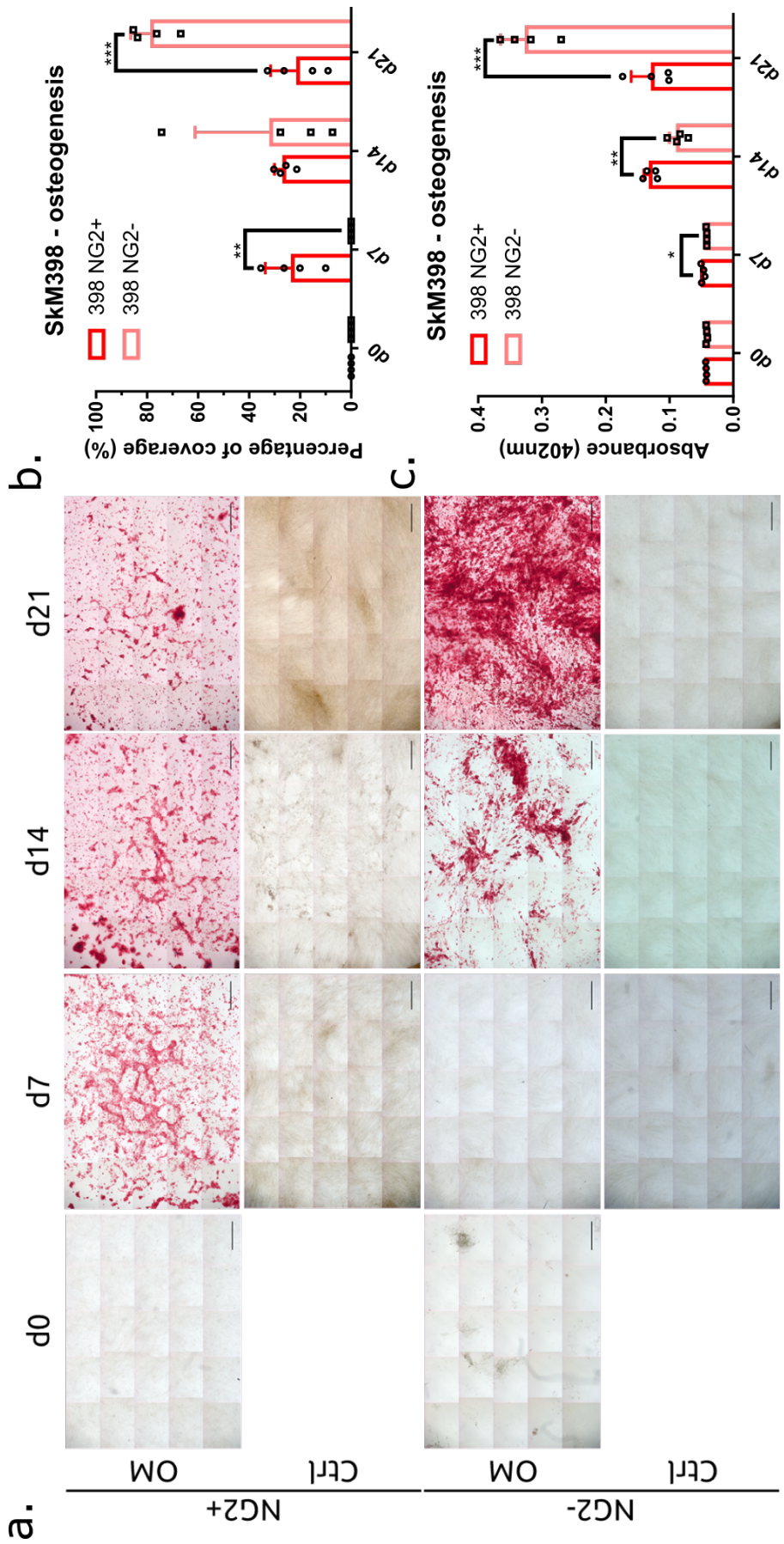

Figure 4.24: **NG2$^-$ pericytes exhibit higher osteogenic potential.** Osteogenesis assay *in vitro* performed on foetal sample SkM398 (14 weeks old) NG2$^\pm$ pericytes derived populations. Alizarin red staining for calcium deposition (a, scale bar=1mm) after culture in osteogenic medium (OM) or standard growth medium (Ctrl). Alizarin red coverage (b) and calcium detection by spectrophotometry (c) revealed that the NG2$^-$ subtype exhibits higher osteogenic potential than the NG2$^+$ counterpart (mean±SD, n=4, multiple T-test, *=p-value$<$0.05,**=p-value$<$0.01,***=p-value$<$0.001).

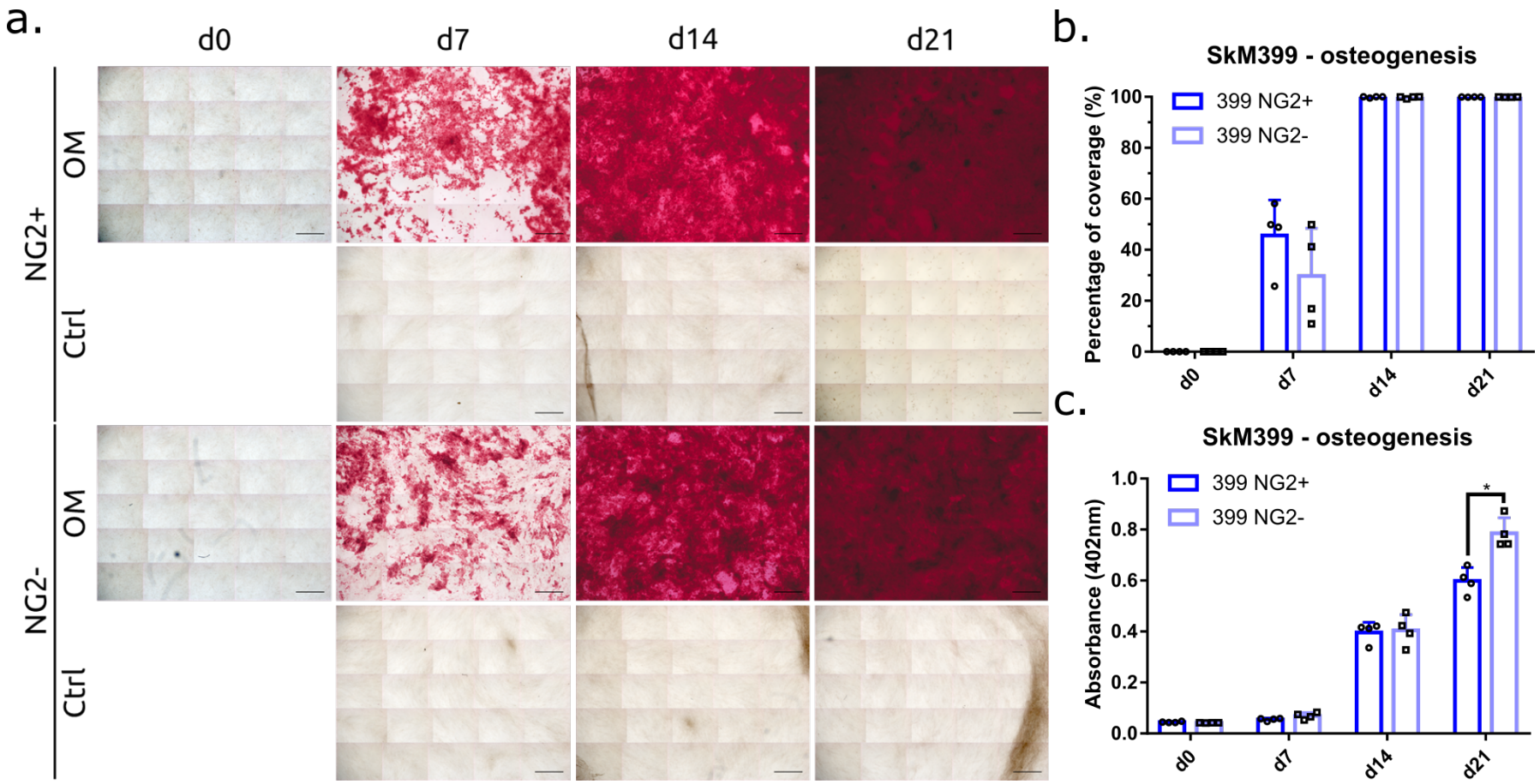

Figure 4.25: **NG2^{-} pericytes exhibit higher osteogenic potential.** Osteogenesis assay *in vitro* performed on foetal sample SkM399 (16 weeks old) NG2$^{\pm}$ pericytes derived populations. Alizarin red staining for calcium deposition (a, scale bar=1mm) after culture in osteogenic medium (OM) or standard growth medium (Ctrl). Alizarin red coverage (b) and calcium detection by spectrophotometry (c) revealed that the NG2^{-} subtype exhibits higher osteogenic potential than the NG2^{+} counterpart (mean$\pm$SD, n=4, multiple T-test, *=p-value$<$0.05,**=p-value$<$0.01,***=p-value$<$0.001).

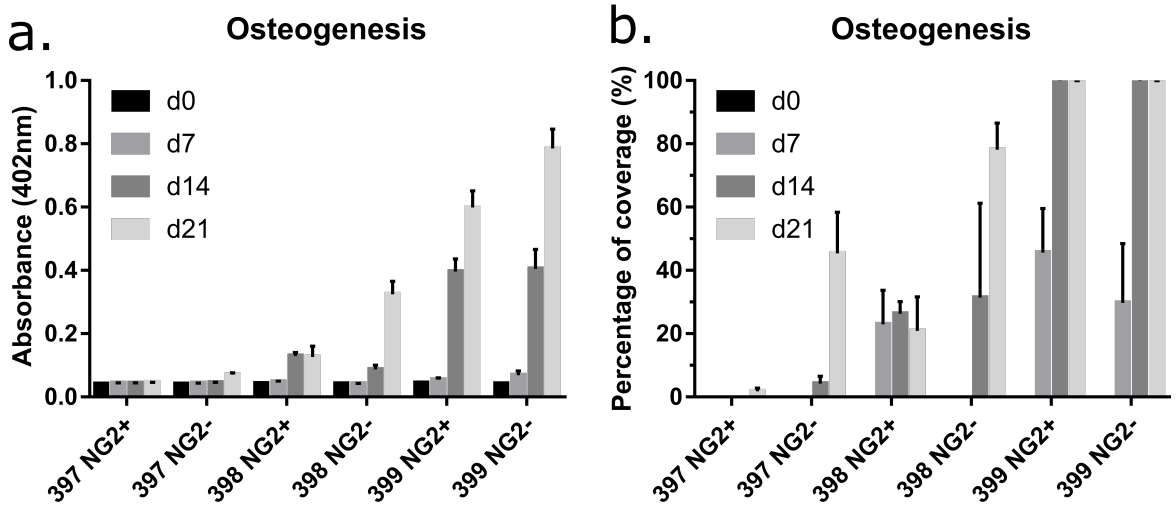

Figure 4.26: **Osteogenesis quantifications.** Calcium deposition was analysed by spectrophotometry (a) and alizarin red coverage (b) for all cell lines (mean±SD, n=4, no statistical analysis showed).

Cultured pericyte populations exhibit no skeletomyogenic potential

When placed in skeletomyogenic medium, none of the subtypes of any of the three donors seem to be able to generate any type of fibre thus not differentiating into skeletal muscle (Figures 4.27 and 4.29).

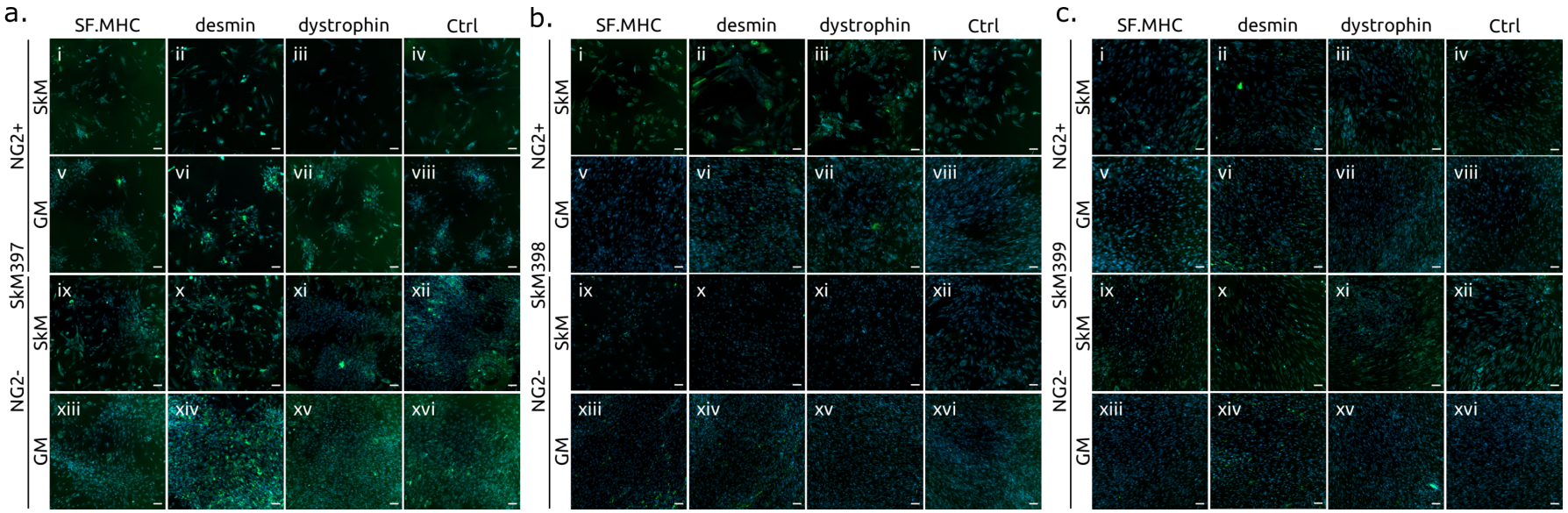

Figure 4.27: **NG2^{-} pericytes no skeletomyogenesis potential in the three donors tested.** NG2$^{+/-}$ pericyte subtypes from the three foetal samples tested. Immunocytochemistry staining following differentiation in skeletomyogenesis medium (SkM; i-iv, ix-xii) or standard growth medium (GM; v-viii,xiii-xvi) for skeletic muscle markers slow fast myosin heavy chain (SF.MHC; i, v, ix, xiii), desmin (ii, vi, x, xiv) and dystrophin (iii, vii, xi, xv). Control isotype (Ctrl; iv, viii, xii, xvi). n=4, scale bar=100μm.

NG2$^-$ pericytes exhibit higher cardiomyogenic potential than NG2$^+$ pericytes

When placed in cardiomyogenic conditions, the NG2$^-$ subtype seemed to differentiate better in two of the three donors tested (Figure 4.28b-c), none of the cell lines differentiating in the third donor (Figure 4.28a). For donor SkM398, fibres were formed and stained positive for troponin (Figure 4.28b$_{iii}$,b$_{xi}$), but only NG2$^-$ stained positive for cardiac myosin heavy chain (Figure 4.28b$_{ii}$,b$_{x}$). None of the cell lines produced fibers positive for αactinin (Figure 4.28b$_{i}$,b$_{ix}$). The NG2$^-$ cells also formed fibers spontaneously when grown with control medium, also staining positive for troponin (Figure 4.28b$_{xv}$).

This did not occur with donor SkM399, where all controls were clean of any fiber formation (Figure 4.28c$_{xiii-xiv}$). The NG2$^-$ subtype formed longer and more numerous fibers thant the NG2$^+$, all staining positive for αactinin, cHCM and troponin (Figure 4.28c$_{ix-xi}$). Fibers formed by the NG2$^+$ subtype only stained positive for αactinin and cHCM (Figure 4.28c$_{i-iii}$).

These results show that while not all isolated subtypes can differentiate into cardiomyogenic fibers, with no statistical differences overall when comparing both subtypes, the NG2$^-$ subtype would seem to hold higher potential (Figure 4.29).

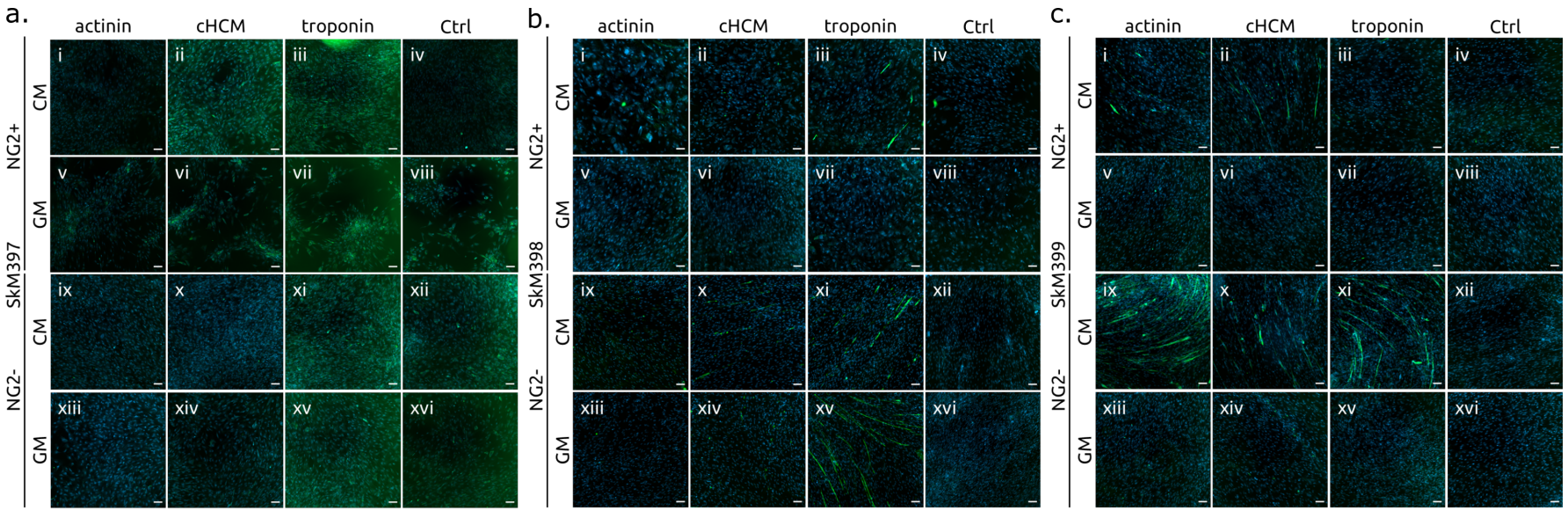

Figure 4.28: **NG2$^-$ pericytes exhibit higher cardiomyogenic potential in two of the three donors tested.** Pericyte NG2$^{+/-}$ subtypes from the three foetal samples tested SkM397 (a; 17 weeks old), SkM398 (b; 14 weeks old) and SkM399 (c; 16 weeks and 5 days old). Representative images show immunocytochemistry staining on cells following differentiation after culture with cardiomyogenic medium (CM; i-iv, ix-xii) or standard growth medium (GM; v-viii,xiii-xvi) for cardiac markers αactinin (actinin; i, v, ix, xiii), cardiac heavy chain myosin (cHCM; ii, vi, x, xiv) and troponin (iii, vii, xi, xv), with a control isotype (Ctrl; iv, viii, xii, xvi). n=4, scale bar=100μm. Subfigure a shows high autofluorescence, although processed and imaged identically to subfigures b and c.

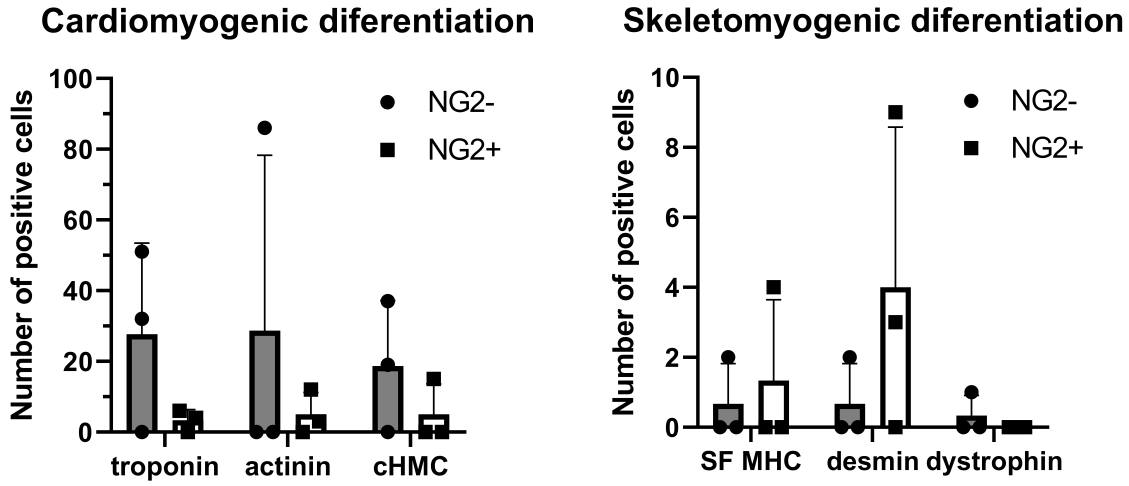

Figure 4.29: **Quantification of diferentiated muscle cells by immunocytochemistry.** Quantifications of positive cells for troponin, actinin and cardiac heavy myosin chain (cHMC) by immunocytochemistry on NG2^{+} and NG2^{-} pericytes cultured in cardiac differentiation medium (left). Quantifications of positive cells for Slow Fast myosin heavy chain (SF HMC), desmin and dystrophin by immunocytochemistry on NG2^{+} and NG2^{-} pericytes cultured in skeletal muscle differentiation medium (right). Showed mean$\pm$SD, n=3, unpaired t-test with Welsh correction.

Brief summary and discussion of the *in vitro* assays

All the results of these series of *in vitro* experiments are summarised in Table 4.2. It is relevant to point out two main conclusions from these experiments.

Table 4.2: Foetal skeletal muscle derived NG2$^{+/-}$ pericytes in culture. Best performers in each assay are indicated.

SAMPLE	SkM397	SkM398	SkM399	Best overall
Metabolic activity	NG2^{-}	NG2^{+}	NG2^{-}	**NG2^{-}**
Migration speed	NG2^{-}	NG2^{+}	No differences	**Inconclusive**
Growth rate	NG2^{-}	NG2^{-}	NG2^{-}	**NG2^{-}**
Clonogenic potential	NG2^{+}	NG2^{-}	No differences	**Inconclusive**
Osteogenic potential	NG2^{-}	NG2^{-}	NG2^{-}	**NG2^{-}**
Skeletomyogenic potential	None	None	None	**None**
Cardiomyogenic potential	None	NG2^{-}	NG2^{-}	**NG2^{-}**

First, when results are homogeneous across donors, the NG2$^-$ subtype appears to hold more abilities than the positive subpopulation. Since it appears that many native NG2$^+$ pericytes die during cell isolation, it is acceptable to assume that characteristics described for previously cultured pericytes would be very similar for the NG2$^-$ pericytes isolated in this experiment. Meanwhile, as only a fraction of surviving NG2$^+$ pericytes was isolated, the limited potentials here observed may be due to damaged cell lines or the fact that NG2$^+$ pericytes -or at least anoikis-resistant ones- have limited MSCs potential.

Second, on the assays where there is divergence between donors, huge differences can be observed on migration and clonogenic ability. It is expected to see cells that migrate more to be in a less proliferative state, and thus the results observed fit this model. The origin of these differences is not known. As discussed earlier, in some assays the cells behave homogeneously across samples, thus indicating that it is not an origin issue. It is not because they originate from different samples that the cells behaved differently. Its the case of the growth potential, where negative cells divide faster than the positive counterpart. Nevertheless, the tissues are from different foetal gestation ages, and when the migration and clonogenic potential of these cells are observed there appears to be a transition of state. It is possible that younger NG2$^-$ pericytes are highly proliferative and little migratory compared to NG2$^+$ pericytes, and transition into the inverse state, therefore younger samples being able to form more colonies with less initial cells. Thus these results would then be an observation of changes in the abilities of the specific subtypes during human development, as seen above with expression of Mef2c on cardiac pericytes.

4.4 Discussion

Overall, the work described in this chapter is insufficient to prove any particular roles of pericyte subtypes based on NG2 and yet less on αSMA expression. Nevertheless, it shows there is a clear diversity in the perivascular cell compartment. The work in this chapter highlights important issues that must be addressed.

4.4.1 There is heterogeneity within perivascular cells

The results here shown indicate there is abundant perivascular cell diversity using canonical markers. First, the distribution of particular cell types differs on the particular area of the tissue, evidenced by the imaging analysis. Second, the existence of multiple subtypes within the tissue is confirmed by flow cytometry. Third, these markers have a varying but apparent role in the fibrotic response to injury, evidenced by the increase of large amounts of cells positive for PC markers around a fraction of the porcine blood vessels. Fourth, when sorted, pericyte subpopulations exhibited significant differences when tested for clonogenicity, migration, growth potential and differentiation ability. Both NG2^{+} and NG2^{-} CD146^{+} pericytes were able to perform as previously described populations of pericytes, thus meaning either of them could be used for *in vitro* and *in vivo* purposes, and possibly even been defined as MSCs.
Like CD146, αSMA and NG2 are well established markers for pericytes, independently used to isolate and characterise them. To date, studies on pericytes based on either of these markers were believed to address the same population of cells, with the previous understanding that there is no unique marker for pericytes. Thus whichever function described in the analysed populations was ascribed to the ”pericyte” brand. It has been known for a long time now that both NG2 and αSMA are not expressed on all pericytes, nevertheless differences within distinct subtypes has not been explored until this work: there is heterogeneity within these pericyte subsets. As NG2 and αSMA

are canonical markers, characterisation of the subtypes should be a priority in future studies, before other minor subsets using novel markers.

4.4.2 Impact of anoikis

The most striking observation of these series of experiments is the anoikis effect observed when trying to isolate NG2$^+$ pericytes from human tissues. NG2 has been used by many groups to isolate pericytes from murine tissues, notably using reporter mice [90] but fewer attempts have been performed on human tissues and not on native cells, thus the contribution of human NG2$^+$ cells in the cultures established and later characterised is not known. This *in vitro* characterisation includes imaging techniques or flow cytometry but, as shown by this work, sorted NG2$^-$ pericyte derived cells can start expressing NG2 at the same level as NG2$^+$ pericyte derived cells. NG2 has been linked to anoikis [187, 188] thus, published studies could very well misinterpret NG2$^+$ cells in culture for the native NG2$^+$ pericyte resident population in human tissues.
Anoikis was confirmed to occur in similar experiments performed by other members of the laboratory. These findings may drive authors to reinterpret their results, replacing pericytes by NG2$^-$ pericytes.
The impact of anoikis is also particularly relevant since it clearly shows the superiority of the NG2$^-$ cells. While it remains unknown whether NG2$^+$ cells that die because of anoikis hold a similar or higher potential to the one described NG2$^-$ cells, it seems that the majority of the MSC potential is restricted to venular NG2$^-$ pericytes. More efforts are required to further characterise the NG2$^-$ and NG2$^+$ cells.

4.4.3 The technical issues of human tissue handling

The second major observation is the donor variability observed in cultured cell lines: differences are greater when comparing samples than when comparing subtypes within the same donor, while trends seemed to be maintained for some of the abilities assessed when comparing one subtype to the other. As per the origin of these variations multiple hypotheses can be formulated.

First, there is the inevitable genetic variability inherent to the handling of human samples. In contrast to animal models in which tissues originate usually from a stable and homogeneous genetic background, foetal samples used in this study originate from a very diverse human population, on which information is not available for ethical reasons.

Second, foetal sample donation during the progression of this work has been growing rare, thus little selection of samples, by developmental stage for instance, can be performed. Lower tissue availability translated into the use of tissues from diverse developmental stages, ranging 9 to 22 weeks in the same experiment. During such period of time, PCs of specific organs are susceptible of change, both in potential, distribution and native roles within the developing tissue. Changes could also be affecting other components of the organ. In particular, modifications of ECM components could alter tissue dissociation.

Third, extending from the previous point, gestational development could also differ in an organ specific manner. Organs with complex architecture such as the kidneys or heart are more likely to present developmental differences in shorter time gaps than more homogeneous tissues such as the bone marrow or skeletal muscle. Which developmental stages can be pooled to minimise this type of variation must be considered.

Finally, foetal samples were collected by the medical staff and later handed to the collection teams. Samples were obtained following induced abortion; delivery of the foetus would vary in time according to patients. This translates into a foetal sample that could be kept at womb temperature for a long period of time, thus tissue decay

was already initiated, as sometimes evidenced by the condition of the liver at the time of dissection.

Normalisation of the data is key to properly compare subpopulations with such donor related differences. Comparisons across sample should only be performed normalising data from one subtype versus the other for instance.

Chapter 5

Identification and isolation of PDGFR$\alpha^{+/-}$ and PDGFR$\beta^{+/-}$ subtypes of human, murine and porcine pericytes

5.1 Introduction

PDGFRβ is one of the major markers to identify perivascular cells, while PDGFRα has been mostly studied as a marker for fibrogenesis. Although they are isoforms of the same receptors, coexpression has been little studied in the perivascular context.

5.2 Hypothesis and Aims

The working hypothesis for this chapter is that PDGFRα and β can be used to identify and isolate functionally distinct subtypes of pericytes, as described in the Introduction, CD146^{+}CD34^{-}. This hypothesis will be articulated in three aims, as follows:

- Identify PDGFRα^+ and PDGFRβ^+ perivascular cells *in situ* in murine, porcine and human tissues.
- Isolate subsets of in murine, porcine and human perivascular cells based on PDGFRα and PDGFRβ expression using FACS and expand them *in vitro*.
- Assess clonogenic, proliferative and differentiation potentials of the different subsets *in vitro*.

5.3 Results

5.3.1 PDGFRα and β are expressed in the perivascular layer of the majority of blood vessels in the human foetal heart

Immunohistological analysis of the human foetal heart showed that the majority of blood vessels are surrounded by a layer of PDGFRβ^+ and PDGFRα^+ cells (Figure 5.1a). Quantified as shown in section 4.3.3, no differences in the number of blood vessels covered by PDGFRα and β positive cells were observed within distinct cardiac compartments (Figure 5.1b). The existence of a fraction of blood vessels with a perivascular layer negative for these markers indicate the presence of PC subtypes based on PDGFRα and β.

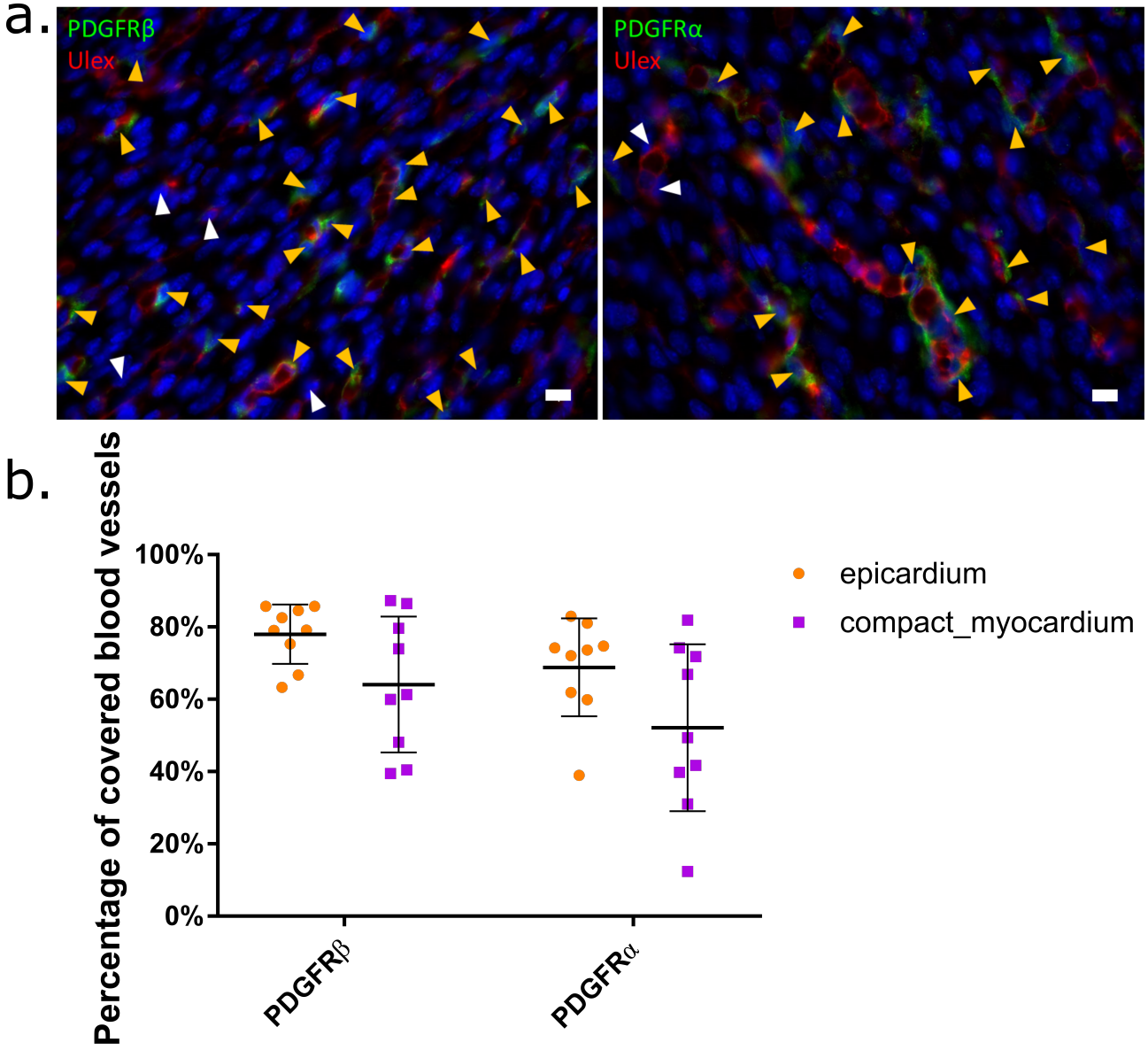

Figure 5.1: **PDGFRα and β are expressed in the perivascular layer of the majority of blood vessels in the human foetal heart.** a. Positive pericytes (orange arrowhead), negative pericytes (white arrowhead) surrounding blood vessels (scale bar=10μm). b. Percentage of PDGFRα and PDGFRβ positive blood vessels, quantified as explained in section 2.5.6, and shown in Figure 4.4 in section 4.3.3 (unpaired T-tests, n=9, non-significance p-value$>$0.05).

5.3.2 Subsets of PDGFRβ^+ cells based on other pericyte markers are present in murine tissues

Immunohistochemical analysis on a PDGFRβ-GFP (Pbag) reporter mouse showed a high efficiency in the PDGFRβ labelling. αSMA, NG2 and PDGFRα label a fraction of PDGFRβ^+ cells, revealing the existence of pericyte subsets (Figures 5.2-5.3). Co-localisation of the endothelial marker isolectin B-4 (IB4) and PDGFRβ was observed only in the endocardium.

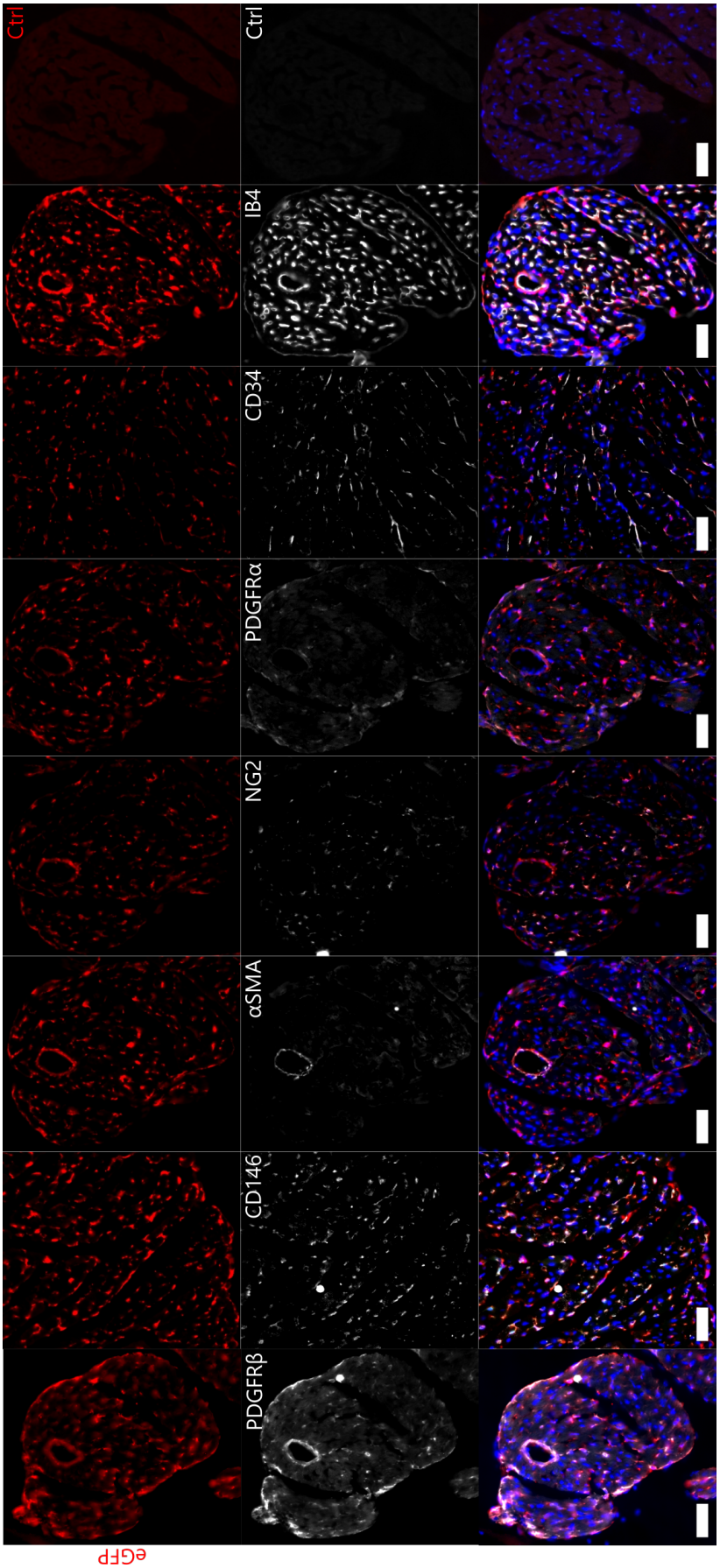

Figure 5.2: **Pbag PDGFRβ-GFP$^+$ cells co-express multiple perivascular markers in the murine heart.** PDGFRβ-GFP$^+$ cells are colocalised with PDGFRβ, CD146, αSMA, NG2 and PDGFRα cardiac perivascular cells. These cells are located around CD34$^+$ and IB4$^+$ endothelial cells (scale bar=100μm).

Figure 5.3: **Pbag PDGFRβ-GFP$^+$ cells co-express multiple perivascular markers in the murine skeletal muscle.** PDGFRβ-GFP$^+$ cells are colocalised with PDGFRβ, CD146, αSMA, NG2 and PDGFRα muscle perivascular cells. These cells are located around CD34$^+$ and IB4$^+$ endothelial cells (scale bar=100μm).

5.3.3 PDGFRα and β label porcine perivascular cells

Immunohistochemical staining of porcine cardiac tissue showed expression of PDGFRα and β around blood vessels, thus validating these markers for the identification of perivascular cells in the pig. As observed in human foetal heart, the majority of the blood vessels are covered by a perivascular layer of PDGFRα and β positive cells (Figure 5.4).

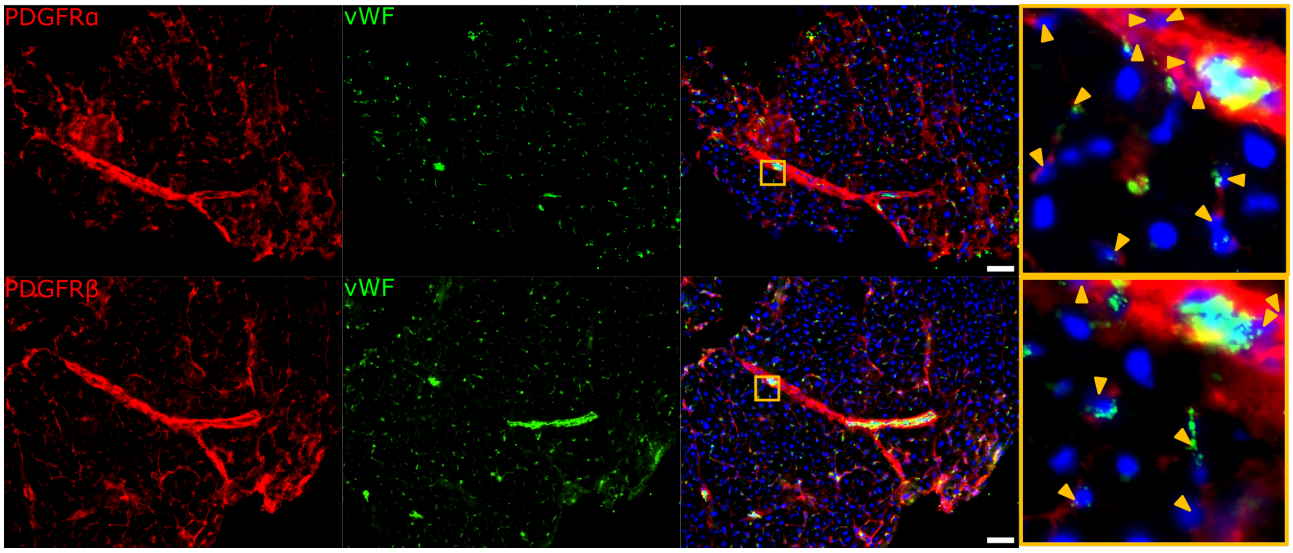

Figure 5.4: **Porcine pericytes express PDGFRα and β.** Immunofluorescence staining of PDGFRα and β and endothelial marker vWF on a healthy area of adult porcine left ventricle 2 days after acute myocardial infarction (scale bar=50μm).

5.3.4 FACS analysis of PDGFRα and β expressing cells in human tissues

Quantification by flow cytometry in the foetal skeletal muscle revealed that only a fraction of CD146$^+$ pericytes are positive for PDGFRα (1.68$\pm$1.48%) and PDGFRβ (3.44$\pm$1.66%, Figure 5.5a,c). Analysis of the CD34$^-$ stromal cell subpopulations shows that over 50% of the total cells are CD146$^+$ while PDGFRα and β account for less than 4% (Figure 5.5b,d). The majority of PDGFRα^+ cells are CD146 negative as are the PDGFRβ^+ cells. Similar results can be found in foetal heart and adult

subcutaneous adipose tissue (Figure 5.5e-f). These results are particularly surprising since they do not match the expected numbers from the histological analysis, where over 50$\%$ of the blood vessels were covered by positive perivascular cells. These differences might be due to a fragility in the isolated cells as seen in previous chapter for the NG2 positive cells, or a fragility in the receptor itself during the isolation process. Nevertheless, flow cytometry confirmed the existence of pericyte subtypes based on PDGFRα and β expression in human tissues.

CD146$^+$PDGFRβ^+PDGFRα^+, CD146$^+$PDGFRβ^+PDGFRα^- and CD146$^+$PDGFRβ^- PDGFRα^+ cell populations were sorted but due to low cell yields cultures were not successfully established.

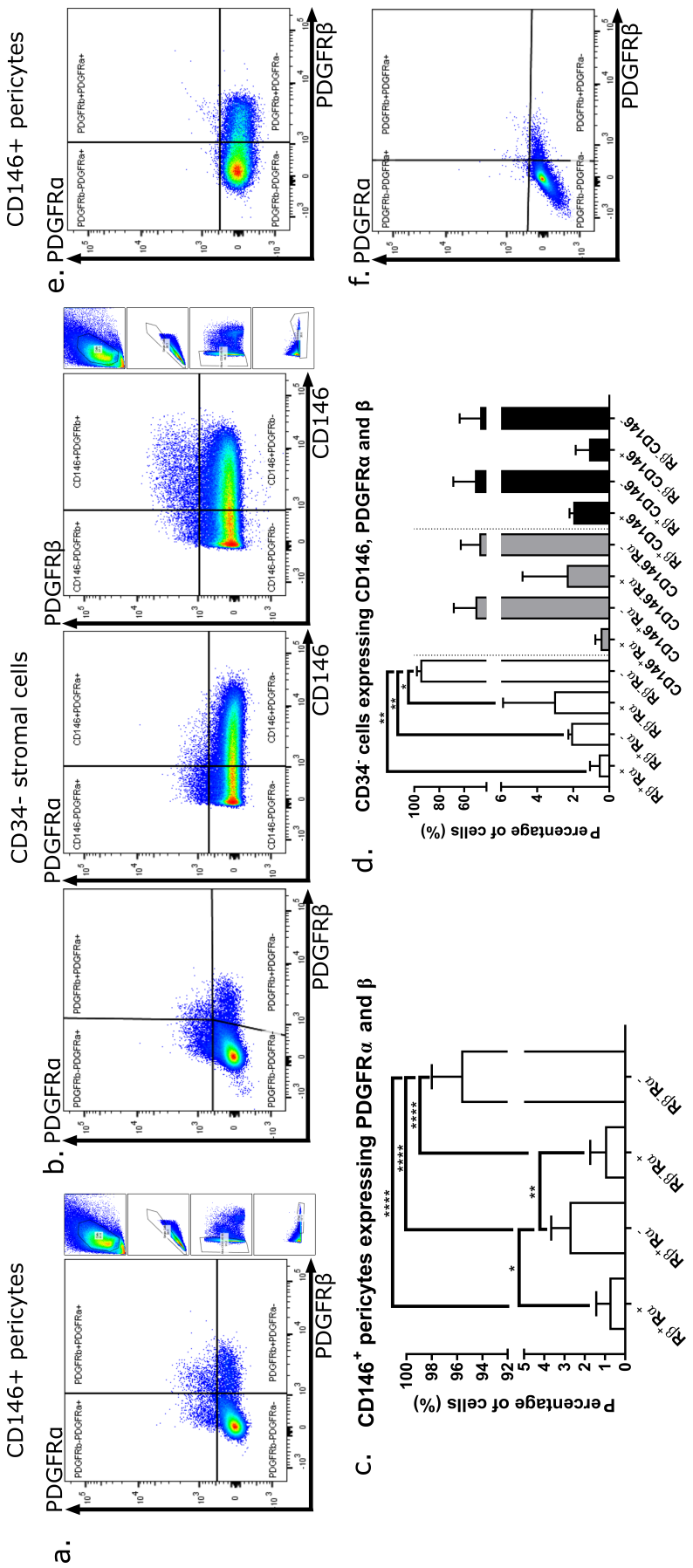

Figure 5.5: **PDGFRα^+ and β^+ cells in human tissues.** CD146$^+$ foetal skeletal muscle pericytes (a) and gated CD34$^-$ cells (b). Percentages of each cell population for CD146$^+$ pericytes (c) and CD34$^-$ stromal cells (d, 1-way ANOVA followed by Tukey's analysis, n=3, non-significative p-value$>$0.05, *=p-value$<$0.05, **=p-value$<$0.01, ****=p-value$<$0.0001). FACS analysis of CD146$^+$ pericytes from foetal heart (e) and adult white adipose tissue (f).

5.3.5 FACS analysis of PDGFRα and β expressing cells in murine tissues

Flow cytometry analysis on Pbag PDGFRβ-GFP reporter mice confirmed the presence of stromal cells subpopulations based on these receptors (Figure 5.6a-b). Analysis revealed similar proportions of the PDGFRβ-GFP^{+}PDGFRα^{+}, PDGFRβ-GFP^{+}PDGFRα^{-} and PDGFRβ-GFP^{-}PDGFRα^{+} cell populations (Figure 5.6c).

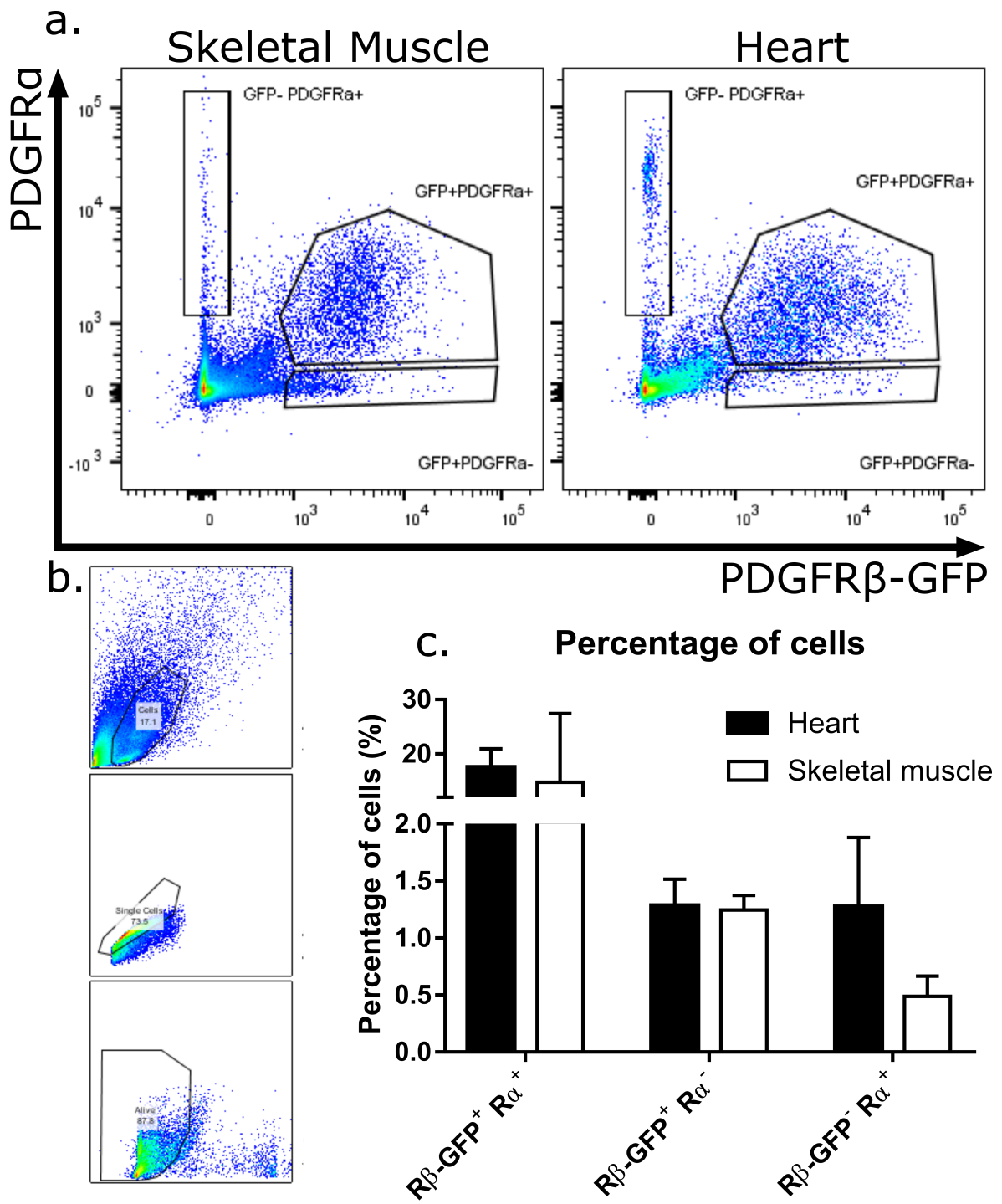

Figure 5.6: **PDGFRα^+ and β-GFP$^+$ cells in murine tissues.** Living cells from Pbag PDGFRβ-GFP reporter mice skeletal muscle and heart tissue (a-b). Percentages of PDGFRβ-GFP$^+$PDGFRα^+ (Rβ-GFP$^+$Rα^+), PDGFRβ-GFP$^+$PDGFRα^- (Rβ-GFP$^+$Rα^-) and PDGFRβ-GFP$^-$PDGFRα^+ (Rβ-GFP$^-$Rα^+) populations (paired T-test, n=3, non-significative p-value$>$0.05).

5.3.6 Early attempts to analyse pig cells by flow cytometry

A standard protocol for cell isolation and flow cytometry on human and murine tissues (see section 2.2) was used on subcutaneous fat and left ventricle from adult pig. Tissues were properly digested yielding living cells, thus the method was deemed adequate to isolate perivascular cells from porcine tissues (Figure 5.7).

As extremely few anti-pig antibodies are commercially available, antibodies against human antigens were tested on pig cells. None of the lineage antibodies to CD31, CD45 and CD56 labelled cells, nor did anti-CD34. The antibody against human CD146 stained cells. Antibodies to PDGFRα and β seemed not to stain any cell, while analysis on the stromal fraction revealed similar percentage of cells as seen in human tissues (Figure 5.7).

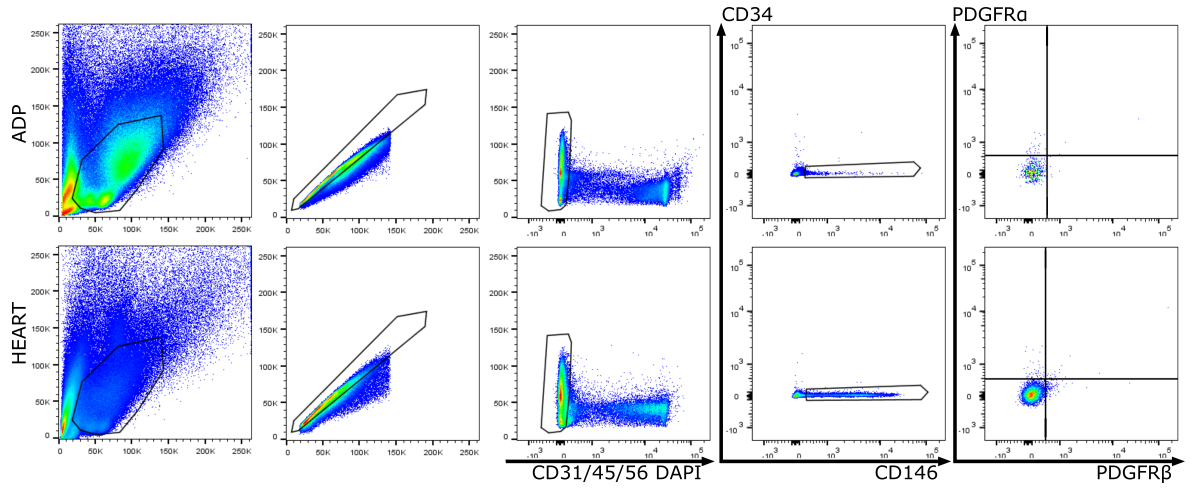

Figure 5.7: **Flow cytometry analysis of porcine tissue.** Porcine cells from heart and subcutaneous adipose (ADP) tissues. Gated cells from left to right: total cells, single cells, living CD31$^-$CD34$^-$CD56$^-$ cells. These cells were additionally gated for CD34 vs. CD146 and PDGFRα vs. PDGFRβ.

5.3.7 Brief summary

PDGFRβ and PDGFRα expression on fractions of perivacular cells in human, pig and mouse were confirmed. In the human developing heart, it was observed that not all

blood vessels are covered by PDGFRβ and PDGFRα positive perivascular layers, although expected numbers do not match when analysed by flow cytometry. This work is the first to show PDGFRβ and PDGFRα expression on porcine cardiac perivascular cells by histological analysis. In murine heart and skeletal muscle 4 different stromal cell populations can be identified by PDGFRβ and PDGFRα expression.

5.4 Discussion

5.4.1 PDGFRα and β identify subsets of perivascular cells in porcine, murine and human tissues

Murine perivascular cell populations based on PDGFRα and β have been long identified, as shown here, but this work also confirms their presence in other species. Subsets of perivascular cells have been confirmed in foetal human cardiac and skeletal muscles [140, 189]. Expression of the same markers has been confirmed in adult porcine heart and subcutaneous fat.

5.4.2 Faint extracellular labelling hinders cell sorting and later culture

Notable differences can be observed when looking at these populations of cells. Histological analysis reveals a majority of perivascular cells expressing at least one PDGF receptor, while the cell numbers observed by flow cytometry are much lower than expected. This is particularly true for PDGFRβ, for which a faint labelling in human tissues can be seen, compared to a clear and distinct signal from the reporter mice used. As a consequence, low cell yields were achieved after sorting, impeding the

establishment of cell cultures derived from porcine and human tissues.

5.4.3 *In vitro* and *in vivo* characteristics of the subtypes based on PDGFRα and β derived from human tissues remains unknown

Our laboratory has been working on PDGFRα and β in murine tissues, particularly the skeletal and cardiac muscle. Murray *et al.* showed the key contribution in the fibrotic response of PDGFRβ^+ cells following injury. Using a cardiac and skeletal muscle acute injury mouse model, PDGFRβ^+ cells were shown to contribute to the fibrotic response via αv integrins to activate the TGFβ pathway. This cascade could be inactivated using an αv integrin inhibitor. Incidentally, an overlap of 44.8$\%$ of cells expressing both PDGFRα and β was detected in uninjured tissues [140].

The PDGFRβ^+PDGFRα^+ and PDGFRβ^+PDGFRα^- subsets were specifically targeted in adult murine skeletal muscle in another study from our laboratory. Jensen *et al.* show that *in vitro* the double positive cell population was extremely adipogenic while the PDGFRβ^+PDGFRα^- subset was unable to produce such a response. Similar observations were made when cell cultures were treated with TGFβ, which response could be attenuated by the use of the same αv integrin inhibitor used in the previous study. *In vivo*, the same response was observed with a dramatic PDGFRβ^+PDGFRα^+ contribution to fibroadipogenesis following the rotator scuff fatty degeneration model [189].

5.4.4 Overall conclusion

PDGFRβ^+PDGFRα^+ and PDGFRβ^+PDGFRα^- perivascular cells show dramatically distinct potential in murine tissues as shown by others in our laboratory. The work pre-

sented here shows presence of both PDGFRβ and PDGFRα in perivascular cells in human and porcine tissues, while their isolation and later cell culture remains elusive. It would be extremely interesting to investigate whether these results can be reproduced in human cells, but further samples are required to establish a working FACS protocol for *in vitro* characterisation.

Chapter 6

General discussion

6.1 Major findings

There are several findings to be highlighted from this work.

First, the work in this thesis shows evidence of perivascular cell heterogeneity. In one hand, positive and negative populations of PCs were observed for each one of the markers tested -CD146, CD34, αSMA, NG2, LepR, PDGFRα and β-. Furthermore, positive and negative subpopulations were also observed when combining multiple markers during the analysis. On the other hand, when examining the distribution of some markers in the foetal human heart, we observe differences in the distribution of αSMA but not PDGFRα and β between the myocardium and epicardium. As marker distribution varies across different tissue areas, PC heterogeneity is not exclusive to diverse marker expression.

Second, this work validates the use of well established perivascular markers CD146, NG2, LepR, PDGFRα and β to identify porcine perivascular cells. Previous published studies only reported the expression of CD34 and αSMA in porcine tissues [190, 191].

Third, this work highlights the donor-derived heterogeneity. While same cell populations have been sorted and treated identically *in vitro*, significant differences have been observed within different donors of similar gestation stage. As shown in chap-

ter 3, LepR$^{+/-}$ perivascular cell derived populations behaved completely differently from one sample to another when tested for clonogeneicity, growth and osteogenic and adipogenic potentials. In chapter 4, NG2$^{+/-}$ derived populations showed convergence of results within donors when tested for metabolic activity, growth, osteogenic and cardiomyogenic potentials -with better performance of the NG2^{-} subpopulation- while exhibiting significant differences in the migratory and clonogeneic abilities.

Fourth, this work has revealed the impact of anoikis on NG2^{+} pericytes. This is the most important finding of this thesis. It questions whether the isolation and characterisation of pericytes so far was able to truly capture the whole population or just the anoikis-resistant ones. This discovery does not directly affect the clinical applications of the already characterised sorted and cultured populations, which are still applicable, but does affect the whole native cell population, as these abilities and features may be unique only to a fraction, and thus not to all pericytes or adventitial cells.

All-together, this work reveals many challenges this field of study is currently facing, which need to be addressed immediately, and other important factors that must be taken into account when characterising PCs.

6.2 Perivascular cell populations need to be standardised

The stromal compartment of an organ corresponds to all cells not directly involved in its function and primarily composes the connective tissue. Characterisation of this compartment has been pushed into the background in favour of the parenchymal cells, thus the stroma remains improperly characterised. As stromal cells, PCs suffer the same fate and are under-characterised. When interest for PCs grew, two major basic issues appeared: the current nomenclature is obsolete and new markers are required.

6.2.1 Perivascular cell nomenclature is obsolete

The current perivascular cell nomenclature, established long before the characterisation of their potential, from MSCs progenitors to their involvement in the fibrotic response, primarily refers to their anatomical location in the vessel. While *in situ* localisation and identification of a particular cell type by morphology and marker expression remains accurate, due to marker overlap, identification and isolation of perivascular cells by flow cytometry is impaired. Current isolated populations, while labelled the same, do not correspond to the original definition. Thus the current nomenclature is obsolete and must be renewed.

In chapters 3 and 4, the cells sorted with the immunophenotype $CD146^{+}CD34^{-}CD31^{-}CD45^{-}CD56^{-}$ were labelled as pericytes, when VSMCs also match this immunophenotype.

6.2.2 Cellular immunophenotype should be used as the new standard

Current nomenclature is a most common subject of argument among the community studying PCs, challenging the validity of any published work on the terminology used for the sorted cells. The clearest example is without any doubt the term ”pericyte”, which is being used to designate cell populations that correspond to pericytes, VSMCs and adventitial cells as described in the Introduction chapter of this thesis [190, 192, 193]. In order to progress, a new standardised system must be adopted, and must be robust enough to withstand paradigmatic shifts that could originate from the new cutting edge techniques being developed. Unique and unequivocal identification of a specific cell type is only achieved using the exact immunophenotype used to

locate and isolate cell populations.

As an example, the cell populations used in this work and designated as ”pericytes” and ”adventitial cells” actually correspond to $CD146^{+}CD34^{-}CD31^{-}CD45^{-}CD56^{-}$ and $CD34^{+}CD146^{-}CD31^{-}CD45^{-}CD56^{-}$ respectively. By using the immunophenotype rather than the obsolete terminology there is no room for misunderstanding and conflict.

6.2.3 New markers are still required

To tackle the heterogeneity new markers should be characterised. Our laboratory alone has identified over a hundred potential markers with the aid of single sequencing and extracellular screening techniques which have shown significant functionally distinct potentials [50]: $CD10^{+}$ adventitial cells exhibit higher proliferative and osteogenic potential compared to $CD10^{-}$; $ALDH^{hi}$ adventitial cells and pericytes express primitive genes in higher levels than the $ALDH^{lo}$; $PDGFR\beta^{+}PDGFR\alpha^{+}$ perivascular cells are fibroadipogenesis while $PDGFR\beta^{+}PDGFR\alpha^{-}$ regenerate muscle fibres [50, 189, 194]. The work here presented also shows differences between $NG2^{+}$ and $NG2^{-}$ perivascular cells.

Nevertheless, a particular question that must be addressed immediately is how to distinguish between traditional pericytes and VSMCs during cell sorting. Overlap for the majority of markers has hindered the possibilities to isolate pure cell populations.

A potential marker is CD39, also known as ectonucleoside triphosphate diphosphohydrolase 1 (ENTPD1), a cell surface enzyme that seems to be uniquely expressed on VSMCs but not on pericytes, while naturally present on endothelial cells in human tissues (Figure 6.1). CD39 was further explored at the end of the experimental work of this study, thus only limited results were obtained. Nevertheless, these preliminary results are extremely promising to finally distinguish true pericytes from VSMCs.

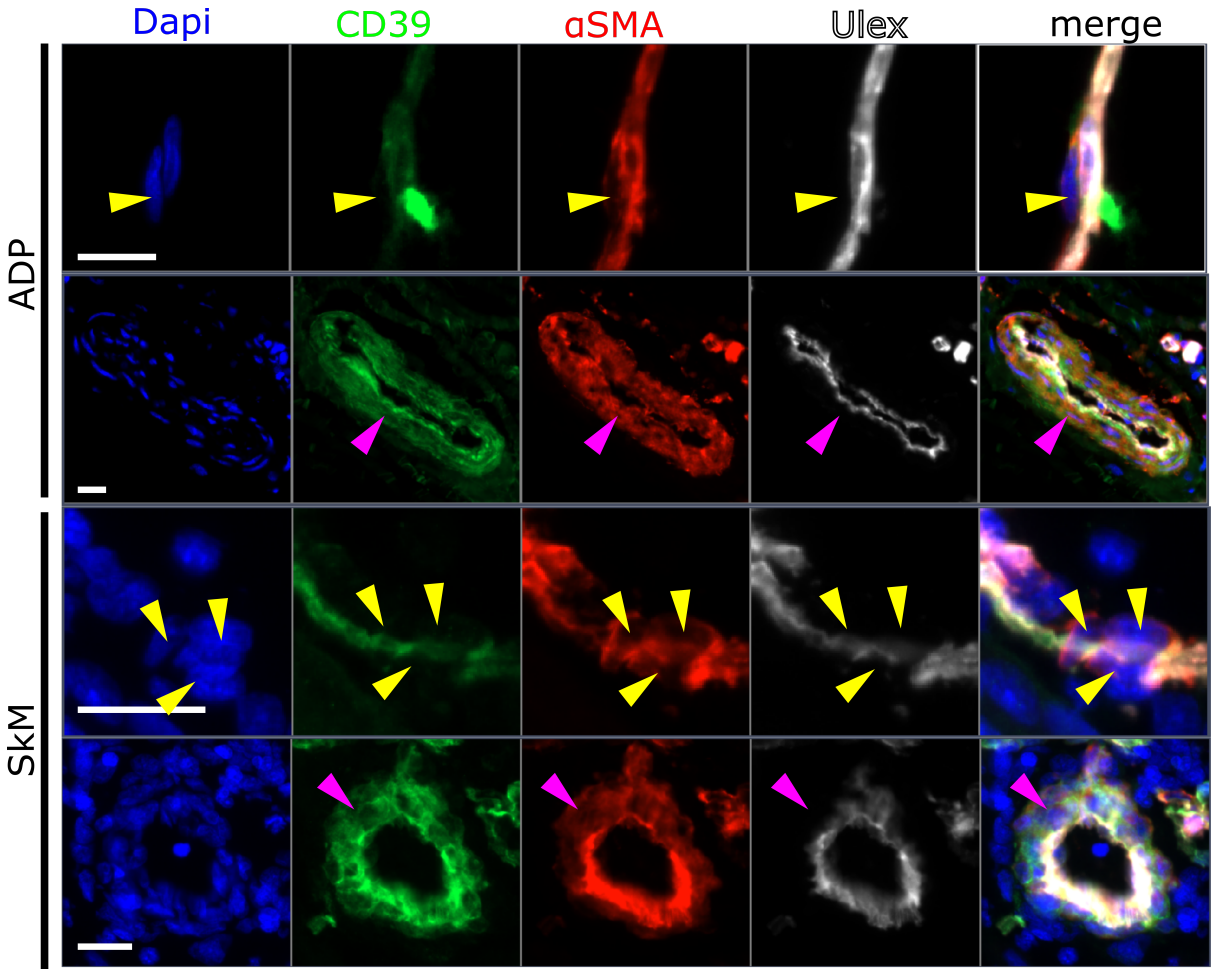

Figure 6.1: **CD39 is expressed on VSMCs but not on pericytes in human tissues.** αSMA$^+$ pericytes (yellow arrowhead) are negative for CD39 on adult subcutaneous white adipose tissue (ADP) and foetal skeletal muscle (SkM), while αSMA$^+$ VSMCs (magenta arrowhead) are positive for CD39. Scale bar = 20μm.

6.2.4 Hierarchy within perivascular cells

Successful identification and characterisation on the different subtypes of perivascular cells naturally leads to the discovery of a perivascular hierarchic system. Our laboratory has identified ALDH as a marker of stemness/primitivity of perivascular cells, where cells with high levels of ALDH are more primitive than cells with low level of this enzyme. Similarly, adventitial cells have been described more primitive than pericytes, as they express genes related to stemness in higher frequencies [50].

6.3 Important factors to consider when studying perivascular cells

Perivascular heterogeneity extends beyond the nomenclature and immunophenotype. Thus there are several important factors that must be taken into account when locating and isolating PCs, whether it is to understand their native contribution or as potential therapeutic agents to be transplanted.

6.3.1 Organ architecture

All organs composing the body can be grouped by their architectural complexity.
Some tissues are very homogeneous in structure such as the adipose tissue, skin or skeletal muscle. Different cell populations are homogeneously distributed along the whole tissue, including perivascular subpopulations.
Other tissues are composed of functional units too small to be individually dissected while keeping cells alive. For instance, the hepatic lobules in the liver or the islets in the pancreas.
Some tissues are composed by larger structure that when arranged spatially compartmentalise the whole organ into different specific areas that can be easily dissected. Isolation from a particular area enriched with the targeted PC population rather than the whole organ yields a purer population. Examples of these are the kidney and heart, where each area has a specific perivascular marker expression pattern [195].
These architectural differences but be taken into account in order to obtain the purest cell population yields.

6.3.2 Variability due to blood vessel type

In chapter 4, sorted CD146$^+$CD34$^-$CD31$^-$CD45$^-$CD56$^-$ cells positive and negative for NG2 exhibited different *in vitro* abilities, with the NG2$^-$ subtype with higher potential. This work and other published studies show NG2$^+$ perivascular cells to have specificity for capillaries, arteries and arterioles, but not veins and venules. This specificity is not observed on CD146, αSMA, PDGFRα and β.

Similarly, other markers have been located around particular blood vessels. In the haematopoietic system, LepR perivascular have been identified around sinusoids. In the kidney, juxtaglomerular but not glomerular pericytes express renin.

Variations in blood vessel size has not been explored either. Pericytes surrounding arterioles, precapillary arterioles, capillaries, postcapillary venules and venules are morphologically very different and have a specific disposition around the blood vessel. These varying pericytes may also have different potentials.

Understanding the distribution of perivascular cell populations surrounding different blood vessel types is crucial for specific cell targeting, whether it is for proper cell isolation or targetted chemotherapy.

6.3.3 Tissue age

In chapter 4, immunohistochemistry on multiple human foetal hearts showed a transient expression of Mef2c in CD146$^+$NG2$^+\alpha$SMA$^+$. This suggests a change in cell populations identified using the same immunophenotype according to the developmental stage of the tissue.

With old age, PCs degenerate and lose functions at different paces. Certain subtypes lose active receptors thus responding differently to the same signalling pathways deriving into a new subtype that, when abundant enough, alters the overall tissue phenotype [195–197]. Eventually, particular cell types will be lost causing impaired and later

total tissue function [198, 199].

Perivascular cell distribution varies according to the donors age. From developmental stages to adulthood, followed by ageing and decay, the perivascular compartment remodels differently for each tissue. Characterising the perivascular distribution across time is crucial to understand the role and potential of resident PCs, whether they belong to a recipient or donor.

6.4 Final remarks

In essence, to characterise perivascular cells it is key to understand their *in situ* location, distribution and immunophenotype before isolating and assess the sorted populations *in vitro* and *in vivo*.

These isolated cells should also be tested in co-culture with other cell types to assess their supportive abilities, such as HSCs [27] or ECs for angiogenic support [200]. Similarly, paracrine properties should be tested by means of secretome arrays [201] and conditioned media cultures [200].

Once identified, their therapeutical potential and mechanism must be assessed to decypher the optimal method to use these cells, whether it is via cell transplantation (direct or using a scaffold system) of progenitor cells for tissue incorporation or release of trophic factors for modulation of signalling pathways and endogenous cell activation, expansion and differentiation *in vitro*, or any novel technique yet to develop. This step is crucial to understand and use the full potential of these cells for medical purposes in regenerative medicine and tissue engineering [202, 203].

Bibliography

[1] Darwin J. Prockop. Marrow stromal cells as stem cells for nonhematopoietic tissues. *Science*, 276(5309):71–74, 1997.

[2] A. J. Friedenstein, R. K. Chailakhjan, and K. S. Lalykina. The development of fibroblast colonies in monolayer cultures of guinea-pig bone marrow and spleen cells. *Cell Proliferation*, 3(4):393–403, 1970.

[3] Mark F. Pittenger, Alastair M. Mackay, Stephen C. Beck, Rama K. Jaiswal, Robin Douglas, Joseph D. Mosca, Mark A. Moorman, Donald W. Simonetti, Stewart Craig, and Daniel R. Marshak. Multilineage potential of adult human mesenchymal stem cells. *Science*, 284(5411):143–147, 1999.

[4] Arnold I. Caplan. Mesenchymal stem cells. *Journal of orthopaedic research : official publication of the Orthopaedic Research Society*, 9(5):641–50, 1991.

[5] Edwind M. Horwitz, Katarina Le Blanc, Massimo Dominici, Ingo Mueller, Ineke Slaper-Cortenbach, Frank C. Marini, Robert J. Deans, Diane S. Krause, and Armand Keating. Clarification of the nomenclature for MSC: The International Society for Cellular Therapy position statement. *Cytotherapy*, 7(5):393–395, 2005.

[6] Massimo Dominici, Katarina Le Blanc, Ingo Mueller, Ineke Slaper-Cortenbach, Frank C. Marini, Diane S. Krause, Robert J. Deans, Armand Keating, Darwin J. Prockop, and Edwind M. Horwitz. Minimal criteria for defining multipotent mes-

enchymal stromal cells. The International Society for Cellular Therapy position statement., 2006.

[7] T M Dexter, T D Allen, and L G Lajtha. Conditions controlling the proliferation of haemopoietic stem cells in vitro. *Journal of cellular physiology*, 91(3):335–344, 1977.

[8] Benedetto Sacchetti, Alessia Funari, Stefano Michienzi, Silvia Di Cesare, Stefania Piersanti, Isabella Saggio, Enrico Tagliafico, Stefano Ferrari, Pamela Gehron Robey, Mara Riminucci, and Paolo Bianco. Self-renewing osteoprogenitors in bone marrow sinusoids can organize a hematopoietic microenvironment. *Cell*, 131(2):324–36, 2007.

[9] Hsiang-yiang Jui, Cheng-hsin Lin, Wan-tseng Hsu, Yi-ru Liu, Ron-bin Hsu, Borluen Chiang, Wen-yih I Tseng, Ming-fong Chen, Kenneth K Wu, and Chii-ming Lee. Autologous Mesenchymal Stem Cells Prevent Transplant Interleukin-10 , Interferon-gamma, and Indoleamine 2,3-dioxygenase. *Cell Transplantation*, 21(7):971–984, 2012.

[10] Arnold I. Caplan and James E. Dennis. Mesenchymal stem cells as trophic mediators. *Journal of Cellular Biochemistry*, 98(5):1076–1084, 2006.

[11] Jiajia Xu, Yiyun Wang, Ching Yun Hsu, Yongxing Gao, Carolyn Ann Meyers, Leslie Chang, Leititia Zhang, Kristen Broderick, Catherine Ding, Bruno Péault, Kenneth Witwer, and Aaron Watkins James. Human perivascular stem cell-derived extracellular vesicles mediate bone repair. *eLife*, 8, 2019.

[12] Iain R. Murray, Christopher C. West, Winters R. Hardy, Aaron W. James, Tea Soon Park, Alan Nguyen, Tulyapruek Tawonsawatruk, Lorenza Lazzari, Chia Soo, and Bruno Péault. Natural history of mesenchymal stem cells, from vessel walls to culture vessels. *Cellular and Molecular Life Sciences*, 71(8):1353–1374, 2014.

[13] Pouya Mafi, Sandip Hindocha, Reza Mafi, Michelle Griffin, and Wasim S. Khan. Adult mesenchymal stem cells and cell surface characterization - a systematic review of the literature. *The open orthopaedics journal*, 5(Suppl 2):253–60, 2011.

[14] Lindolfo da Silva Meirelles, Pedro C. Chagastelles, and Nance B. Nardi. Mesenchymal stem cells reside in virtually all post-natal organs and tissues. *Journal of Cell Science*, 119(11):2204–2213, 2006.

[15] C. Farrington-Rock, N. J. Crofts, M. J. Doherty, B. a. Ashton, C. Griffin-Jones, and a. E. Canfield. Chondrogenic and adipogenic potential of microvascular pericytes. *Circulation*, 110(15):2226–2232, 2004.

[16] Mihaela Crisan, Solomon Yap, Louis Casteilla, Chien-wen Chen, Mirko Corselli, Tea Soon Park, Gabriella Andriolo, Bin Sun, Bo Zheng, Li Zhang, Cyrille Norotte, Pang-Ning Teng, Jeremy Traas, Rebecca Schugar, Bridget M Deasy, Stephen Badylak, Hans-jörg Bühring, Jean-Paul Giacobino, Lorenza Lazzari, Johnny Huard, and Bruno Péault. A perivascular origin for mesenchymal stem cells in multiple human organs. *Cell stem cell*, 3(3):301–13, 2008.

[17] Guiting Lin, Maurice Garcia, Hongxiu Ning, Lia Banie, Ying-Lu Guo, Tom F Lue, and Ching-Shwun Lin. Defining stem and progenitor cells within adipose tissue. *Stem cells and development*, 17(6):1053–1063, 2008.

[18] Paola Campagnolo, Daniela Cesselli, Ayman Al Haj Zen, Antonio Paolo Beltrami, Nicolle Kränkel, Rajesh Katare, Gianni Angelini, Costanza Emanueli, and Paolo Madeddu. Human adult vena saphena contains perivascular progenitor cells endowed with clonogenic and proangiogenic potential. *Circulation*, 121(15):1735–1745, 2010.

[19] Mirko Corselli, Chien W. Chen, Mihaela Crisan, Lorenza Lazzari, and Bruno Péault. Perivascular ancestors of adult multipotent stem cells. *Arteriosclerosis, Thrombosis, and Vascular Biology*, 30(6):1104–1109, 2010.

[20] Ludovic Zimmerlin, Vera S. Donnenberg, Melanie E. Pfeifer, E. Michael Meyer, Bruno Péault, J. Peter Rubin, and Albert D. Donnenberg. Stromal vascular progenitors in adult human adipose tissue. *Cytometry Part A*, 77(1):22–30, 2010.

[21] Tea Soon Park, Manuela Gavina, Chien Wen Chen, Bin Sun, Pang Ning Teng, Johnny Huard, Bridget M. Deasy, Ludovic Zimmerlin, and Bruno Péault. Placental perivascular cells for human muscle regeneration. *Stem Cells and Development*, 20(3):451–463, 2011.

[22] Jörg C. Gerlach, Patrick Over, Morris E. Turner, Robert L. Thompson, Hubert G. Foka, William C.W. Chen, Bruno Péault, Bruno Gridelli, and Eva Schmelzer. Perivascular mesenchymal progenitors in human fetal and adult liver. *Stem Cells and Development*, 21(18):3258–3269, 2012.

[23] Aaron W. James, Janette N. Zara, Mirko Corselli, Michael Chiang, Wei Yuan, Virginia Nguyen, Asal Askarinam, Raghav Goyal, Ronald K. Siu, Victoria Scott, Min Lee, Kang Ting, Bruno Péault, and Chia Soo. Use of human perivascular stem cells for bone regeneration. *Journal of Visualized Experiments*, 63:e2952, 2012.

[24] Aaron W. James, Janette N. Zara, Mirko Corselli, Asal Askarinam, Ann M. Zhou, Alireza Hourfar, Alan Nguyen, Silva Megerdichian, Greg Asatrian, Shen Pang, David Stoker, Xinli Zhang, Ben Wu, Kang Ting, Bruno Peault, and Chia Soo. An Abundant Perivascular Source of Stem Cells for Bone Tissue Engineering. *Stem Cells Translational Medicine*, 1(9):673–684, 2012.

[25] Asal Askarinam, Aaron W. James, Janette N. Zara, Raghav Goyal, Mirko Corselli, Angel Pan, Pei Liang, Le Chang, Todd Rackohn, David Stoker, Xinli

Zhang, Kang Ting, Bruno Péault, and Chia Soo. Human perivascular stem cells show enhanced osteogenesis and vasculogenesis with Nel-like molecule I protein. *Tissue Engineering - Part A*, 19(11-12):1386–1397, 2013.

[26] Mirko Corselli, Mihaela Crisan, Iain R. Murray, Christopher C. West, Jessica Scholes, Felicia Codrea, Nusrat Khan, and Bruno Péault. Identification of Perivascular Mesenchymal Stromal / Stem Cells by Flow Cytometry. *Cytometry A*, 83(8):714–20, 2013.

[27] Mirko Corselli, Chee Jia Chin, Chintan Parekh, Arineh Sahaghian, Wenyuan Wang, Shundi Ge, Denis Evseenko, Xiaoyan Wang, Elisa Montelatici, Lorenza Lazzari, Gay M. Crooks, and Bruno Péault. Perivascular support of human hematopoietic stem / progenitor cells. *Blood*, 121(15):2891–2901, 2013.

[28] Chien-Wen Chen, Masaho Okada, Jonathan D Proto, Xueqin Gao, Naosumi Sekiya, Sarah A Beckman, Mirko Corselli, Mihaela Crisan, Arman Saparov, Kimimasa Tobita, Bruno Péault, and Johnny Huard. Human pericytes for ischemic heart repair. *Stem cells (Dayton, Ohio)*, 31(2):305–16, 2013.

[29] Olivia Chen and Li Qian. Direct Cardiac Reprogramming: Advances in Cardiac Regeneration. *Biomed Res Int*, 2015:580406, 2015.

[30] Paul Hindle, Nusrat Khan, Leela Biant, and Bruno Péault. The Infrapatellar Fat Pad as a Source of Perivascular Stem Cells with Increased Chondrogenic Potential for Regenerative Medicine. *Stem Cells Translational Medicine*, 6(1):77–87, 2017.

[31] Ania Stefanska, Christopher Kenyon, Helen C. Christian, Charlotte Buckley, Isaac Shaw, John J. Mullins, and Bruno Péault. Human kidney pericytes produce renin. *Kidney International*, 90(6):1251–1261, 2016.

[32] Christopher C. West, Winters R. Hardy, Iain R. Murray, Aaron W. James, Mirko Corselli, Shen Pang, Cameron Black, S. E. Lobo, Kunal Sukhija, Ping Liang,

Venu Lagishetty, David C. Hay, Keith L. March, K. Ting, Chia Soo, and Bruno Péault. Prospective purification of perivascular presumptive mesenchymal stem cells from human adipose tissue: process optimization and cell population metrics across a large cohort of diverse demographics. *Stem Cell Res Ther*, 7(1):47, 2016.

[33] Claire D. Eliasberg, Ayelet Dar, Andrew R. Jensen, Iain R. Murray, Winters R. Hardy, Tomasz J. Kowalski, Cameron A. Garagozlo, Kyle M. Natsuhara, Adam Z. Khan, Owen J. McBride, Peter I. Cha, Benjamin V. Kelley, Denis Evseenko, Brian T. Feeley, David R. McAllister, Bruno Peault, and Frank A. Petrigliano. Perivascular stem cells diminish muscle atrophy following massive rotator cuff tears in a small animal model. *Journal of Bone and Joint Surgery - American Volume*, 99(4):331–341, 2017.

[34] Charles Marie Rouget. Memoire sur le development, la structure et les proprietes 846 physiologiques des capillaires sanguins et lymphatiques. *Arch Physiol Norm Pathol*, 5, 1873.

[35] Charles Marie Rouget. Note sur le developpement de la tunique contractile des vaisseaux. *Compt Rend Acad Sci*, 59:559–562, 1874.

[36] K Zimmermann. Die feinere Ban der Blutcapinaren. *Z. Anat. Entwickl.*, 68:29–209, 1923.

[37] Russell Ross, Newton B. Everett, and Ruth Tyler. Wound healing and collagen formation. VI. The origin of the wound fibroblast studied in parabiosis. *Journal of Cell Biology*, 44(3):645–654, 1970.

[38] Lucio Diaz-Flores, Ricardo Gutierrez, Hilda Varela, N. Rancel, and F. Valladares. Microvascular pericytes: A review of their morphological and functional characteristics. *Histology and Histopathology*, 6(2):269–286, 1991.

[39] Lucio Diaz-Flores, Ricardo Gutierrez, Pilar Gonzalez, and Hilda Varela. Inducible perivascular cells contribute to the neochondrogenesis in grafted perichondrium. *The Anatomical Record*, 229(1):1–8, 1991.

[40] William C. W. Chen, James E. Baily, Mirko Corselli, Mary Diaz, Bin Sun, Guosheng Xiang, Gillian A. Gray, Johnny Huard, and Bruno Péault. Human Myocardial Pericytes : Multipotent Mesodermal Precursors Exhibiting Cardiac Specificity. *Stem Cells*, 33(2):557–573, 2014.

[41] William C. W. Chen, Bruno Péault, and Johnny Huard. Regenerative Translation of Human Blood-Vessel-Derived MSC Precursors. *Stem Cells International*, 2015:375187, 2015.

[42] Yuya Kunisaki, Ingmar Bruns, Cristoph Scheiermann, Jalal Ahmed, Sandra Pinho, Dachuan Zhang, Toshihide Mizoguchi, Quiaozhi Wei, Daniel Lucas, Keisuke Ito, Jessica C. Mar, Aviv Bergman, and Paul S. Frenette. Arteriolar niches maintain haematopoietic stem cell quiescence. *Nature*, 502(7473):637–643, 2013.

[43] Lei Ding, Thomas L. Saunders, Grigori Enikolopov, and Sean J. Morrison. Endothelial and perivascular cells maintain haematopoietic stem cells. *Nature*, 481(7382):457–462, 2012.

[44] Diana Sá da Bandeira, Joan Casamitjana, and Mihaela Crisan. Pericytes, integral components of adult hematopoietic stem cell niches. *Pharmacology and Therapeutics*, 171:104–113, 2017.

[45] Annika Armulik, Guillem Genové, Maarja Mäe, Maya H. Nisancioglu, Elisabet Wallgard, Colin Niaudet, Liqun He, Jenny Norlin, Per Lindblom, Karin Strittmatter, Bengt R. Johansson, and Christer Betsholtz. Pericytes regulate the blood-brain barrier. *Nature*, 468(7323):557–561, 2010.

[46] Annika Armulik, Alexandra Abramson, and Christer Betsholtz. Endothelial/Pericyte Interactions. *Circulation Research*, 97(6):512–523, 2005.

[47] Mirko Corselli, Chien-Wen Chen, Bin Sun, Solomon Yap, J. Peter Rubin, and Bruno Péault. The Tunica Adventitia of Human Arteries and Veins As a Source of Mesenchymal Stem Cells, 2012.

[48] Rafael Kramann, Claudia Goettsch, Janewit Wongboonsin, Hiroshi Iwata, Rebekka K. Schneider, Christoph Kuppe, Nadine Kaesler, Monica Chang-Panesso, Flavia G. Machado, Susannah Gratwohl, Kaushal Madhurima, Joshua D. Hutcheson, Sanjay Jain, Elena Aikawa, and Benjamin D. Humphreys. Adventitial MSC-like Cells Are Progenitors of Vascular Smooth Muscle Cells and Drive Vascular Calcification in Chronic Kidney Disease. *Cell Stem Cell*, 19(5):628–642, 2016.

[49] Ulrich Tigges, Masanobu Komatsu, and William B. Stallcup. Adventitial pericyte progenitor/mesenchymal stem cells participate in the restenotic response to arterial injury. *Journal of Vascular Research*, 50(2):134–144, 2013.

[50] W. Reef Hardy, Mirko Corselli, Iain R. Murray, Bruno Péault, Dmitry O. Traktuev, Keith March, Nicanor I. Moldovan, Leni Moldovan, Kenneth J. Livak, Krishna Datta, and Chirayu Goswami. Transcriptional Networks in Single Perivascular Cells Sorted from Human Adipose Tissue Reveal a Hierarchy of Mesenchymal Stem Cells. *Stem Cells*, 35(5):1273–1289, 2017.

[51] Mariana di Luca, Roya Hakimjavadi, Denise Burtenshaw, Emma Fitzpatrick, Pattie Mathiue, Catriona Lally, Eileen M. Redmond, and Paul A. Cahill. The Dichotomy of Vascular Smooth Muscle Differentiation/De- Differentiation in Health and Disease. In *Muscle Cell and Tissue - Current Status of Research Field*, pages 259–285. 2018.

[52] Aaron W. B. Joe, Lin Yi, Anuradha Natarajan, Fabien Le Grand, Leslie So, Joy Wang, Michael A. Rudnicki, and Fabio M.V. Rossi. Muscle injury activates resident fibro/adipogenic progenitors that facilitate myogenesis. *Nat Cell Biol*, 12(2):153–63, 2010.

[53] Shuei Liong Lin, Tatiana Kisseleva, David A. Brenner, and Jeremy S. Duffield. Pericytes and perivascular fibroblasts are the primary source of collagen-producing cells in obstructive fibrosis of the kidney. *American Journal of Pathology*, 173(6):1617–1627, 2008.

[54] Shuei Liong Lin, Fan Chi Chang, Claudia Schrimpf, Yi Ting Chen, Ching Fang Wu, Vin Cent Wu, Wen Chih Chiang, Frank Kuhnert, Calvin J. Kuo, Yung Ming Chen, Kwan Dun Wu, Tun Jun Tsai, and Jeremy S. Duffield. Targeting endothelium-pericyte cross talk by inhibiting VEGF receptor signaling attenuates kidney microvascular rarefaction and fibrosis. *American Journal of Pathology*, 178(2):911–923, 2011.

[55] Rafael Kramann, Rebekka K. Schneider, Derek P. Dirocco, Flavia Machado, Susanne Fleig, Philip A. Bondzie, Joel M. Henderson, Benjamin L. Ebert, and Benjamin D. Humphreys. Perivascular Gli1+ progenitors are key contributors to injury-induced organ fibrosis. *Cell Stem Cell*, 16(1):51–66, 2015.

[56] Dhruv Lowe, Terrence Sanvictores, and Savio John. Alkaline Phosphatase, 2020.

[57] Arianna Dellavalle, Maurilio Sampaolesi, Rossana Tonlorenzi, Enrico Tagliafico, Benedetto Sacchetti, Laura Perani, Anna Innocenzi, Beatriz G Galvez, Graziella Messina, Roberta Morosetti, Sheng Li, Marzia Belicchi, Giuseppe Peretti, Jeffrey S Chamberlain, Woodring E Wright, Yvan Torrente, Stefano Ferrari, Paolo Bianco, and Giulio Cossu. Pericytes of human skeletal muscle are myogenic precursors distinct from satellite cells. *Nat Cell Biol*, 9(3):255–267, 2007.

[58] Mattia Quattrocelli, Giacomo Palazzolo, Giuseppe Floris, Patrick Schöffski, Luigi Anastasia, Aldo Orlacchio, Thierry Vandendriessche, Marinee K L Chuah, Giulio Cossu, Catherine Verfaillie, and Maurilio Sampaolesi. Intrinsic cell memory reinforces myogenic commitment of pericyte-derived iPSCs. *The Journal of pathology*, 223(5):593–603, 2011.

[59] Jordi Díaz-Manera, Eduard Gallardo, Noemi De Luna, Miquel Navas, Laura Soria, Matteo Garibaldi, Ricard Rojas-García, Rossana Tonlorenzi, Giulio Cossu, and Isabel Illa. The increase of pericyte population in human neuromuscular disorders supports their role in muscle regeneration in vivo. *Journal of Pathology*, 228(4):544–553, 2012.

[60] Upinder Singh, Rene H. Quintanilla, Scott Grecian, Kyle R. Gee, Mahendra S. Rao, and Uma Lakshmipathy. Novel Live Alkaline Phosphatase Substrate for Identification of Pluripotent Stem Cells. *Stem Cell Reviews and Reports*, 8(3):1021–1029, 2012.

[61] Ratti Ram Sharma, Kathryn Pollock, Allison Hubel, and David McKenna. Mesenchymal stem or stromal cells: A review of clinical applications and manufacturing practices. *Transfusion*, 54(5):1418–1437, 2014.

[62] Kateřina Štefková, Jiřina Procházková, and Jiří Pacherník. Alkaline phosphatase in stem cells. *Stem Cells Int*, 2015:628368, 2015.

[63] Henk Jan Prins, A. Koen Braat, D. Gawlitta, Wouter J.A. Dhert, David A. Egan, Estel Tijssen-Slump, Huipin Yuan, Paul J. Coffer, Henk Rozemuller, and Anton C. Martens. In vitro induction of alkaline phosphatase levels predicts in vivo bone forming capacity of human bone marrow stromal cells. *Stem Cell Research*, 12(2):428–440, 2014.

[64] Volker Nehls and Detlev Drenckhahn. Heterogeneity of microvascular pericytes for smooth muscle type alpha-actin. *Journal of Cell Biology*, 113(1):147–154, 1991.

[65] Tailoi Chan-Ling, Matthew Philip Page, Tom Gardiner, Louise Baxter, Emilia Rosinova, and Suzanne Hughes. Desmin ensheathment ratio as an indicator of vessel stability: Evidence in normal development and in retinopathy of prematurity. *American Journal of Pathology*, 165(4):1301–1313, 2004.

[66] Jörg Kunz, Dorothee Krause, Marian Kremer, and Rolf Dermietzel. The 140 kDa Protein of Blood Brain Barrier Associated Pericytes Is Identical to Aminopeptidase N. *Journal of Neurochemistry*, 62(6):2375–2386, 1994.

[67] C. I. Civin, L. C. Strauss, C. Brovall, M. J. Fackler, J. F. Schwartz, and J. H. Shaper. Antigenic analysis of hematopoiesis. III. A hematopoietic progenitor cell surface antigen defined by a monoclonal antibody raised against KG-1a cells. *Journal of immunology*, 133(1):157–65, 1984.

[68] Laura E. Sidney, Matthew J. Branch, Siobhán E. Dunphy, Harminder S. Dua, and Andrew Hopkinson. Concise Review : Evidence for CD34 as a Common Marker for Diverse Progenitors. *Stem Cells*, 32:1380–1389, 2014.

[69] Ie-Ming Shih. The role of CD146 (Mel-CAM) in biology and pathology. *Journal of Pathology*, 189:4–11, 1999.

[70] Christine Sers, Gert Riethmüller, and Judith P. Johnson. MUC18, a Melanoma-Progression Associated Molecule, and Its Potential Role in Tumor Vascularization and Hematogenous Spread. *Cancer Research*, 54(21):5689–5694, 1994.

[71] Ariane Tormin, Ou Li, Jan Claas Brune, Stuart Walsh, Birgit Schütz, Mats Ehinger, and Nicholas Ditzel. CD146 expression on primary non-hematopoietic bone marrow stem cells correlates to in situ localization CD146 Expression on

Primary Non-Hematopoietic Bone Marrow Stem Cells Correlates to In situ Localization. *Blood*, 117(19):5067–5077, 2011.

[72] Dimas T. Covas, Rodrigo A. Panepucci, Aparecida M. Fontes, Wilson A. Silva, Maristela D. Orellana, Marcela C.C. Freitas, Luciano Neder, Anemari R.D. Santos, Luiz C. Peres, Maria C. Jamur, and Marco A. Zago. Multipotent mesenchymal stromal cells obtained from diverse human tissues share functional properties and gene-expression profile with CD146+ perivascular cells and fibroblasts. *Experimental Hematology*, 36(5):642–654, 2008.

[73] Mats Hellström, Mattias Kalén, Per Lindahl, Alexandra Abramsson, and Christer Betsholtz. Role of PDGF-B and PDGFR-beta in recruitment of vascular smooth muscle cells and pericytes during embryonic blood vessel formation in the mouse. *Development*, 126(14):3047–3055, 1999.

[74] Steven Song, Andrew J Ewald, William Stallcup, Zena Werb, and Gabriele Bergers. PDGFRβ+ perivascular progenitor cells in tumours regulate pericyte differentiation and vascular survival. *Nature Cell Biology*, 7(9):870–879, 2005.

[75] Michelle D. Tallquist, Wendy J. French, and Philippe Soriano. Additive effects of PDGF receptor β signaling pathways in vascular smooth muscle cell development. *PLoS Biology*, 1(2):E52, 2003.

[76] Robert D. Bell, Ethan A. Winkler, Abhay P. Sagare, Itender Singh, Barb LaRue, Rashid Deane, and Berislav V. Zlokovic. Pericytes Control Key Neurovascular Functions and Neuronal Phenotype in the Adult Brain and during Brain Aging. *Neuron*, 68(3):409–427, 2010.

[77] Erzsebet Kokovay, Lu Li, and Lee A. Cunningham. Angiogenic recruitment of pericytes from bone marrow after stroke. *Journal of Cerebral Blood Flow and Metabolism*, 26:545–555, 2006.

[78] Leon C.D. Smyth, Justin Rustenhoven, Emma L. Scotter, Patrick Schweder, Richard L.M. Faull, Thomas I.H. Park, and Mike Dragunow. Markers for human brain pericytes and smooth muscle cells. *Journal of Chemical Neuroanatomy*, 92:48–60, 2018.

[79] Faming Zhang, Margret B. Basinski, John M. Beals, Stephen L. Briggs, Lisa M. Churgay, David K. Clawson, Richard D. DiMarchi, Thomas C. Furman, John E. Hale, Hansen M. Hsiung, Brigitte E. Schoner, Dennis P. Smith, Xing Y. Zhang, Jean-Pierre Wery, and Richard W. Schevitz. Crystal structure of the obese protein leptin-E100. *Nature*, 387(6629):206–9, 1997.

[80] Douglas L. Coleman. Obese and diabetes: two mutant genes causing diabetes-obesity syndromes in mice. *Diabetologia*, 14(3):141–8, 1978.

[81] Tian-Jie Han and Xin Wang. Leptin and its receptor in hematologic malignancies. *International journal of clinical and experimental medicine*, 8(11):19840–9, 2015.

[82] Marina Konopleva, Adel Mikhail, Zeev Estrov, Shourong Zhao, David Harris, Gisela Sanchez-Williams, Steven M. Kornblau, Joan Dong, Kay-Oliver Kliche, Shuwei Jiang, H. Ralph Snodgrass, Elihu H. Estey, and Michael Andreeff. Expression and function of leptin receptor isoforms in myeloid leukemia and myelodysplastic syndromes: Proliferative and anti-apoptotic activities. *Blood*, 93(5):1668–1676, 1999.

[83] Xu Xu Chen and Tianfu Yang. Roles of leptin in bone metabolism and bone diseases. *J Bone Miner Metab*, 33(5):474–85, 2015.

[84] Bo O. Zhou, Rui Yue, Malea M. Murphy, James G. Peyer, and Sean J. Morrison. Leptin-Receptor-Expressing Mesenchymal Stromal Cells Represent the Main Source of Bone Formed by Adult Bone Marrow. *Cell Stem Cell*, 15(2):154–168, 2014.

[85] Johanna Donovan, Xu Shiwen, Jill Norman, and David Abraham. Platelet-derived growth factor alpha and beta receptors have overlapping functional activities towards fibroblasts. *Fibrogenesis and Tissue Repair*, 6(1):1–9, 2013.

[86] Satoru Morikawa, Yo Mabuchi, Yoshiaki Kubota, Yasuo Nagai, Kunimichi Niibe, Emi Hiratsu, Sadafumi Suzuki, Chikako Miyauchi-Hara, Narihito Nagoshi, Takehiko Sunabori, Shigeto Shimmura, Atsushi Miyawaki, Taneaki Nakagawa, Toshio Suda, Hideyuki Okano, and Yumi Matsuzaki. Prospective identification, isolation, and systemic transplantation of multipotent mesenchymal stem cells in murine bone marrow. *The Journal of Experimental Medicine*, 206(11):2483–2496, 2009.

[87] Peter C. Stapor, Richard S. Sweat, Derek C. Dashti, Aline M. Betancourt, and Walter Lee Murfee. Pericyte dynamics during angiogenesis: New insights from new identities. *Journal of Vascular Research*, 51(3):163–174, 2014.

[88] Lorin E. Olson and Philippe Soriano. PDGFRβ signaling regulates mural cell plasticity and inhibits fat development. *Developmental Cell*, 20(6):815–826, 2011.

[89] Peter M. Steinert, Ying-Hao Chou, Veena Prahlad, David A. D. Parry, Lyuben N. Marekov, Kenneth C. Wu, Shyh-Ing Jang, and Robert D. Goldman. A High Molecular Weight Intermediate Filament-associated Protein in BHK-21 Cells Is Nestin, a Type VI Intermediate Filament Protein. *The Journal of Biological Chemistry*, 274(14):9881–90, 1999.

[90] Alexander Birbrair, Tan Zhang, Zhong-Min Wang, Maria Laura Messi, Grigori N. Enikolopov, Akiva Mintz, and Osvaldo Delbono. Role of Pericytes in Skeletal Muscle Regeneration and Fat Accumulation. *Stem Cells and Development*, 22(16):2298–2314, 2013.

[91] Urban Lendahl, Lyle B. Zimmerman, and Ronald D.G. McKay. CNS stem cells express a new class of intermediate Filament Protein. *Cell*, 60:585–595, 1990.

[92] Sayuri Suzuki, Jun Namiki, Shinsuke Shibata, Yumi Mastuzaki, and Hideyuki Okano. The neural stem/progenitor cell marker nestin is expressed in proliferative endothelial cells, but not in mature vasculature. *Journal of Histochemistry and Cytochemistry*, 58(8):721–730, 2010.

[93] Jaroslav Mokrý, Dana Čížková, Stanislav Filip, Jiří Ehrmann, Jan Österreicher, Zdeněk Kolář, and Denis English. Nestin Expression by Newly Formed Human Blood Vessels. *Stem Cells and Development*, 13(6):658–664, 2004.

[94] Yuka Kishaba, Daisuke Matsubara, and Toshiro Niki. Heterogeneous expression of nestin in myofibroblasts of various human tissues. *Pathology International*, 60(5):378–385, 2010.

[95] Olga Kruppkova, Tomas Loja, Iva Zambo, and Renata Veselska. Nestin expression in human tumors and tumor cell lines. *Neoplasma*, 57(4):291–298, 2010.

[96] Walter L. Murfee, Michael R. Rehorn, Shayn M. Peirce, and Thomas C. Skalak. Perivascular cells along venules upregulate NG2 expression during microvascular remodeling. *Microcirculation*, 13(3):261–273, 2006.

[97] Mario Berger, Gabriele Bergers, Bernd Arnold, Günter J. Hämmerling, and Ruth Ganss. Regulator of G-protein signaling-5 induction in pericytes coincides with active vessel remodeling during neovascularization. *Blood*, 105(3):1094–1101, 2005.

[98] Cecilia Bondjers, Mattias Kalén, Mats Hellström, Stefan J. Scheidl, Alexandra Abramsson, Oliver Renner, Per Lindahl, Hyeseon Cho, John Kehrl, and Christer Betsholtz. Transcription profiling of platelet-derived growth factor-B-deficient mouse embryos identifies RGS5 as a novel marker for pericytes and vascular smooth muscle cells. *American Journal of Pathology*, 162(3):721–729, 2003.

[99] Mitali Manzur and Ruth Ganss. Regulator of G Protein Signaling 5: A New Player in Vascular Remodeling. *Trends in Cardiovascular Medicine*, 19(1):26–30, 2009.

[100] Jia Shen, Swati Shrestha, Yu Hsin Yen, Michelle A. Scott, Chia Soo, Kang Ting, Bruno Peault, Sarah M. Dry, and Aaron W. James. The pericyte antigen RGS5 in perivascular soft tissue tumors. *Human Pathology*, 47(1):121–131, 2016.

[101] Avital Tidhar, Moshe Reichenstein, Dana Cohen, Alexander Faerman, Neal G. Copeland, Debra J. Gilbert, Nancy A. Jenkins, and Moshe Shani. A novel transgenic marker for migrating limb muscle precursors and for vascular smooth muscle cells. *Developmental Dynamics*, 220(1):60–73, 2001.

[102] Richard A. Klinghoffer, Peter F. Mueting-Nelsen, Alexander Faerman, Moshe Shani, and Philippe Soriano. The two PDGF receptors maintain conserved signaling in vivo despite divergent embryological functions. *Molecular Cell*, 7(2):343–354, 2001.

[103] Pascal Stuelsatz, Paul Keire, Ricardo Almuly, and Zipora Yablonka-Reuveni. A Contemporary Atlas of the Mouse Diaphragm: Myogenicity, Vascularity, and the Pax3 Connection. *Journal of Histochemistry and Cytochemistry*, 60(9):638–657, 2012.

[104] Toyoshi Fujimoto and S. J. Singer. Immunocytochemical Studies of Desmin and Vimentin in Pericapillary Cells of Chicken. *Journal of Histochemistry and Cytochemistry*, 35(10):1105–1115, 1987.

[105] Y. Kapanci, C. Ribaux, C. Chaponnier, and G. Gabbiani. Cytoskeletal features of alveolar myofibroblasts and pericytes in normal human and rat lung. *Journal of Histochemistry and Cytochemistry*, 40(12):1955–1963, 1992.

[106] Ramesh C. Nayak, Audrey B. Berman, Katherine L. George, George S. Eisenbarth, and George L. King. A monoclonal antibody (3G5)-defined ganglioside antigen is expressed on the cell surface of microvascular pericytes. *Diabetes*, 167(3):1003–1015, 1988.

[107] Yang Kim, Riffat Y. Imdad, Alan H. Stephenson, Randy S. Sprague, and Andrew J. Lomgro. Vascular Endothelial Growth Factor mRNA in Pericytes Is Upregulated by Phorbol Myristate Acetate. *Hypertension*, 31[part2]:511–515, 1998.

[108] Peter Helmbold, Johannes Wohlrab, Wolfgang C. Marsch, and Ramesh C. Nayak. Human dermal pericytes express 3G5 ganglioside - A new approach for microvessel histology in the skin. *Journal of Cutaneous Pathology*, 28(4):206–210, 2001.

[109] Akira Gushi, Masashi Tanaka, Shinichiro Tsuyama, Taku Nagai, Tamotsu Kanzaki, Takuro Kanekura, and Takami Matsuyama. The 3G5 antigen is expressed in dermal mast cells but not pericytes. *Journal of Cutaneous Pathology*, 35(3):278–284, 2008.

[110] Domenico Ribatti, Roberto Tamma, Simona Ruggieri, Tiziana Annese, and Enrico Crivellato. Surface markers: An identity card of endothelial cells. *Microcirculation*, 00:e12587, 2019.

[111] M. G. Lampugnani, M. Resnati, M. Raiteri, R. Pigott, A. Pisacane, G. Houen, L. P. Ruco, and E. Dejana. A novel endothelial-specific membrane protein is a marker of cell-cell contacts. *Journal of Cell Biology*, 118(6):1511–1522, 1992.

[112] Peter J. Lenting, Olivier D. Christophe, and Cécile V. Denis. Von Willebrand factor biosynthesis, secretion, and clearance: Connecting the far ends. *Blood*, 125(13):2019–2028, 2015.

[113] Richard L. Benton, Melissa A. Maddie, Danielle R. Minnillo, Theo Hagg, and Scott R. Whittemore. Griffonia simplicifolia Isolectin B4 Identifies a Specific Subpopulation of Angiogenic Blood Vessels Following Contusive Spinal Cord Injury in the Adult Mouse. *The Journal of Comparative Neurology*, 507(1):1031–1052, 2008.

[114] Andreas Rheinländer, Burkhart Schraven, and Ursula Bommhardt. CD45 in human physiology and clinical medicine. *Immunology Letters*, 196:22–32, 2018.

[115] Gunhild Mechtersherimer, Martina Stauder, and Peter Moller. Expression of the Natural Killer (NK) Cell-Associated Antigen CD56(Leu-19), Which Is Identical to the 140-kDa Isoform of N-CAM, in Neural and Skeletal Muscle Cells and Tumors Derived Therefrom. *Ann N Y Acad Sci*, 650:311–316, 1992.

[116] Luisa Boldrin, Francesco Muntoni, and Jennifer E. Morgan. Are human and mouse satellite cells really the same? *Journal of Histochemistry and Cytochemistry*, 58(11):941–955, 2010.

[117] Paolo Bianco, M. Costantini, L. C. Dearden, and E. Bonucci. Alkaline phosphatase positive precursors of adipocytes in the human bone marrow. *British Journal of Haematology*, 68(4):401–403, 1988.

[118] Volker Nehls, Kristin Denzer, and Detlev Drenckhahn. Pericyte involvement in capillary sprouting during angiogenesis in situ. *Cell and Tissue Research*, 270(3):469–474, 1992.

[119] Per Lindahl, Bengt R Johansson, Per Levéen, and Christer Betsholtz. Pericyte Loss and Microaneurysm Formation in PDGF-B-Deficient Mice. *Science*, 277(5323), 1997.

[120] Hyeseon Cho, Tohru Kozasa, Cecilia Bondjers, Christer Betsholtz, and John H. Kehrl. Pericyte-specific expression of Rgs5: implications for PDGF and EDG receptor signaling during vascular maturation. *The FASEB Journal*, 17(3):440–2, 2003.

[121] Amy M. Mellgren, Christopher L. Smith, Gregory S. Olsen, Banu Eskiocak, Bin Zhou, Michelle N. Kazi, Fernanda R. Ruiz, William T. Pu, and Michelle D. Tallquist. Platelet-Derived Growth Factor Receptor β Signaling Is Required for Ef-

ficient Epicardial Cell Migration and Development of Two Distinct Coronary Vascular Smooth Muscle Cell Populations. *Circ Res*, 103(12):1393–1401, 2008.

[122] J. N. Passman, X. R. Dong, S.-P. Wu, C. T. Maguire, K. A. Hogan, V. L. Bautch, and M. W. Majesky. A sonic hedgehog signaling domain in the arterial adventitia supports resident Sca1+ smooth muscle progenitor cells. *Proceedings of the National Academy of Sciences*, 105(27):9349–9354, 2008.

[123] Ayelet Dar, Hagit Domev, Oren Ben-Yosef, Maty Tzukerman, Naama Zeevi-levin, Atara Novak, Igal Germanguz, Michal Amit, and Joseph Itskovitz-Eldor. Multipotent Vasculogenic Pericytes From Human Pluripotent Stem Cells Promote Recovery of Murine Ischemic Limb Ayelet Dar, Hagit Domev, Oren Ben-Yosef, Maty Tzukerman, Naama Zeevi-Levin, Atara Novak, Igal Germanguz, Michal Amit and Joseph Itskovitz-Eldor. *Circulation*, 125(1):87–99, 2012.

[124] Aaron W. James, Janette N. Zara, Xinli Zhang, Asal Askarinam, Raghav Goyal, Michael Chiang, Wei Yuan, Le Chang, Mirko Corselli, Jia Shen, Shen Pang, David Stoker, Ben Wu, Kang Ting, Bruno Péault, and Chia Soo. Perivascular stem cells: a prospectively purified mesenchymal stem cell population for bone tissue engineering. *Stem cells translational medicine*, 1(6):510–9, 2012.

[125] Stephan Nees, Gerd Juchem, Nicola Eberhorn, Martin Thallmair, Stefan Forch, Maria E. Knott, Anton Senftl, Theodor Fischlein, Bruno Reichart, and Dominik R. Weiss. Wall structures of myocardial precapillary arterioles and postcapillary venules reexamined and reconstructed in vitro for studies on barrier functions. *AJP: Heart and Circulatory Physiology*, 302(1):H51–H68, 2012.

[126] Valerie S. Lebleu, Gangadhar Taduri, Joyce O'Connell, Yingqi Teng, Vesselina G. Cooke, Craig Woda, Hikaru Sugimoto, and Raghu Kalluri. Origin and function of myofibroblasts in kidney fibrosis. *Nature Medicine*, 19(8):1047–1053, 2013.

[127] C. Soderblom, X. Luo, E. Blumenthal, E. Bray, K. Lyapichev, J. Ramos, V. Krishnan, C. Lai-Hsu, K. K. Park, P. Tsoulfas, and J. K. Lee. Perivascular Fibroblasts Form the Fibrotic Scar after Contusive Spinal Cord Injury. *Journal of Neuroscience*, 33(34):13882–13887, 2013.

[128] Alexander Birbrair, Tan Zhang, Daniel Clark Files, Sandeep Mannava, Thomas Smith, Zhong-Min Wang, Maria Laura Messi, Akiva Mintz, and Osvaldo Delbono. Type-1 pericytes accumulate after tissue injury and produce collagen in an organ-dependent manner. *Stem Cell Res Ther*, 5(6):122, 2014.

[129] Lina Chen, Fengming Qin, Menghua Ge, Qiang Shu, and Jianguo Xu. Application of adipose-derived stem cells in heart disease. *Journal of cardiovascular translational research*, 7(7):651–63, 2014.

[130] Hu Zhao, Jifan Feng, Kerstin Seidel, Songtao Shi, Ophir Klein, Paul Sharpe, and Yang Chai. Secretion of shh by a neurovascular bundle niche supports mesenchymal stem cell homeostasis in the adult mouse incisor. *Cell Stem Cell*, 14(2):160–173, 2014.

[131] Jia Shen, Swati Shrestha, Yu Hsin Yen, Greg Asatrian, Marco Mravic, Chia Soo, Kang Ting, Sarah M. Dry, Bruno Peault, and Aaron W. James. Pericyte antigens in perivascular soft tissue tumors. *International Journal of Surgical Pathology*, 23(8):638–648, 2015.

[132] Andreas Svensson, Ilknur Özen, Guillem Genové, Gesine Paul, and Johan Bengzon. Endogenous brain pericytes are widely activated and contribute to mouse glioma microvasculature. *PLoS ONE*, 10(4):e0123553, 2015.

[133] Katharina S. Volz, Andrew H. Jacobs, Heidi I. Chen, Aruna Poduri, Andrew S. McKay, Daniel P. Riordan, Natalie Kofler, Jan Kitajewski, Irving Weissman, and Kristy Red-Horse. Pericytes are progenitors for coronary artery smooth muscle. *eLife*, 4:1–22, 2015.

[134] Liqun He, Michael Vanlandewijck, Elisabeth Raschperger, Maarja Andaloussi Maë, Bongnam Jung, Thibaud Lebouvier, Koji Ando, Jennifer Hofmann, Annika Keller, and Christer Betsholtz. Analysis of the brain mural cell transcriptome. *Scientific Reports*, 6(35108):1–13, 2016.

[135] Henar Cuervo, Brianna Pereira, Taliha Nadeem, Mika Lin, Frances Lee, Jan Kitajewski, and Chyuan Sheng Lin. PDGFRβ-P2A-CreERT2 mice: a genetic tool to target pericytes in angiogenesis. *Angiogenesis*, 20(4):655–662, 2017.

[136] Robert A. Hill, Lei Tong, Peng Yuan, Sasidhar Murikinati, Shobhana Gupta, and Jaime Grutzendler. Regional Blood Flow in the Normal and Ischemic Brain Is Controlled by Arteriolar Smooth Muscle Cell Contractility and Not by Capillary Pericytes. *Neuron*, 87(1):95–110, 2015.

[137] Yi Ting Chen, Fan Chi Chang, Ching Fang Wu, Yu Hsiang Chou, Huan Lun Hsu, Wen Chih Chiang, Juqun Shen, Yung Ming Chen, Kwan Dun Wu, Tun Jun Tsai, Jeremy S. Duffield, and Shuei Liong Lin. Platelet-derived growth factor receptor signaling activates pericyte-myofibroblast transition in obstructive and post-ischemic kidney fibrosis. *Kidney International*, 80(11):1170–1181, 2011.

[138] Chi Hung, Geoffrey Linn, Yu Hua Chow, Akio Kobayashi, Kristen Mittelsteadt, William A. Altemeier, Sina A. Gharib, Lynn M. Schnapp, and Jeremy S. Duffield. Role of lung Pericytes and resident fibroblasts in the pathogenesis of pulmonary fibrosis. *American Journal of Respiratory and Critical Care Medicine*, 188(7):820–830, 2013.

[139] John L. Mignone, Valery Kukekov, Ann Shyn Chiang, Dennis Steindler, and Grigori Enikolopov. Neural Stem and Progenitor Cells in Nestin-GFP Transgenic Mice. *Journal of Comparative Neurology*, 469(3):311–324, 2004.

[140] Iain R. Murray, Zaniah N. Gonzalez, James Baily, Ross Dobie, Robert J. Wallace, A. C. Mackinnon, Jamie R. Smith, Stephen N. Greenhalgh, A. I. Thompson,

K. P. Conroy, David W. Griggs, P. G. Ruminski, Gillian A. Gray, M. Singh, M. A. Campbell, Timothy J. Kendall, J. Dai, Yong Li, John P. Iredale, Hamish Simpson, Johnny Huard, Bruno Péault, and Neil C. Henderson. αv integrins on mesenchymal cells regulate skeletal and cardiac muscle fibrosis. *Nature Communications*, 8(1):1118, 2017.

[141] Aaron W. James, Paul Hindle, Iain R. Murray, Christopher C. West, Tulyapruek Tawonsawatruk, Jia Shen, Greg Asatrian, Xinli Zhang, Vi Nguyen, A. Hamish Simpson, Kang Ting, Bruno Péault, and Chia Soo. Pericytes for the treatment of orthopedic conditions. *Pharmacology and Therapeutics*, 171:93–103, 2017.

[142] Paul Hindle, James Baily, Nusrat Khan, Leela C. Biant, A. Hamish R. Simpson, and Bruno Péault. Perivascular Mesenchymal Stem Cells in Sheep: Characterization and Autologous Transplantation in a Model of Articular Cartilage Repair. *Stem Cells and Development*, 25(21):1659–1669, 2016.

[143] Cristina L. Esteves, Tara A. Sheldrake, Lucy Dawson, Timothy Menghini, Burgunde Elisabeth Rink, Karin Amilon, Nusrat Khan, Bruno Péault, and Francesc Xavier Donadeu. Equine Mesenchymal Stromal Cells Retain a Pericyte-Like Phenotype. *Stem Cells and Development*, 26(13):964–972, 2017.

[144] Cristina L Esteves, Tara A Sheldrake, Simone P Mesquita, Juan J Pesántez, Timothy Menghini, Lucy Dawson, Bruno Péault, and F Xavier Donadeu. Isolation and characterization of equine native MSC populations. *Stem Cell Research and Therapy*, 8(1):1–12, 2017.

[145] Heather C. Etchevers, Claude Vincent, Nicole M. Le Douarin, and Gerard F. Couly. The cephalic neural crest provides pericytes and smooth muscle cells to all blood vessels of the face and forebrain. *Development*, 128(7):1059–1068, 2001.

[146] Mark W. Majesky. Developmental basis of vascular smooth muscle diversity. *Arteriosclerosis, Thrombosis, and Vascular Biology*, 27(6):1248–1258, 2007.

[147] Mark W. Majesky, Xiu Rong Dong, Jenna N. Regan, and Virginia J. Hoglund. Vascular smooth muscle progenitor cells: Building and repairing blood vessels. *Circulation Research*, 108(3):365–377, 2011.

[148] Annika Armulik, Guillem Genové, and Christer Betsholtz. Pericytes: Developmental, Physiological, and Pathological Perspectives, Problems, and Promises. *Developmental Cell*, 21(2):193–215, 2011.

[149] Maria G. Minasi, Mara Riminucci, Luciana De Angelis, Ugo Borello, Barbara Berarducci, Anna Innocenzi, Arianna Caprioli, Dario Sirabella, Marta Baiocchi, Ruggero De Maria, Renata Boratto, Thierry Jaffredo, Vania Broccoli, Paolo Bianco, and Giulio Cossu. The meso-angioblast: A multipotent, self-renewing cell that originates from the dorsal aorta and differentiates into most mesodermal tissues. *Development*, 129(11):2773–2783, 2002.

[150] Giulio Cossu and Paolo Bianco. Mesoangioblasts - Vascular progenitors for extravascular mesodermal tissues. *Current Opinion in Genetics and Development*, 13(5):537–542, 2003.

[151] Maurilio Sampaolesi, Yvan Torrente, Anna Innocenzi, Rossana Tonlorenzi, Giuseppe D'Antona, M. Antonietta Pellegrino, Rita Barresi, Nereo Bresolin, M. Gabriella Cusella De Angelis, Kevin P. Campbell, Roberto Bottinelli, and Giulio Cossu. Cell therapy of α-sarcoglycan null dystrophic mice through intra-arterial delivery of mesoangioblasts. *Science*, 301(5632):487–492, 2003.

[152] D. Galli, A. Innocenzi, L Staszewsky, L Zanetta, M. Sampaolesi, A. Bai, E. Martinoli, E. Carlo, G. Balconi, F. Fiordaliso, S. Chimenti, G. Cusella, E. Dejana, G. Cossu, and R. Latini. Mesoangioblasts, Vessel-Associated Multipotent Stem

Cells, Repair the Infarcted Heart by Multiple Cellular Mechanisms: A Comparison With Bone Marrow Progenitors, Fibroblasts, and Endothelial Cells. *Arteriosclerosis, Thrombosis, and Vascular Biology*, 25(4):692–697, 2005.

[153] Maurilio Sampaolesi, Stephane Blot, Giuseppe D'Antona, Nicolas Granger, Rossana Tonlorenzi, Anna Innocenzi, Paolo Mognol, Jean Lauren Thibaud, Beatriz G. Galvez, Ines Barthélémy, Laura Perani, Sara Mantero, Maria Guttinger, Orietta Pansarasa, Chiara Rinaldi, M. Gabriella Cusella De Angelis, Yvan Torrente, Claudio Bordignon, Roberto Bottinelli, and Giulio Cossu. Mesoangioblast stem cells ameliorate muscle function in dystrophic dogs. *Nature*, 444(7119):574–579, 2006.

[154] Holger Gerhardt and Christer Betsholtz. Endothelial-pericyte interactions in angiogenesis. *Cell and Tissue Research*, 314(1):15–23, 2003.

[155] Konstantin Gaengel, Guillem Genové, Annika Armulik, and Christer Betsholtz. Endothelial-mural cell signaling in vascular development and angiogenesis. *Arteriosclerosis, Thrombosis, and Vascular Biology*, 29(5):630–638, 2009.

[156] Fergus M. O'Farrell and David Attwell. A role for pericytes in coronary no-reflow. *Nature reviews Cardiology*, 11(7):427–432, 2014.

[157] Ania M Stefańska, Bruno Péault, and John J. Mullins. Renal pericytes: Multifunctional cells of the kidneys. *Pflugers Archiv European Journal of Physiology*, 465(6):767–773, 2013.

[158] Catherine N. Hall, Clare Reynell, Bodil Gesslein, Nicola B. Hamilton, Anusha Mishra, Brad A. Sutherland, Fergus M. O'Farrell, Alastair M. Buchan, Martin Lauritzen, and David Attwell. Capillary pericytes regulate cerebral blood flow in health and disease. *Nature*, 508(7494):55–60, 2014.

[159] Claudia Schrimpf and Jeremy S. Duffield. Mechanisms of fibrosis: The role of the pericyte. *Current Opinion in Nephrology and Hypertension*, 20(3):297–305, 2011.

[160] Benjamin D. Humphreys, Shuei Liong Lin, Akio Kobayashi, Thomas E. Hudson, Brian T. Nowlin, Joseph V. Bonventre, M. Todd Valerius, Andrew P. McMahon, and Jeremy S. Duffield. Fate tracing reveals the pericyte and not epithelial origin of myofibroblasts in kidney fibrosis. *American Journal of Pathology*, 176(1):85–97, 2010.

[161] Alexander Birbrair. *Pericyte Biology in Different Organs*, volume 1122. 2019.

[162] Takaaki Higashi, Scott L. Friedman, and Yujin Hoshida. Hepatic stellate cells as key target in liver fibrosis. *Advanced Drug Delivery Reviews*, 121:27–42, 2017.

[163] Ramon Bataller and David A. Brenner. Hepatic stellate cells as a target for the treatment of liver fibrosis. *Seminars in Liver Disease*, 21(3):437–451, 2001.

[164] John P Iredale. Models of liver fibrosis: exploring the dynamic nature of inflammation and repair in a solid organ. 117(3):539–548, 2007.

[165] Koichi Arimura, Tetsuro Ago, Masahiro Kamouchi, Kuniyuki Nakamura, Koji Ishitsuka, Junya Kuroda, Hiroshi Sugimori, Hiroaki Ooboshi, Tomio Sasaki, and Takanari Kitazono. PDGF Receptor Beta; Signaling in Pericytes Following Ischemic Brain Injury. *Current Neurovascular Research*, 9(1):1–9, 2012.

[166] David A. Brenner, Tatiana Kisseleva, David Scholten, Yong Han Paik, Keiko Iwaisako, Sayaka Inokuchi, Bernd Schnabl, Ekihiro Seki, Samuele De Minicis, Christoph Oesterreicher, and Kojiro Taura. Origin of myofibroblasts in liver fibrosis. *Fibrogenesis and Tissue Repair*, 5(SUPPL.1):2–5, 2012.

[167] Ching Fang Wu, Wen Chih Chiang, Chun Fu Lai, Fan Chi Chang, Yi Ting Chen, Yu Hsiang Chou, Ting Hui Wu, Geoffrey R. Linn, Hong Ling, Kwan Dun Wu,

Tun Jun Tsai, Yung Ming Chen, Jeremy S. Duffield, and Shuei Liong Lin. Transforming growth factor β-1 stimulates profibrotic epithelial signaling to activate pericyte-myofibroblast transition in obstructive kidney fibrosis. *American Journal of Pathology*, 182(1):118–131, 2013.

[168] Marion Scharpfenecker, Ben Floot, Nicola S. Russell, Rob P. Coppes, and Fiona A. Stewart. Thalidomide ameliorates inflammation and vascular injury but aggravates tubular damage in the irradiated mouse kidney. *International Journal of Radiation Oncology Biology Physics*, 89(3):599–606, 2014.

[169] Sophie Dulauroy, Selene E. Di Carlo, Francina Langa, Gérard Eberl, and Lucie Peduto. Lineage tracing and genetic ablation of ADAM12 + perivascular cells identify a major source of profibrotic cells during acute tissue injury. *Nature Medicine*, 18(8):1262–1270, 2012.

[170] Christian Göritz, David O. Dias, Nikolay Tomilin, Mariano Barbacid, Oleg Shupliakov, and Jonas Frisén. A pericyte origin of spinal cord scar tissue. *Science*, 333(6039):238–242, 2011.

[171] Alexander Birbrair, Tan Zhang, Zhong-Min Wang, Maria L. Messi, Akiva Mintz, and Osvaldo Delbono. Pericytes: multitasking cells in the regeneration of injured, diseased, and aged skeletal muscle. *Frontiers in Aging Neuroscience*, 6:245, 2014.

[172] Yuehua Jiang, Ben Vaessen, Todd Lenvik, Mark Blackstad, Morayma Reyes, and Catherine M. Verfaillie. Multipotent progenitor cells can be isolated from postnatal murine bone marrow, muscle, and brain. *Experimental Hematology*, 30(8):896–904, 2002.

[173] Patricia A. Zuk, Min Zhu, Peter Ashjian, Daniel A. De Ugarte, Jerry I. Huang, Hisroshi Mizuno, Zeni C. Alfonso, John K. Fraser, Prosper Benhaim, and Marc H.

Hedrick. Human Adipose Tissue Is a Source of Multipotent Stem Cells. *Molecular Biology of the Cell*, 13:4279–4295, 2002.

[174] Kenneth R. McGaffin, Cheuk-Kwan Sun, Jennifer J. Rager, Lia C. Romano, Baobo Zou, Michael A. Mathier, Robert M. O'Doherty, Charles F. McTiernan, and Christopher P. O'Donnell. Leptin signalling reduces the severity of cardiac dysfunction and remodelling after chronic ischaemic injury. *Cardiovascular Research*, 77(1):54–63, 2008.

[175] Daniela Klaffenbach, Udo Meißner, Michael Raake, Fabian Fahlbusch, Miguel A. Alejandre Alcazar, Ida Allabauer, Jürgen Kratzsch, Wolfgang Rascher, and Jörg Dötsch. Upregulation of leptin-receptor in placental cells by Hypoxia. *Regulatory Peptides*, 167(1):156–162, 2011.

[176] Xinyang Hu, Rongrong Wu, Zhi Jiang, Lihan Wang, Panpan Chen, Ling Zhang, Lu Yang, Yan Wu, Han Chen, Huiqiang Chen, Yinchuan Xu, Yu Zhou, Xin Huang, Keith A Webster, Hong Yu, and Jian'an Wang. Leptin signaling is required for augmented therapeutic properties of mesenchymal stem cells conferred by hypoxia preconditioning. *Stem cells*, 32(10):2702–13, 2014.

[177] Kenneth R. McGaffin, William G. Witham, Keith A. Yester, Lia C. Romano, Robert M. O'Doherty, Charles F. McTiernan, and Christopher P. O'Donnell. Cardiac-specific leptin receptor deletion exacerbates ischaemic heart failure in mice. *Cardiovascular Research*, 89(1):60–71, 2011.

[178] Michael E Hall, Romain Harmancey, and David E Stec. Lean heart: Role of leptin in cardiac hypertrophy and metabolism. *World journal of cardiology*, 7(9):511–24, 2015.

[179] Hiroki Matsui, Masahiko Motooka, Hiroto Koike, Masahiro Inoue, Tsutomu Iwasaki, Tadashi Suzuki, Masahiko Kurabayashi, and Tomoyuki Yokoyama. Is-

chemia/reperfusion in rat heart induces leptin and leptin receptor gene expression. *Life Sciences*, 80(7):672–680, 2007.

[180] Kenneth R. McGaffin, Christine S. Moravec, and Charles F. McTiernan. Leptin signaling in the failing and mechanically unloaded human heart. *Circulation: Heart Failure*, 2(6):676–683, 2009.

[181] Josette M Northcott, Azadeh Yeganeh, Carla G Taylor, Peter Zahradka, and Jeffrey T Wigle. Adipokines and the cardiovascular system: mechanisms mediating health and disease. *Canadian journal of physiology and pharmacology*, 90(8):1029–59, 2012.

[182] Mark F. McCarty and James J. DiNicolantonio. The Molecular Biology and Pathophysiology of Vascular Calcification. *Postgraduate Medicine*, 126(2):54–64, 2014.

[183] Amaia Rodríguez, Javier Gómez-Ambrosi, Victoria Catalán, Ana Fortuño, and Gema Frühbeck. Leptin inhibits the proliferation of vascular smooth muscle cells induced by angiotensin II through nitric oxide-dependent mechanisms. *Mediators of inflammation*, 2010:105489, 2010.

[184] Asad Zeidan, Daniel M Purdham, Venkatesh Rajapurohitam, Sabzali Javadov, Subrata Chakrabarti, and Morris Karmazyn. Leptin Induces Vascular Smooth Muscle Cell Hypertrophy through Angiotensin II- and Endothelin-1-Dependent Mechanisms and Mediates Stretch-Induced Hypertrophy. *The journal of pharmacology and experimental therapeutics*, 315(3):1075–1084, 2005.

[185] Georgina M. Ellison, Daniele Torella, Santo Dellegrottaglie, Claudia Perez-Martinez, Armando Perez De Prado, Carla Vicinanza, Saranya Purushothaman, Valentina Galuppo, Claudio Iaconetti, Cheryl D. Waring, Andrew Smith, Michele Torella, Carlos Cuellas Ramon, Jose Manuel Gonzalo-Orden, Valter Agosti,

Ciro Indolfi, Manuel Galianes, Felipe Fernandez-Vazquez, and Bernardo Nadal-Ginard. Endogenous cardiac stem cell activation by insulin-like growth factor-1/hepatocyte growth factor intracoronary injection fosters survival and regeneration of the infarcted pig heart. *Journal of the American College of Cardiology*, 58(9):977–986, 2011.

[186] Georgina M. Ellison, Bernardo Nadal-Ginard, and Daniele Torella. Optimizing cardiac repair and regeneration through activation of the endogenous cardiac stem cell compartment. *Journal of Cardiovascular Translational Research*, 5(5):667–677, 2012.

[187] Nam E. Joo, Toshiya Watanabe, C. Chen, Martha Chekenya, William B. Stallcup, and Yvonne L. Kapila. NG2, a novel proapoptotic receptor, opposes integrin α4 to mediate anoikis through PKCα-dependent suppression of FAK phosphorylation. *Cell Death and Differentiation*, 15(5):899–907, 2008.

[188] Nam E. Joo, Di Miao, Mercedes Bermúdez, William B. Stallcup, and Yvonne L. Kapila. Shedding of NG2 by MMP-13 Attenuates Anoikis. *DNA and Cell Biology*, 33(12):854–862, 2014.

[189] Andrew R. Jensen, Benjamin V. Kelley, Gina M. Mosich, Allison Ariniello, Claire D. Eliasberg, Brandon Vu, Paras Shah, Sai K. Devana, Iain R. Murray, Bruno Péault, Ayelet Dar, and Frank A. Petrigliano. Neer Award 2018: Platelet-derived growth factor receptor α co-expression typifies a subset of platelet-derived growth factor receptor β–positive progenitor cells that contribute to fatty degeneration and fibrosis of the murine rotator cuff. *Journal of Shoulder and Elbow Surgery*, 27(7):1149–1161, 2018.

[190] Valeria Vincenza Alvino, Rodrigo Fernández-Jiménez, Iker Rodriguez-Arabaolaza, Sadie Slater, Giuseppe Mangialardi, Elisa Avolio, Helen Spencer, Lucy Culliford, Sakinah Hassan, Lorena Sueiro Ballesteros, Andrew Herman,

Ali Ayaon-Albarrán, Carlos Galán-Arriola, Javier Sánchez-González, Helena Hennessey, Catherine Delmege, Raimondo Ascione, Costanza Emanueli, Gianni Davide Angelini, Borja Ibanez, and Paolo Madeddu. Transplantation of allogeneic pericytes improves myocardial vascularization and reduces interstitial fibrosis in a swine model of reperfused acute myocardial infarction. *Journal of the American Heart Association*, 7(2):e006727, 2018.

[191] Hiroshi Ando, Thomas Kubin, Wolfgang Schaper, and Jutta Schaper. Cardiac microvascular endothelial cells express α-smooth muscle actin and show low NOS III activity. *American Journal of Physiology - Heart and Circulatory Physiology*, 276(5):H1755–68, 1999.

[192] Rajesh Katare, Federica Riu, Kathryn Mitchell, Miriam Gubernator, Paola Campagnolo, Yuxin Cui, Orazio Fortunato, Elisa Avolio, Daniela Cesselli, Antonio Paolo Beltrami, Gianni Angelini, Costanza Emanueli, and Paolo Madeddu. Transplantation of Human Pericyte Progenitor Cells Improves the Repair of Infarcted Heart Through Activation of an Angiogenic Program Involving MicroRNA-132. *Circulation research*, 109(8):894–906, 2011.

[193] E. Avolio, I. Rodriguez-Arabaolaza, H. L. Spencer, F. Riu, G. Mangialardi, S. C. Slater, J. Rowlinson, V. V. Alvino, O. O. Idowu, S. Soyombo, a. Oikawa, M. M. Swim, C. H. T. Kong, H. Cheng, H. Jia, M. T. Ghorbel, J. C. Hancox, C. H. Orchard, G. Angelini, C. Emanueli, M. Caputo, and P. Madeddu. Expansion and Characterization of Neonatal Cardiac Pericytes Provides a Novel Cellular Option for Tissue Engineering in Congenital Heart Disease. *Journal of the American Heart Association*, 4(6):e002043–e002043, 2015.

[194] Lijun Ding, Bianca Vezzani, Nusrat Khan, Jing Su, Lu Xu, Guijun Yan, Yong Liu, Ruotian Li, Anushri Gaur, Zhenyu Diao, Yali Hu, Zhongzhou Yang, W. Reef Hardy, Aaron W. James, Haixiang Sun, and Bruno Péault. CD10 expression

identifies a subset of human perivascular progenitor cells with high proliferation and calcification potentials. *Stem Cells*, (February):1–22, 2019.

[195] Isaac William Shaw. *Perivascular cells and their sub-types in healthy , aged and diseased kidney .* PhD thesis, University of Edinburgh, 2018.

[196] Suchitra D. Gopinath and Thomas A. Rando. Stem Cell Review Series: Aging of the skeletal muscle stem cell niche. *Aging Cell*, 7(4):590–598, 2008.

[197] Alexander Birbrair, Tan Zhang, Zhong Min Wang, Maria Laura Messi, Akiva Mintz, and Osvaldo Delbono. Pericytes at the intersection between tissue regeneration and pathology. *Clinical Science*, 128(2):81–93, 2015.

[198] Suzanne Hughes, Tom Gardiner, Ping Hu, Louise Baxter, Emelia Rosinova, and Tailoi Chan-Ling. Altered pericyte-endothelial relations in the rat retina during aging: Implications for vessel stability. *Neurobiology of Aging*, 27(12):1838–1847, 2006.

[199] Tapas Chandra Nag, Meenakshi Maurya, and Tara Sankar Roy. Age-related changes of the human retinal vessels: Possible involvement of lipid peroxidation. *Annals of Anatomy*, 226:35–47, 2019.

[200] Chien-Wen Chen, Masaho Okada, Jonathan D. Proto, Xueqin Gao, Naosumi Sekiya, Sarah A. Beckman, Mirko Corselli, Mihaela Crisan, Arman Saparov, Kimimasa Tobita, Bruno Péault, and Johnny Huard. Human Pericytes for Ischemic Heart Repair. *Stem Cells*, 31(2):305–316, 2013.

[201] Bianca Vezzani, Isaac Shaw, Hanna Lesme, Li Yong, Nusrat Khan, Carlo Tremolada, and Bruno Péault. Higher Pericyte Content and Secretory Activity of Microfragmented Human Adipose Tissue Compared to Enzymatically Derived Stromal Vascular Fraction. *Stem Cells Translational Medicine*, 7(12):876–886, dec 2018.

[202] Mark F. Pittenger, Dennis E. Discher, Bruno M. Péault, Donald G. Phinney, Joshua M. Hare, and Arnold I. Caplan. Mesenchymal stem cell perspective: cell biology to clinical progress. *npj Regenerative Medicine*, 4(1), 2019.

[203] Mario Gomez-Salazar, Zaniah N. Gonzalez, Joan Casamitjana, Mihaela Crisan, Aaron W. James, and Bruno Péault. Five decades later, are mesenchymal stem cells still relevant? *Front. Bioeng. Biotechnol.*, 2020.

Appendices

Macros

Macros were scripted in IJ1 Macro language using the FIJI/imageJ software. Key input on better code was provided by Dr. Bertrand Vernay, head of the SCRM Imaging facility, and Isaac Shaw.

.1 Stitching Operetta whole scan images

This macro was scripted in collaboration with Dr. Bertrand Vernay, head of the SCRM Imaging facility.

```
/*
MACRO FOR OPERETTA v2.1 (22022017)

AUTHORS: Joan Casamitjana*, Bertrand Vernay and Isaac Shaw
*Main coder, any doubt contact Joan (s1478844@sms.ed.ac.uk).

Aims: This macro will generate a reconstruction of your Operetta scan as viewed in Columbus when all fields are selected, but with full resolution.

This macro only works with single channel images and a maximum of 4 channels (downloaded folder from Columbus when you back up your data).

This macro automatically detects number of files, channels, reset max intensity (as fiji is applying autocontrast), merges single images, calculates their relative position, stitches them, treats single channels (as an option) an
By default, this macro treats the single channels of your montage by Substract background and setting B/C in Auto, in that order.
If other treatments are required, user will have to change treatments settings on the script.
*/

macro "Operetta Stitching [F1]" { //installs this macro with F1 botton as a shortcut -- has to be done manually

//set batch mode to true for faster processing
setBatchMode(true);

//DIALOG BOX - WARNING
Dialog.create("WARNING");
Dialog.addMessage("1- To run this macro properly, all windows will be closed and clipboard content will be erased. Pressing OK will close them without option to save them."+'\n'+ "2- Stiching in FIJI does not like long directory
Dialog.show();

//Clear log window
print("\\Clear");

//Start message
print("------ MACRO STARTED ------");

//Input & output directories
folder = getDirectory("Select the folder containing your raw files");

//Variables initialisation
var count=0;
var xCoordinate = newArray(1);      //one indexed value of 0
var newxCoordinate = newArray(1);   //one indexed value of 0
var newyCoordinate = newArray(1);   //one indexed value of 0
var ycoordinate = newArray(1);      //one indexed value of 0
var newX = newArray(1); //one indexed value of 0
var tileName = newArray("tile");    //one indexed string of "tile"
var tileInX =1;
var tileInY=1;
var xInterval = 1;
var yInterval = 1;
var minX=0;
var manX=0;
var minY=0;
var maxY=0;
var num_single_images=0

//Main body of macro
```

```
//selects the beginning of your files (assuming it is always something like '001002-')
listFiles(folder);
function listFiles(folder) {
    list1 = getFileList(folder);
    for (i=0; i<1; i++) { //picks up the first file only
        beginning_of_your_file = substring(list1[i],0,7); //takes first 7 characters of the file name
        String.copy(beginning_of_your_file); //copies the string into the clipboard
    }
}
beginning_of_your_file = String.paste //generates the object with the content of the clipboard, THIS HAS TO GO WITH THE PREVIOUS!!!

//Counting number of total single images (we still inside the previous function)
listFiles2(folder);
function listFiles2(folder) {
    list2 = getFileList(folder);
    for (i=0; i<list2.length; i++){
        tifs=indexOf(list2[i], ".tif"); //look for all tif files and counts them
        if (tifs != -1) {
            num_single_images++;
        }
    }
}

//DIALOG BOX - INPUT VALUES (external information that user need to introduce manually)
Dialog.create("Introducing parameters");
Dialog.addNumber("Percentage of overlap", 10);
//Dialog.addChoice("Objective used:", newArray("2x", "10x", "20x", "40x", "60x", "100x"));
//Dialog.addNumber("Scale bar in microns", 100);
Dialog.addString("Save your final image as (.tif)", "Montage");
Dialog.addCheckbox("Delete Composite folder", true);
Dialog.addCheckbox("Delete Tile folder", true);
Dialog.addCheckbox("Enhance image (modify the pixel data)", false);
Dialog.show();
overlap = Dialog.getNumber();
//objective_used = Dialog.getChoice();
//dim_scalebar = Dialog.getNumber();
montage_name = Dialog.getString();
del_CompositeFolder = Dialog.getCheckbox();
del_TileFolder = Dialog.getCheckbox();
enhance = Dialog.getCheckbox();

run("Close All");
print("\\Clear"); //Reset log
print("The working folder path is: " + folder);
print("Your files begin with '" + beginning_of_your_file + "'");
//print("Your montage will be displayed at " + (montage_scale*100) + "% of its total resolution.");
//print("Objective used: " + objective_used);
//print("Scale bar displayed: " + dim_scalebar + "um");
print("Your montage will be saved as: " + montage_name + ".tif");

field_heigth = 1024 //in pixels. Dimension of your images. Required for blank images.
field_width = 1360 //in pixels
startingTime = getTime();
```

```
//find metadata *.xml file and extract coordinates and number of tiles
list = getFileList(folder);
    for (m=0; m<list.length; m++){
        print(list[m]);
        if (endsWith(list[m], "ImageIndex.ColumbusIDX.xml")) {
            //Open metadata file as a string
    filestring=File.openAsString(folder+list[m]);
    delimiters='(<URL BufferNo="0">)';      //create line return after <URL BufferNo="0">
    rows=split(filestring, delimiters);     //create line return after <URL BufferNo="0">

    //Counting number of tiles listed in metadata: based on first channel (there is always a channel1)
    for (i=0; i<rows.length; i++){
        indexTileNameTif=indexOf(rows[i], ".tif");          //Check if line contains ".tif"
        row_channel1=indexOf(rows[i], "1.tif");             //Check if line contains "1.tif"
            if ((indexTileNameTif != -1) && (row_channel1 != -1)) {  //selecting only first channel for each tile
                count++;
                }
        }
    print("Number of tiles= "+count);

    //Extraction X and Y coordinates for each tile
    for (i=0; i<rows.length; i++){
        indexTileNameTif=indexOf(rows[i], ".tif");          //Check if line contains ".tif"
        row_channel1=indexOf(rows[i], "1.tif");
            if ((indexTileNameTif != -1) && (row_channel1 != -1)) {         //Conditions only process line containig both ".tif" & "1.tif"
                name =substring(rows[i], 0, indexTileNameTif+4);    //Extract tile file name from metadata
                //print("Tile name= "+name);
                xPositionStart= (indexOf(rows[i], '<PositionX Unit="m">'));
                xPositionStop= (indexOf(rows[i],'</PositionX>'));
                yPositionStart= (indexOf(rows[i], '<PositionY Unit="m">'));
                yPositionStop= (indexOf(rows[i],'</PositionY>'));
                TileXPosition= substring(rows[i],xPositionStart+20,xPositionStop);  //Get TileXPosition position coordinates
                TileXPosition= 10000000000000*parseFloat(TileXPosition);                    //TileXPosition in float, it is multiplied by 10^14 since operetta gives 14 decimal numbers
                TileYPosition= substring(rows[i],yPositionStart+20,yPositionStop);  //Get TileYPosition position coordinates
                TileYPosition= 10000000000000*parseFloat(TileYPosition);                    //TileYPosition in float
                TileXPosition= parseInt(TileXPosition);                             //TileXPosition as integer
                TileYPosition= parseInt(TileYPosition);                             //TileYPosition as integer
                //print(TileXPosition);
                //print(TileYPosition);
                tileName = Array.concat(tileName, name);
                xCoordinate = Array.concat(xCoordinate, TileXPosition);             //add x coordinate to array
                yCoordinate = Array.concat(yCoordinate, TileYPosition);             //add y coordinate to array
                //print("X coordinates");
                //Array.print(xCoordinate);
                //print("Y coordinates");
                //Array.print(yCoordinate);
                }
        }

        //Final list of X & Y coordinates and name for tiles
        print("***********************************************");
        //print("X coordinates");
        xCoordinate = Array.slice(xCoordinate,1);               //remove first value created at initialisation of array
```

```
      //Array.print(xCoordinate);
      for (h=0;h<xCoordinate.length; h++){
      //print(xCoordinate[h]);
      }
      //print("Y coordinates");
      yCoordinate = Array.slice(yCoordinate,1);              //remove first value created at initialisation of array
      //Array.print(yCoordinate);
      for (h=0;h<yCoordinate.length; h++){
      //print(yCoordinate[h]);
      }

   //Determining mosaic size in width and height
   xStats=Array.getStatistics(xCoordinate, min, max, mean, stdDev);       //min and max value of x coordinates
   minX = min;
   print("min X= "+minX);
   maxX = max;
   print("max X= "+maxX);

   yStats = Array.getStatistics(yCoordinate, min, max, mean, stdDev);     //min and max value of y coordinates
   minY = min;
   print("min Y= "+minY);
   maxY= max;
   print("max Y= "+maxY);

//Getting the tile interval
   superArrayX= Array.copy(xCoordinate);
   superArrayX= Array.sort(superArrayX);
   for (i=0; i+1<superArrayX.length; i++){
       x1num =(superArrayX[i]);
       x2num = (superArrayX[i+1]);
       if (x1num != x2num){
           xInterval = x2num -x1num;
           //print("Tile X Interval = "+xInterval);
       }
   }
   superArrayY= Array.copy(yCoordinate);
   superArrayY= Array.sort(superArrayY);
   for (i=0; i+1<superArrayY.length; i++){
       y1num =(superArrayY[i]);
       y2num = (superArrayY[i+1]);
       if (y1num != y2num){
           yInterval = y2num -y1num;
           //print("Tile Y Interval = "+yInterval);
       }
   }

//Obtaining coordinates (simple numbers)
   for (h=0; h<xCoordinate.length; h++){
       newX = xCoordinate[h];
       newX = round((newX-minX)/xInterval);
       newxCoordinate = Array.concat(newxCoordinate, newX);
       }
   newxCoordinate = Array.slice(newxCoordinate,1);
   for (h=0; h<yCoordinate.length; h++){
       newY = yCoordinate[h];
       newY= abs(round((newY-maxY)/yInterval)); //y numbers are negative, we need them positive
       //print(newY);
       newyCoordinate = Array.concat(newyCoordinate, newY);
       }
    newyCoordinate = Array.slice(newyCoordinate,1);

//resuming the size
    tileInX=parseInt((maxX-minX)/xInterval)+1;  // add 1 to make it works WHY?
    print(tileInX +" tiles in X");

    tileInY=parseInt((maxY-minY)/yInterval)+1;  // add 1 to make it works WHY?
    print(tileInY +" tiles in Y");
          }
    }

print("You are processing " + count + " fields.");

//Calculating number of channels
number_of_channels = num_single_images/count
print("You are processing " + number_of_channels + " channels.");

//Creating output folder: Composites
Composites = folder+"Composites"+File.separator;
File.makeDirectory(Composites);
CompositeFolder = folder+ "Composites\\"
print("Generated files can be located in: " + CompositeFolder);

for (i = 1; i < count+1 ; i++) {
   //1 CHANNEL
   if (number_of_channels == 1) {
       open(folder + beginning_of_your_file + i + "-001001001.tif");
       n1= beginning_of_your_file + i + "-001001001.tif";
       selectWindow(n1);
       setMinAndMax(0, 16384);
       }
   //2 CHANNELS
   if (number_of_channels == 2) {
       open(folder + beginning_of_your_file + i + "-001001001.tif");
       n1= beginning_of_your_file + i + "-001001001.tif";
       selectWindow(n1);
       setMinAndMax(0, 16384);
       open(folder + beginning_of_your_file + i + "-001001002.tif");
       n2= beginning_of_your_file + i + "-001001002.tif";
       selectWindow(n2);
       setMinAndMax(0, 16384);
       run("Merge Channels...", "c2=" + n2 + " c3=" + n1 + " create");
       }
   //3 CHANNELS
   if (number_of_channels == 3) {
       open(folder + beginning_of_your_file + i + "-001001001.tif");
       n1= beginning_of_your_file + i + "-001001001.tif";
```

```
        selectWindow(n1);
        setMinAndMax(0, 16384);
        open(folder + beginning_of_your_file + i + "-001001002.tif");
        n2= beginning_of_your_file + i + "-001001002.tif";
        selectWindow(n2);
        setMinAndMax(0, 16384);
        open(folder + beginning_of_your_file + i + "-001001003.tif");
        n3= beginning_of_your_file + i + "-001001003.tif";
        selectWindow(n3);
        setMinAndMax(0, 16384);
        run("Merge Channels...", "c1=" + n3 + " c2=" + n2 + " c3=" + n1 + " create");
        }
    //4 CHANNELS
    if (number_of_channels == 4) {
        open(folder + beginning_of_your_file + i + "-001001001.tif");
        n1= beginning_of_your_file + i + "-001001001.tif";
        selectWindow(n1);
        setMinAndMax(0, 16384);
        open(folder + beginning_of_your_file + i + "-001001002.tif");
        n2= beginning_of_your_file + i + "-001001002.tif";
        selectWindow(n2);
        setMinAndMax(0, 16384);
        open(folder + beginning_of_your_file + i + "-001001003.tif");
        n3= beginning_of_your_file + i + "-001001003.tif";
        selectWindow(n3);
        setMinAndMax(0, 16384);
        open(folder + beginning_of_your_file + i + "-001001004.tif");
        n4= beginning_of_your_file + i + "-001001004.tif";
        selectWindow(n4);
        setMinAndMax(0, 16384);
        run("Merge Channels...", "c1=" + n3 + " c2=" + n2 + " c3=" + n1 + " c4=" + n4 + " create");
        }

saveAs("Tiff", CompositeFolder + "Field " + i);
print("Field " + i + " processed...");
close();
}

//Creating a blank image to fill empty spaces
newImage("Field b", "16-bit black", field_width, field_heigth, 1);
if (number_of_channels == 2) {
    run("Merge Channels...", "c2=[Field b] c3=[Field b] create"); //if you have more than one channel, add cx=[Field b] per channel. The channel selected should be the same as your initial image
    }
if (number_of_channels == 3) {
    run("Merge Channels...", "c1=[Field b] c2=[Field b] c3=[Field b] create"); //if you have more than one channel, add cx=[Field b] per channel. The channel selected should be the same as your initial image
    }
if (number_of_channels == 4) {
    run("Merge Channels...", "c1=[Field b] c2=[Field b] c3=[Field b] c4=[Field b] create"); //if you have more than one channel, add cx=[Field b] per channel. The channel selected should be the same as your initial image
    }
saveAs("Tiff", CompositeFolder + "Field b");
print("Blank field generated...");
close();

//Creating the tile folder and adding the images. First full y*x grid, then real images will be copied on top of those, a full grid with blank images and actual images.
Tiles = folder+"Tiles"+File.separator;
File.makeDirectory(Tiles);
TileFolder = folder+ "Tiles\\";

var Xarray = newArray(1);
var Yarray = newArray(1);
var blankXarray = newArray(1);
var blankYarray = newArray(1);
var blankArray = newArray(1);

//blank X and Y array
Xarray = Array.getSequence(tileInX);
for (i=0; i<tileInY; i++){
    blankXarray = Array.concat(blankXarray,Xarray);
}
blankXarray = Array.slice(blankXarray,1,(tileInX*tileInY)+1); //previous loops generates a first array with one value "0" as the first blank array does not actually exists.

Yarray = Array.getSequence(tileInY);
for (i=0; i<tileInY+1; i++){
    blankYarray = Array.concat(blankYarray,Yarray);
}
blankYarray = Array.slice(blankYarray,1,(tileInX*tileInY)+1);
blankYarray = Array.sort(blankYarray);

//renaming the tile files. First total blank images, then actual images
print("Generating blank tiles copies ...");
for (n=0; n<(tileInX*tileInY); n++){
    File.copy(CompositeFolder+"Field b.tif", TileFolder+"Field_x"+blankXarray[n]+"_y"+blankYarray[n]+".tif");
    //print(TileFolder+"Field_x"+blankXarray[n]+"_y"+blankYarray[n]+".tif");
}
print("Blank tiles copies generated...");
print("Renaming and replacing real images in Tile folder...");
for (h=0; h<count; h++){
    File.copy(CompositeFolder+"Field "+ (h+1) +".tif", TileFolder+"Field_x"+newxCoordinate[h]+"_y"+newyCoordinate[h]+".tif");
}
print("Real images in Tile folder...");


//Stiching & renaming your image
print("Stiching...");
run("Grid/Collection stitching", "type=[Filename defined position] order=[Defined by filename         ] grid_size_x="+tileInX+" grid_size_y="+tileInY+" tile_overlap="+overlap+" first_file_index_x=0 first_file_index_y=0 directory=
print("Stiching completed...");
selectWindow("Fused");
run("Scale...", "x=1 y=1 interpolation=Bilinear average create title=Montage");
selectWindow("Fused");
close();

if (enhance == true)
    {
        autoContrast();
    }
```

```
//saving your montage
Montages = folder+"Montages"+File.separator;
File.makeDirectory(Montages);
MontageFolder = folder+ "Montages\\";

saveAs("Tiff", MontageFolder + montage_name);
run("Close All");

//deleting additonal folder - to make it lighter
if(del_CompositeFolder == true){
    for (i = 1; i < count+1 ; i++) {
        File.delete(CompositeFolder+"Field " + i +".tif");
    }
    File.delete(CompositeFolder+"Field b.tif");
    File.delete(CompositeFolder);
    print("Folder containing merged images deleted...");
}
if(del_TileFolder == true){
    for (n=0; n<(tileInX*tileInY); n++){
        File.delete(TileFolder+"Field_x"+blankXarray[n]+"_y"+blankYarray[n]+".tif");
    }
    File.delete(TileFolder+"TileConfiguration.registered.txt");
    File.delete(TileFolder+"TileConfiguration.txt");
    File.delete(TileFolder);
    print("Folder containing tile images deleted...");
}

//farewell messages
print("************************************************");
print("HUZZAH! Your montage has succesfully been processed and saved!");

time = getTime()-startingTime;
mins= time/60000;
mins=floor(mins);
secs=time%60000;
secs=round(secs/1000);
if(mins == 0){
    print("This macro was executed in " +secs+ " seconds.");
}
else {
    print("This macro was executed in " + mins + "minutes and "+secs+ " seconds.");
}

print("Hope you enjoyed using this macro.");
print("------ MACRO FINISHED ------");

setBatchMode(false);

/*
OPERETTA CALIBRATIONS
if (objective_used == "2x"){
    run("Set Scale...", "distance=1024 known=5086 pixel=[] unit=um global");
    }
if (objective_used == "10x"){
    run("Set Scale...", "distance=1024 known=1017 pixel=[] unit=um global");
    }
if (objective_used == "20x"){
    run("Set Scale...", "distance=1024 known=509 pixel=[] unit=um global");
    }
if (objective_used == "40x"){
    run("Set Scale...", "distance=1024 known=254 pixel=[] unit=um global");
    }
if (objective_used == "60x"){
    run("Set Scale...", "distance=1024 known=170 pixel=[] unit=um global");
    }
if (objective_used == "100x"){
    run("Set Scale...", "distance=1024 known=102 pixel=[] unit=um global");
    }
*/

//Applying autocontrast - conditional function
function autoContrast(){
    print("Enhancing...");
    selectWindow("Montage");
        //1 CHANNEL
    if (number_of_channels == 2) {
        run("Subtract Background...", "rolling=50");
        run("Enhance Contrast", "saturated=0.35");
        run("Apply LUT");
        }
        //2 CHANNELS
    if (number_of_channels == 2) {
        run("Split Channels");
        selectWindow("C2-Montage");
        run("Subtract Background...", "rolling=50");
        run("Enhance Contrast", "saturated=0.35");
        run("Apply LUT");
        selectWindow("C1-Montage");
        run("Subtract Background...", "rolling=50");
        run("Enhance Contrast", "saturated=0.35");
        run("Apply LUT");
        run("Merge Channels...", "c2=C1-Montage c3=C2-Montage create");
        }
        //3 CHANNELS
    if (number_of_channels == 3) {
        run("Split Channels");
        selectWindow("C1-Montage");
        run("Subtract Background...", "rolling=50");
        run("Enhance Contrast", "saturated=0.35");
        run("Apply LUT");
        selectWindow("C2-Montage");
        run("Subtract Background...", "rolling=50");
        run("Enhance Contrast", "saturated=0.35");
        run("Apply LUT");
        selectWindow("C3-Montage");
        run("Subtract Background...", "rolling=50");
        run("Enhance Contrast", "saturated=0.35");
        run("Apply LUT");
        run("Merge Channels...", "c1=C1-Montage c2=C2-Montage c3=C3-Montage create");
        }
        //4 CHANNELS
    if (number_of_channels == 4) {
        run("Split Channels");
        selectWindow("C1-Montage");
        run("Subtract Background...", "rolling=50");
        run("Enhance Contrast", "saturated=0.35");
        run("Apply LUT");
        selectWindow("C2-Montage");
        run("Subtract Background...", "rolling=50");
        run("Enhance Contrast", "saturated=0.35");
        run("Apply LUT");
        selectWindow("C3-Montage");
        run("Subtract Background...", "rolling=50");
        run("Enhance Contrast", "saturated=0.35");
        run("Apply LUT");
        selectWindow("C4-Montage");
        run("Subtract Background...", "rolling=50");
        run("Enhance Contrast", "saturated=0.35");
        run("Apply LUT");
        run("Merge Channels...", "c1=C1-Montage c2=C2-Montage c3=C3-Montage c4=C4-Montage create");
        }
    selectWindow("Montage");
    print("Enhacing complete...");
}

}//this one ends the macro function
```

.2 Blood vessel quantification

```
/*
Macro - counting blood vessels and characterising the blood vessel type
v1.0 23/03/2017

Working with previously defined ROIs in the whole scanned image, this macro quantifies "independent vessels" and character

All calculations are made based on pixels!!!
*/

BigFolder = getDirectory("Choose the working directory");
folder = BigFolder+"OriginalData"+File.separator;
file = "sample";

lableArray = newArray("Epicardium", "Compact_myocardium", "Trabecular_myocardium");

setBatchMode(true);

print("MACRO started");
startingTime = getTime();

open(folder+file+".tif");
roiManager("reset");
roiManager("Open", folder+"RoiSet.zip");

run("Clear Results");

RoiArea = newArray((roiManager("count"))); //calculates the area of the original ROIs (tissue area)
for(roi=0; roi<(roiManager("count")); roi++){
    roiManager("Select", roi);
    roiManager("Measure");
    roiArea = getResult("Area", roi);
    RoiArea[roi] = roiArea;
}

run("Clear Results");
selectWindow(file+".tif");
close();

//each ROI correspond to an area of the heart. 1 outmost to 4 innermost.
for(roi=0; roi<(roiManager("count")); roi++){
    print("Analysing ROI "+roi+"...");

    open(folder+file+".tif");

    run("Split Channels");
    selectWindow("C3-"+file+".tif");
    close();
    selectWindow("C1-"+file+".tif");
    close();
    selectWindow("C2-"+file+".tif");
    roiManager("Select", roi);
    run("Duplicate...", " ");
    run("Make Inverse");
    setForegroundColor(2, 2, 2); //that should be black background
    run("Fill", "slice");
    selectWindow("C2-"+file+".tif");
    close();
    selectWindow("C2-"+file+"-1.tif");
        run("Duplicate...", "C2-"+roi+"-1.tif");
        saveAs("Tiff", BigFolder+"C2-"+roi+"-1.tif");
        close();
    selectWindow("C2-"+file+"-1.tif");

    //thresholding
    run("Make Inverse");
    setAutoThreshold("Li dark");
    setOption("BlackBackground", false);
    run("Convert to Mask");

    //saves mask for future checks
    roiManager("reset");
    run("Clear Results");
    run("Analyze Particles...", "size=30-Infinity show=Outlines display add"); //particles less than 30px are background g
    selectWindow("Drawing of C2-"+file+"-1.tif");
    saveAs("Tiff", BigFolder+lableArray[roi]+" particle mask.tif");
    roiManager("Save", BigFolder+"RoiSetMask "+lableArray[roi]+".zip");
    run("Close All"); //closes open images

    print("Analysing the endothelial vessels...");
    //counting total blood vessels
    TotalBloodVessels = nResults;

    //getting the areas of each individual blood vessel
    resultArray= newArray(TotalBloodVessels); //creates an array as long as the results list
    for(row=0; row<nResults; row++){
        result = getResult("Area",row); //will generate an annoying extra window
        resultArray[row] = result; //change the values in the array with the values
    }
    areaArray = Array.concat("Area (px)",resultArray); //adds title to the array

```

```
105     run("Split Channels");
106     selectWindow("C3-"+file+".tif");
107     close();
108     selectWindow("C2-"+file+".tif");
109     close();
110     selectWindow("C1-"+file+".tif");
111     roiManager("Select", roi);
112     run("Duplicate...", " ");
113     run("Make Inverse");
114     setForegroundColor(2, 2, 2); //that should be black background
115     run("Fill", "slice");
116     selectWindow("C1-"+file+".tif");
117     close();
118     selectWindow("C1-"+file+"-1.tif");
119         run("Duplicate...", "C1-"+roi+"-1.tif");
120         saveAs("Tiff", BigFolder+"C1-"+roi+"-1.tif");
121         close();
122     selectWindow("C1-"+file+"-1.tif");
123 
124     run("Make Inverse");
125     setAutoThreshold("MaxEntropy dark");
126     setOption("BlackBackground", false);
127     run("Convert to Mask");
128     run("Clear Results");
129 
130     roiManager("reset");
131     roiManager("Open", BigFolder+"RoiSetMask "+lableArray[roi]+".zip");
132     for(i=0; i<TotalBloodVessels; i++) {
133         roiManager("Select", i);
134         run("Enlarge...", "enlarge=10"); //enlarge current ROIs by 10px, a nuclei size
135         roiManager("Update");
136     }
137 
138     for(i=0; i<TotalBloodVessels; i++) {
139         selectWindow("C1-"+file+"-1.tif");
140         roiManager("Select", i);
141         run("Analyze Particles...", "size=0-Infinity show=Outlines display summarize"); //analyse particles for the periva
142         selectWindow("Drawing of C1-sample-1.tif");
143         close();
144     }
145 
146     print("Counting blood vessel types...");
147     selectWindow("Summary"); //count the pos/neg vessels from the summary -- you cannot use the built in function getResul
148     lines = split(getInfo(), "\n");
149     for(i=0; i<TotalBloodVessels; i++){
150         count_value = split(lines[i], "\t");
151         if(count_value[1] <= 10){ //numbers of pixels to consider positive
152             negBV++;
153         }
154         else {posBV++;}
155     }
156 
```

```
    selectWindow("Summary"); //extracting actual perivascular counts from the summary
    PeriMarkerArray = newArray(TotalBloodVessels);
    for(i=0; i<TotalBloodVessels; i++){
        count_value = split(lines[i], "\t");
        PeriMarkerArray[i] = count_value[1];
    }
    PeriMarkerArray = Array.slice(PeriMarkerArray, 1);
    PeriMarkerArray = Array.concat("Perivascular marker count", PeriMarkerArray);

    EndoArray = newArray ("Total vessels", TotalBloodVessels);
    posArray = newArray("Positive vessels", posBV);
    negArray = newArray("Negative vessels", negBV);
    percPosBV = (posBV*100/TotalBloodVessels);
    percPosArray = newArray("Percentage positive vessels", percPosBV);
    percNegBV = (negBV*100/TotalBloodVessels);
    percNegArray = newArray("Percentage negative vessels", percNegBV);

    var TotalVesselArea=0;
    for (i=1; i<(TotalBloodVessels+1); i++){
        TotalVesselArea=TotalVesselArea+areaArray[i];
    }
    percTotVesselArea = (TotalVesselArea*100/RoiArea[roi]);
    percTotVesselAreaArray = newArray("Percentage Total blood vessels area", percTotVesselArea);

    TotTissueArea = newArray("Total tissue area", RoiArea[roi]);

    summaryArray = Array.concat(TotTissueArea, EndoArray, percTotVesselAreaArray, posArray, percPosArray, negArray, percNe

    //SUMMARY RESULTS
    print("Saving report...");
    Array.show("ROI "+roi, particlesArray, areaArray, PeriMarkerArray, summaryArray);
    selectWindow("ROI "+roi);
    saveAs("Results", BigFolder+lableArray[roi]+".xls");
    print("ROI "+roi+" analysed...");

    run("Close All");

    roiManager("reset");
    roiManager("Open", folder+"RoiSet.zip");//restore original roi
}//area loop ends here

print("HUZZAH!");
print("Macro finished!!!");
time = getTime()-startingTime;
mins= time/60000;
mins=floor(mins);
secs=time%60000;
secs=round(secs/1000);
if(mins == 0){
    print("Analysis took " +secs+ " seconds.");
}
else {
    print("Analysis took " + mins + "minutes and "+secs+ " seconds.");
}
setBatchMode(false);
```

.3 Adipogenesis/osteogenesis quantification

```
dir = getDirectory("Select folder containing images to analyse");
list = getFileList(dir);

setBatchMode(true);
roiManager("reset");

for(i=0; i<list.length; i++){
    open(dir+list[i]);
    setMinAndMax(0, 65535);
    call("ij.ImagePlus.setDefault16bitRange", 16);
    run("Split Channels");

    imageCalculator("Add create", "C2-"+list[i],"C3-"+list[i]);
    imageCalculator("Subtract create", "Result of C2-"+list[i],"C1-"+list[i]);
    selectWindow("Result of Result of C2-"+list[i]);

    setThreshold(0, 18500);
    //waitForUser("Check the threshold levels. Press OK.");
    selectWindow("Result of Result of C2-"+list[i]);
    setOption("BlackBackground", false);
    run("Convert to Mask");
    rename(list[i]);

    run("Analyze Particles...", "summarize add");
    roiManager("Save", dir+list[i]+"_RoiSet.zip");
    roiManager("reset");
    run("Close All");
    print((i+1)+"/"+list.length+" images processed...");
}

selectWindow("Summary");
saveAs("Results", dir+"Summary.csv");
print("Huzzah. Done.");
```